CENTRO DE INVESTIGACIÓN Y DE ESTUDIOS AVANZADOS DEL INSTITUTO POLITÉCNICO NACIONAL

UNIDAD QUERÉTARO

"Metanol monohidratado bajo presión: un estudio de primeros principios"

Tesis que presenta

L.Q.I. Rosa Elena Dávila Martínez

Para obtener el grado de

Maestra en ciencias

en la Especialidad de

Materiales

Directores de Tesis:

Dr. Aldo Humberto Romero Castro
Prof. Razvan Caracas

Santiago de Querétaro, Qro. Marzo de 2010

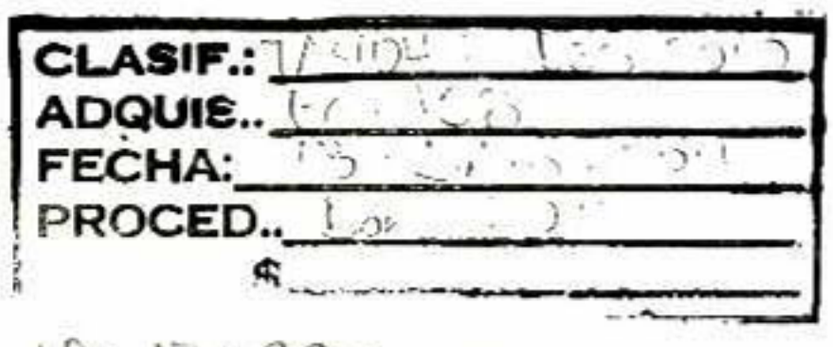

ID: 173916 00

CENTRO DE INVESTIGACIÓN Y DE ESTUDIOS AVANZADOS DEL INSTITUTO POLITÉCNICO NACIONAL

UNIDAD QUERÉTARO

"Methanol monohydrate under pressure: a first principles study"

Thesis presented by

L.Q.I. Rosa Elena Dávila Martínez

To obtain the degree of

Master in Science

With specialty in

Materials

Thesis Directors:

Dr. Aldo Humberto Romero Castro
Prof. Razvan Caracas

Santiago de Querétaro, Qro. March, 2010

Resumen

El metanol monohidratado es un sólido molecular orgánico y una de varias fases cristalinas presentes en el sistcma metanol-agua. A condiciones de presión atmosférica y bajas temperaturas, este compuesto es polar y tiene una estructura desordenada, es decir, algunos protónes pueden localizarse en distintas posiciones. En el presente trabajo se estudió el comportamiento del metanol monohidratado bajo distintas presiones (0 a 40 GPa), dentro del marco teórico de la Teoraí Funcional de la Densidad, con la Aproximación del Gradiente Generalizado. Se propusieron siete configuraciones iniciales idealmente ordenadas, basadas en la estructura encontrada experimentalmente, las cuales se optimizaron estructuralmente a distintas presiones. Tras la optimización se encontraron dos grupos de estructuras, en términos de energía y estabilidad. Las estructuras del grupo de menor energía y más estable preesentan simetría baja o nula, y las diferencias de energía entre las estructuras que lo forman, son muy pequeas (∼meV). Por lo tanto, las diferentes configuraciones pueden ir fácilmente de una a otra por reordenamiento de los átomos de hidrógeno. El grupo con mayor energía está formado por estructuras en las cuales el proton se localiza simétricamente entre dos átomos de oxígeno. Se calcularon y analizaron las geometrías, compresibilidad, patrones de difracción de rayos X, polarizacin espontánea, constante dieléctrica, modos y frecuencias de vibración de las estructuras optimizadas, así como su modificación en función de la presión. Se observó el mecanismo de compresin del sólido, en el cual las estructuras presentaron una alta compresibilidad en la dirección del eje b. De acuerdo con la ecuación de estado de las diferentes configuraciones, se predijo que la simetrización del protón puede ocurrir a 54 GPa. Tambin se encontró que algunas configuraciones presentan una polarización espontánea considerablemente grande para un sólido orgánico, de hasta ∼31 $\mu C/cm^2$ a 10 GPa. Bajo el marco de la Teoría Funcional de la Densidad de Perturbaciones se realizó el estudio vibracional, el que mostró que las configuraciones pertenecientes al grupo de menor energía son dinámicamente estables, mientras que las del grupo de mayor energía, no lo son.

Abstract

Methanol monohydrate is an organic molecular solid and one of several crystalline phases present in the methanol-water system. At ambient conditions of pressure and low temperature, this compound is polar and has a disordered structure, i.e some protons can occupy different positions. In this work, methanol monohydrate behavior under pressure (0 to 40 GPa) was studied, using the Density Functional Theory with the General Gradient Approximation. Based on the experimental structure, seven initial ideally ordered configurations were proposed, which were structurally optimized at different pressures. After optimization two groups of structures were found, in terms of energy and stability. The structures of the group with lowest energies and more stable, have low or no symmetry, and the energy differences among them are very small (~meV difference). Therefore, the different configurations can go from one to the other easily by hydrogen reordering. The higher energy group is formed by structures in which the proton is situated symmetrically between two oxygen atoms. The optimized structures geometry, enthalpy, compressibility, X-Ray diffraction pattern, spontaneous polarization, dielectric constant, vibrational modes and frequencies were calculated and analyzed, as well as their modification as a function of pressure. The compression mechanism of the solid was analyzed, in which the structures presented a high compressibility in the b-axis direction. According to the equations of state of the different configurations, it has been predicted that the symmetrization of the protons might occur at 54 GPa. It was also found that some configurations have spontaneous polarizations considerably large for an organic solid of up to ~31 $\mu C/cm^2$ at 10 GPa. Within the frame of the Density Functional Perturbation Theory, the vibrational study was done, which showed that the configurations that belong to the group of lower energy are dynamically stable, while the ones of the higher energy group are not.

Acknowledgements

I would like to thank to:

Dios, por permitirme cumplir este sueño y estar siempre a mi lado.

Mi familia, por su amor y apoyo incondicional: Papi, Mami, Bueli, Carlos, Susi y Gera; tíos y primos.

My advisors: Dr. Aldo Humberto Romero and Prof. Razvan Caracas, for allowing me to work with them and learn from them; and for kindly guided me to the conclusion of this work.

Mis sinodales, por sus revisiones y acertados comentarios: Dr. Sergio Jiménez y Dr. Gerardo Torres.

Mis amigos de Cinvestav y Cideteq, por ser mi familia en Quéretaro: Diana, Ale, Daisy, Gerardo, Víctor, Gervacio, Zorba, Abril, Tere, Andrés, Saraí, Mine, Zahyra, Julio y Jaime.

Mis amigos de Monterrey, por siempre estar al pendiente de mi: Rogelio, Coco y Manuel.

Cinvestav Querétaro, compañeros y profesores, por su ayuda y enseñanzas.

Les Laboratoire de Sciences de la Terre de la ENS de Lyon.

For computational time to: The Instituto Potosino de Investigación Científica y Tecnológica (Ipicyt); the Centre Informatique National de lEnseignement Suprieur (Cines), at France: Dr. Alfonso Muñoz from the Physics department of the Universidad de La Laguna, at Spain.

Agradecimientos especiales al Consejo Nacional de Ciencia y Tecnología (Conacyt) por el apoyo económico brindado con el número de becario 210030, para la realización de este trabajo de investigación de maestría. Así como por el apoyo del programa de Becas Mixtas para realizar la estancia de investigación en la ENS de Lyon, por el proyecto con número J-59853-F, y el proyecto México-Bélgica.

Contents

List of Figures

List of Tables

Chapter 1

Introduction

Among the several approaches of studying materials science, a broad division can be made: experimental and theoretical studies. Since the appearance of the Schrödinger equation, the latter have become more and more useful with the pass of the time. Nowadays they offer an important alternative to complement experimental data which cannot be easily reached in the laboratory.

The Diamond Anvil Cell is a device used in the laboratory to perform high pressure studies in crystals. It uses two culet diamonds which can be easily broken if the experiment is not performed correctly, making each experiment very expensive. In such case, theoretical calculations offer a great alternative to it, exploring the properties of a material under pressure before even actually making it in the laboratory.

Moreover, the use of theoretical calculations has been enormously benefited by the improvements in computers technology, and the constant development of physical and chemical theories and algorithms, allowing to make calculations faster and for larger systems.

One of this theories is the Density Functional Theory (DFT), which permits to compute properties of a system by finding the ground state density of it, using only fundamental physical constats, i.e. first principles. It is based on the studies of Hohenberg and Kohn of 1964[1], and complemented by the Kohn and Sham set of equations, presented in 1965[2].

Abinit is a DFT software that can be used for the computation of many properties, useful for solid state studies, such as structural, electric, elastic, spectroscopic and vibrational properties, among others[3, 4]. Hence, it has been selected to study the system of interest.

High pressure studies in molecular solids are of great significance since their interactions, and therefore their properties, depend widely on their interatomic distances, and can then be affected under these conditions when atoms are forced to be closer. Some molecular systems have already been widely studied, such as water or ammonia. These studies have been very useful not only to understand changes of structures and properties with pressure, but to use this

data to comprehend the composition and evolution of planets and moons.

Methanol monohydrate is a simple molecular organic solid at low temperatures, pertaining to the methanol-water system. It is a rich hydrogen system, so studies of it can give a better understanding of hydrogen bond. Such bonds cannot be casily experimentally studied under high pressures, because protons are invisible to X-rays and, eventhough they are detected by neutron diffraction, this technique cannot be performed at such pressures; but some answers may be given by optical studies.

Considering all mentioned, first principles studies are a convenient way of studying structural, dielectric and vibrational properties of methanol monohydrate under pressure.

The overall goal of this work is to perform a structural, dielectric and vibrational characterization of methanol monohydrate under pressure, using first principles calculations. To accomplish it, several particular goals were stated:

1. Structural optimization of methanol monohydrate when subjected to different pressures.
2. Structural characterization of methanol monohydrate when subjected to different pressures.
3. Spontaneous polarization calculations of methanol monohydrate at several pressures.
4. Dielectric constant calculations of methanol monohydrate at several pressures.
5. Vibrational characterization of methanol monohydrate when subjected to pressures.
6. Comparison of the results obtained by ab-initio calculations with experimental data.

This work is divided into 6 chapters. The present one is an introduction to the subjet. The second consists of the theoretical background of the Density Functional Theory, Density Functional Perturbation Theory and Polarization, needed to perform the calculations presented in posterior chapters. It also contains the importance and description of the system of interest, methanol monohydrate, and of the high pressure conditions. Chapter 3 is about the crystal structure of methanol monohydrate, including the modification of it under pressure, compressibility and equation of state. Chapter 4 deals with the polarization of the material under pressure. The fifth chapter is dedicated to the calculations done with Response Function, which is based on DFPT, and include the vibrational mode frquencies and the dielectric constant calculations. Finally, the conclusions and perspectives are presented.

Chapter 2

Theoretical Background

The calculations in this work are done under the theoretical framework of the Density Functional Theory (DFT) and a variant of it, called Density Functional Perturbation Theory (DFPT). Therefore the first section of this chapter is devoted to DFT and the second to DFPT, presenting a general explanation, as well as their relationship with the studied properties. The Berry phase approach to calculate the polarization is then explained. The code used, Abinit, is described in the fourth section. Then, the system under study, methanol monohydrate, is described, as well as the conditions, that are high pressures. Finally a brief explanation of X-Ray Diffraction is given.

2.1 Density Functional Theory

All the information of a system is contained in its wave function, Ψ, and it can be found by solving the system's corresponding Schrödinger equation. Nevertheless, this equation becomes impossible to solve for systems that contain more than one electron due to the interactions among them. Its solution can be approximated to a high extent -depending on the system- by semiempirical methods which use parameters that have to be adjusted to experimental data, or by first principles calculations (also called *ab-initio* methods) which do not use empirical data, but only fundamental physical constants. The Density Functional Theory is one of these latter methods.

DFT is a way of approaching the interacting problem by mapping it in principle exactly to an easier to solve non-interacting problem of non-interacting particles in an external potential $v(\mathrm{r})$. Then, the dependence on the external potential can be replaced by a dependence on the density distribution $n(\mathrm{r})$ and consequently the observables can be expressed as a function of the ground state density.

DFT is based on two core elements, the Hohenberg-Kohn theorem and the Kohn-Sham equations[5, 6, 7].

2.1.1 Hohenberg-Kohn Theorem

Hohenberg and Kohn theorem states that the total energy of an electron gas is a unique *functional* of the electron density. The minimum value of the total-energy functional is the ground-state energy of the system, and the density that yields this minimum value is the exact single-particle ground-state density[6]. Its original demonstration can be found somewhere else[1].

2.1.2 Kohn-Sham Method

Hohenberg and Kohn theorem can be solved by the Kohn-Sham equations. This method consists in replacing the many-electron problem by an exactly equivalent set of self consistent one-electron equations[2, 6]. The Kohn-Sham equations are:

$$v_s(\mathbf{r}) = v(\mathbf{r}) + v_H(\mathbf{r}) + v_{xc}(\mathbf{r}) \tag{2.1}$$

$$\left[-\frac{\hbar^2\nabla^2}{2m} + v_s(\mathbf{r})\right]\phi_i(\mathbf{r}) = \epsilon_i\phi_i(\mathbf{r}) \tag{2.2}$$

$$n(\mathbf{r}) \equiv n_s(\mathbf{r}) = \sum_i^N f_i\,|\phi_i(\mathbf{r})|^2 \tag{2.3}$$

Where $\mathbf{r}$ are the electronic coordinates, $v_s(\mathbf{r})$ is the potential where the non-interacting particles move in (s for single-particle), $v(\mathbf{r})$ is the external potential of the interacting (many-body) system, $v_H(\mathbf{r})$ is the Hartree potential, $v_{xc}(\mathbf{r})$ is the exchange-correlation potential, ϕ_i are single particle orbitals of the electronic state i (Kohn-Sham orbitals), ϵ_i is the Kohn-Sham eigenvalue, and $n(\mathbf{r})$ is the original system's density.

The Hartree potential is given by:

$$v_H(\mathbf{r}) = q^2\int d^3\mathbf{r}'\frac{n(\mathbf{r}')}{|\mathbf{r}-\mathbf{r}'|} \tag{2.4}$$

The exchange-correlation potential is given by:

$$v_{xc}(\mathbf{r}) = \frac{\delta\mathbf{E}_{xc}\,[n(\mathbf{r})]}{\delta n(\mathbf{r})} \tag{2.5}$$

The common approach to solve the Kohn-Sham equations is to make an initial guess of the density $n(\mathbf{r})$ to calculate the v_s with equation 2.1 since v_H and v_{xc} depend on $n(\mathbf{r})$. The resulting v_s is substituted in equation 2.2 so the differential equation can be solved to find ϕ_i. The latter is used to calculate a new density with equation 2.3 and start the cycle again. Different variables and algorithms for convergence can be used.

The ground state total energy, E_0, can be found once a converged density has been chosen, by means of:

$$E_0 = \sum_i^N \epsilon_i - \frac{q^2}{2}\int d^3r\int d^3r'\frac{n_o(\mathbf{r})n_o(\mathbf{r}')}{|\mathbf{r}-\mathbf{r}'|} - \int d^3r v^{xc}(\mathbf{r})n_0(\mathbf{r}) + E_{xc}[n_0] \tag{2.6}$$

Where N is the electron number.

2.1.3 Exchange and Correlation Energy

From the prior equations, the only unknown term is the exchange correlation energy, $\mathbf{E}_{xc}$. These contribution to the total energy have been described as follows:

The wave function of a many-electron system must be antisymmetric under exchange of any two electrons because the electrons are fermions. The antisymmetry of the wave function produces a spatial separation between electrons that have the same spin and thus reduces the Coulomb energy of the electronic system. The reduction in the energy of the electronic system due to the antisymmetry of the wave function is called exchange energy. It is straightforward to include exchange energy in a total energy calculation, and this is generally referred to as the Hartree-Fock approximation.

The Coulomb energy of the electronic system can be reduced below its Hartree-Fock value if electrons that have opposite spins are also spatially separated. In this case the Coulomb energy of the electronic system is reduced at the cost of increasing the kinetic energy of the electrons. The difference between the many-body energy of an electronic system and the energy of the system calculated in the Hartree-Fock approximation is called the correlation energy[6].

Other ways of describing correlation energy have been explained by Capelle with different approaches[7]. He mentions a *variational*, a *probabilistic* and the *beyond-mean-field* approaches, as well as a *holes* description. All of them referring to the correlation energy as an energy lowering when considering the interaction of electrons.

2.1.4 Local Density Approximation

If the exchange-correlation energy was known, the exact total energy could be found. Hence, there exists the need of making approximations to it. The simplest and one of the most successful is the Local Density Approximation (LDA) in which the functional is:

$$E_{xc}[n] \approx \int d^3 r e_{xc}^{hom}(n(\mathbf{r})) \tag{2.7}$$

where $e_{xc}^{hom}(n(\mathbf{r}))$ is the exchange-correlation energy per electron at each point in space of an homogeneous interacting electron gas of density n.

The LDA has been shown to give very good results for many atomic, molecular and crystalline interacting electron systems, even though their electron density does not varies slowly[8].

2.1.5 Generalized Gradient Approximation

When highly correlated systems are studied, such as organic molecular solids, there is an approximation that has been found to work better, which is the Generalized Gradient Approximation (GGA).

Any real system has a spatially varying density $n(\mathbf{r})$ and it is useful to include the rate of this variation in the E_{xc} functional, i.e. the gradient $\nabla n(\mathbf{r})$. A gradient-correction is done in the form of a general function of $n(\mathbf{r})$ and $\nabla n(\mathbf{r})$, of the form:

$$E_{xc}^{GGA}[n] = \int d^3r f\left(n(\mathbf{r}), \nabla n(\mathbf{r})\right) \tag{2.8}$$

This is the generalized gradient approximation. It has worked better than LDA for some problems but at the cost of an increase in the computational time.

2.1.6 Pseudopotentials

An important contribution to the computational time reduction in DFT is the use of pseudopotentials. This approach takes advantage of the fact that the outer or valence electrons are the ones that mostly account for many properties. The real external potential is substituted by a pseudopotential that acts on a set of pseudo wavefunctions, as illustrated in figure 2.1[6].

The pseudopotential considers that the inner electrons retain an atomic-like configuration under a modification in the solid or molecule, so only the valence electrons* density is allowed to change in the self-consistency cycle.

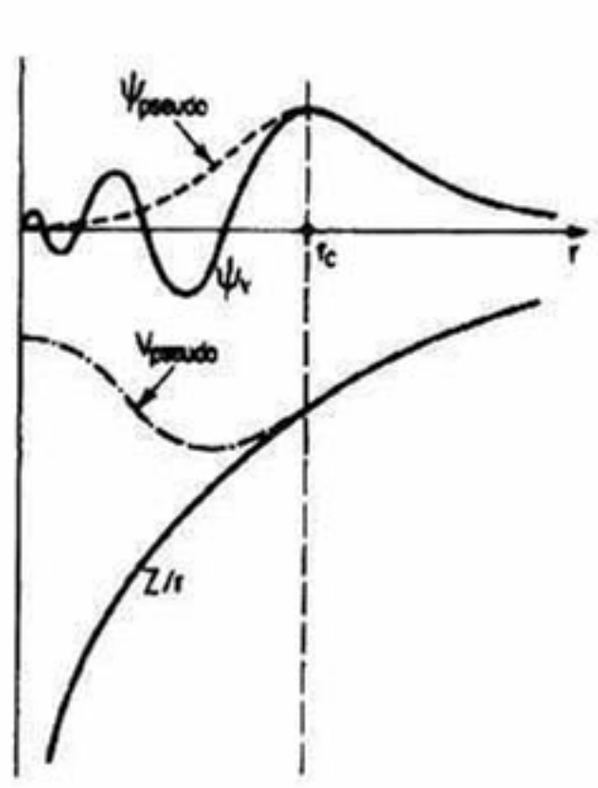

Figure 2.1: Schematic illustration of all-electron (solid lines) and pseudoelectron(dashed lines) potentials and their corresponding wave functions. The radius at which all-electron and pseudoelectron values match is designated as r_c. Outside the core region the two potentials are identical. (After [6]).

Most pseudopotentials are constructed in such way that they satisfy four general conditions. The first one is that the valence pseudo wavefunctions generated from the pseudopotential should contain no nodes. Second, the normalized atomic radial pseudo wavefunctions with angular momentum l is equal to

*The electrons considered as valence ones may vary with the type of pseudopotential and they are determined by the r_c.

the normalized radial all-electron wavefunction beyond the chosen cutoff radius, r_c, or converges rapidly to that value. Third, the charge enclosed within r_c for the two wavefunctions must be equal. The fourth condition is that the valence all-electron and pseudopotential eigenvalues must be equal[9].

2.1.7 Periodic Systems

The valence electrons mentioned in the preceding section are then represented with the Kohn-Sham orbitals, but they are still a large number of electrons moving in a potential of a huge number of nuclei or ions, and need a basis set to suitably represent them.

Bloch's Theorem states that in a periodic solid each electronic wave function can be written as the product of a cell periodic part and a wavelike part. The cell periodic part of the wave function can be expanded using a basis set of *plane waves* whose wavevectors are reciprocal lattice vectors of the crystal. Accordingly, each electronic wave can be written as a sum of plane waves.

$$\phi_i(\mathbf{r}) = \sum_G c_{i,\mathbf{k}+\mathbf{G}} \exp[i(\mathbf{k}+\mathbf{G})\cdot\mathbf{r}] \tag{2.9}$$

where $\mathbf{G}$ are reciprocal lattice vectors.

Bloch's theorem permits to calculate a finite number of electronic wave functions at an infinite number of $\mathbf{k}$ points, instead of calculating an infinite number of wavefunctions. A special set of $\mathbf{k}$ points can be selected since the electronic wave functions at very close $\mathbf{k}$ points will be almost identical. Therefore, only a finite number of $\mathbf{k}$ points are required to calculate the electronic potential and determine the total energy of the solid[6]. An efficient method to generate sets of special points in the Brillouin zone is given by Monkhorst and Pack[10].

Besides, Bloch's theorem allows the electronic wave functions to be expanded in terms of a discrete set of plane waves, instead of a continuum. The coefficients for the plane waves can be truncated up to a finite *cutoff energy*, because the coefficients $c_{i,\mathbf{k}+\mathbf{G}}$ for the plane waves with small kinetic energy are more important than the ones with large kinetic energy. This will lead to an error in the total energy, but a convergence study can be performed to reduce it.

2.1.8 The use of DFT

DFT is one of the most popular and successful quantum mechanical approaches to matter. It is nowadays applied for calculating, e.g., the binding energy of molecules and the band structure of solids. Superconductivity, atoms in the focus of strong laser pulses, relativistic effects in heavy elements and in atomic nuclei, classical liquids, and magnetic properties of alloys have all been studied with DFT[7].

In the present work, DFT is used to optimize the structure of methanol monohydrate by finding the structure of minimum energy. The equilibrium lattice constants and angles of the structure, are those that minimize the total energy. The computed energies can then used to calculate differences in enthalpies. Some other properties were computed, which will be explained in subsequent sections.

2.1.8.1 Enthalpy from DFT

Two phases in equilibrium, denoted by ' and '', must have the same molar free energy, or Gibbs energy, G:

$$G' = G'' \tag{2.10}$$

The Gibbs free energy of a phase is given by:

$$G = E + PV - TS = H - TS, \tag{2.11}$$

and DFT calculations are performed at 0 K, therefore, it is necessary that:

$$H' = H'' \tag{2.12}$$

or $\Delta H = 0$, for a phase transformation to happen.

H can then be calculated using the data found in a DFT calculation without any further treatment, only with the equation:

$$H = E + PV \tag{2.13}$$

E being the total energy, P, the pressure, and V, the unit cell volume.

2.1.9 Accuracy

When covalent, metallic or ionic bonds are present in the studied system, the differences between experiment and theory are commonly 2-3% for geometry (cell parameters, bond lengths), and $\sim 0.007Ha$ (0.2 eV)[†] for bonding energies (with GGA). When weak bonds such as hydrogen bonds or van der Waals interactions play an important role in the structures, this differences are larger.

2.1.10 Van der Waals interactions in DFT

As mentioned before, DFT is exact in principle, then it includes all interactions among the atoms. Nevertheless, van der Waals interactions are among the ones that give place to correlation energy and because of the approximations used, they are not included in the DFT total energy calculations.

[†] 1 hartree = 27.2107 eV

As they are small in comparison with other interactions, in particular for high pressure conditions, its exclusion in the calculation does not affect considerably the total energy and differences of energies. To support this, some studies of similar systems to the one of the present work can be mentioned, which employed DFT and GGA leading to good agreement between theory and experiment: methane hydrate's lattice parameters change under high pressure[11], P-V relations of ice X and ice VII[12], and the crystal structure and pressure dependence of normal mode frequencies of the high pressure phase of sodium formate dihydrate[13].

When relevant, some corrections can be done to include van der Waals interactions in DFT, with a corresponding computational cost.

2.2 Density Functional Perturbation Theory

DFPT is a variant of DFT where the external potential of a quantum mechanical system suffers infinitesimal perturbations.

Within DFPT, the perturbed quantity X is expressed as a Taylor expansion, in terms of a small parameter λ, around the unperturbed values, $X^{(0)}$:

$$X(\lambda) = X^{(0)} + X^{(1)}\lambda + X^{(2)}\lambda^{(2)} + X^{(3)}\lambda^{(3)} \ldots, \tag{2.14}$$

where

$$X^{(n)} = \frac{1}{n!}\frac{d^n X}{d\lambda^n}\Big|_{\lambda=0} \tag{2.15}$$

X can be E, $\phi_\alpha(\mathbf{r})$, $n(\mathbf{r})$, among other quantities. λ represents infinitesimal perturbations, which can be atomic displacements, electric and magnetic fields, strains, etc.

Due to the fact that E satisfies the variational principle, an important theorem has been derived:

A variational principle can be established for the even order perturbations:

$$E^{(2n)} = \min_{\phi_\alpha^{(n)}} \left\{ E_{(\lambda)} \left[\sum_{i=0}^{n} \lambda^i \phi_\alpha^{(i)} \right] \right\}^{(2n)} \tag{2.16}$$

It establishes that that the n^{th}-order derivatives of the wave functions can be calculated by the minimization of the functional expression of energy, $E^{(2n)}$ with respect to $\phi_\alpha^{(n)}$ For example, the first-order derivatives of the wave functions can be computed by minimizing the variational expression of the second-order energy derivatives $E^{(2)}$[14].

Another theorem for odd order energy derivatives has also been derived. The explanation of both theorems can be found somewhere else, as well as a more extensive description of DFPT[15, 16, 17, 18].

The computation of the first order derivatives of the wave functions, density and self-consistent potential with respect to perturbations is described by Gonze in reference [15]. Then, the computation of the second-order derivatives of the total energy is explained in reference [17].

With DFPT, changes in total energies due to adiabatic perturbations are obtained within a few percent of experimental data[15] The perturbations considered in this work belong to two classes: a) collective displacements of atoms characterized by a wavevector, which generates the *phonons*, and b) homogeneous static electric fields, which gives the *dielectric constant*. Many other properties of materials -mechanical, electrostatic, magnetic, thermal, etc.- can be determined by this method[18].

2.2.1 Phonons

The quantum unit of a crystal vibration is a phonon. The energy of the phonon is $\hbar\omega$, where ω is its angular frequency, and $\hbar$ is the Plank constant.

In equation 2.14, when λ stands for the displacements of atoms, the phonons can be obtained. The first term, $X^{(0)}$ represents the static energy with unmoved atoms, it is the total energy from the standard SCF calculation. The second term $X^{(1)}$ gives the forces. If the structure is at equilibrium then the forces are zero and this term dissapears. The third term, $X^{(2)}$, is related to the dynamical matrices.

ω^2 is obtained by diagonalizing the dynamical matrices, if $\omega^2 > 0$ then the phonons have positive frequencies ω and the structure is stable. If $\omega^2 = 0$, it belongs to the acoustic modes if all atoms move parallel the same distance, or to soft optical modes that induce a phase transition. If $\omega^2 < 0$ then ω is imaginary, that is, unphysical, and the crystal structure must be unstable. If such modes are present in the crystal, then it will transform spontaneously to a more stable structure.

The second-order derivatives of the total energy with respect to atomic displacements can be ontained with DFPT as explained above. Once they have been computed, it is possible to use them to calculate dynamical matrices and phonon frequencies. The detailed procedure is described in reference [17]. Theoretical calculations for phonon frequencies have been done for many materials, and agreement with experimental frequencies within $\approx 5\%$ is common[18].

The phonon frequencies are the key ingredient in vibrational spectroscopies. A wealth of information about materials is provided by the vibrational spectra that are measured experimentally by infrared and Raman absorptions, light scattering, inelastic neutron scattering, and other techniques. Then, theoretical calculations can help understand or predict the experimental results, in order to have a better understanding of the materials composition and structure.

2.2.2 Dielectric constant

In this calculations the perturbation is an homogeneous electric field, which results in a change of potential.

The dielectric permitivity constant $\epsilon_{\hat{q}}$ along $\hat{\mathbf{q}}$[‡] can also be calculated within DFPT from the dielectric permitivity tensor $\epsilon_{\alpha\beta}$, by:

$$\epsilon_{\hat{\mathbf{q}}}(\omega) = \sum_{\alpha\beta} \hat{q}_\alpha \epsilon_{\alpha\beta}(\omega) \hat{q}_\beta \tag{2.17}$$

The dielectric permitivity tensor is obtained from the polarization matrix, which can be obtained from the second-derivatives of the total energy with respect to changes in the potential. The detailed formalism can be found in reference [17].

2.3 Polarization

A pair of equal and opposite charges with magnitude q, situated at a distance d, is called an electric dipole, μ. μ is a vector quantity, pointing from the negative to the positive charge and has the unit of Cm[19].

Macroscopic polarization in a dielectric material with finite volume V, can be defined as the dipole moment per unit volume:

$$\mathcal{P} = \frac{\mu}{V} \tag{2.18}$$

or

$$\mathcal{P} = \frac{1}{V}\left[-e\sum_l Z_l \mathbf{R}_l + \int d\mathbf{r}\mathbf{r}\rho(\mathbf{r})\right], \tag{2.19}$$

where e is the electron charge, V is the sample volume, l runs over the ionic sites, $-eZ_l$ are the bare ionic charge, and $\rho(\mathbf{r})$ is the electronic charge density. Although such a dipole is in principle well defined, $\mathcal{P}$ is not a bulk property since it depends upon truncation and shape of the sample. Simplified models are ill defined for periodic crystals, since charge density cannot be "cut", it is a continuous function of $\mathbf{r}$. In contrast, the difference in polarization $\Delta\mathcal{P}$ between two different states of the same solid, is measured as a bulk material property in several circumstances[20, 18].

A theory of polarization formulated directly in terms of the quantum mechanical wavefunction has only recently been derived, in terms of the geometric phase or Berry's phase and alternative expressions using Wannier functions[18], although the latter were not used in the calculations of this thesis. In this work, the polarization of solids is described as a manifestation of a Berry phase.

Polarization is an observable which cannot be cast as the expectation value of any operator. Instead, macroscopic polarization is a gauge invariant phase

[‡] $\mathbf{q}$ is the wavevector of a perturbation, and q=0 is the Gamma point.

feature of the electronic wave function, as a Berry phase. The geometric phase approach provides an extremely powerful computational tool for dealing with spontaneous polarization[20].

The computation of polarization changes within first-principles total-energy calculations is based on what King-Smith and Vanderbilt demonstrated in [21]. They proved that adiabatic changes in the Kohn-Sham Hamiltonian led to polarization changes in the solid which can be computed in terms of the initial and final valence-band wave functions of the system.

The explanation starts by considering an insulator crystal with N doubly occupied bands, and a continuous adiabatic transformation of the crystalline potential connecting two states of the crystal. The transformation is parametcrized by a variable λ, and $\lambda 1$ and $\lambda 2$ denote the initial and final states, respectively. The change in polarization due to this transformation is given by:

$$\Delta \boldsymbol{\mathcal{P}} = \int_{\lambda 1}^{\lambda 2} d\lambda \frac{\partial \boldsymbol{\mathcal{P}}}{\partial \lambda} = \boldsymbol{\mathcal{P}}(\lambda 2) - \boldsymbol{\mathcal{P}}(\lambda 1) \tag{2.20}$$

The polarization $\boldsymbol{\mathcal{P}}(\lambda)$ can be decomposed as the sum of a bare ionic and an electronic polarization:

$$\boldsymbol{\mathcal{P}}(\lambda) = \boldsymbol{\mathcal{P}}_{ion}(\lambda) + \boldsymbol{\mathcal{P}}_{el}(\lambda) \tag{2.21}$$

The ionic polarization can be computed through the expression:

$$\boldsymbol{\mathcal{P}}_{ion}(\lambda) = \frac{e}{\Omega_0} \sum_{\kappa}^{cell} Z_\kappa R_\kappa \tag{2.22}$$

where Z_κ y R_κ are the atomic number and position, Ω_0 is the volume of the unit cell and the sum runs over all atoms in the unit cell.

The electronic polarization can be computed as a Berry phase of the occupied bands:

$$\boldsymbol{\mathcal{P}}_{el}(\lambda) = -\frac{2ie}{(2\pi)^3} \sum_{n=1}^{N} \int_{BZ} d\mathbf{k} \, \langle u_{n\mathbf{k}} \mid \nabla_k \mid u_{n\mathbf{k}} \rangle \tag{2.23}$$

where BZ is the Brillouin zone, $u_{n\mathbf{k}}(\mathbf{r})$ is the periodic part of the Bloch functions and the factor of 2 accounts for the spin degeneracy. The Bloch functions are chosen to satisfy the periodic gauge condition:

$$e^{i\mathbf{G}\cdot\mathbf{r}} u_{n\mathbf{k}+\mathbf{G}}(\mathbf{r}) = u_{n\mathbf{k}}(\mathbf{r}) \tag{2.24}$$

where $\mathbf{G}$ is a reciprocal lattice vector. With this choice of gauge, the polarization changes in equation 2.20 are given to within a factor $(e/\Omega_0)\mathbf{R}$, where $\mathbf{R}$ is a lattice vector.

In order to use equation 2.23 for practical calculations, the integration over the BZ, as well as the differentiation with respect to $\mathbf{k}$, have to be performed on a discrete mesh of $M_k = M_1 \times M_2 \times M_3$ $\mathbf{k}$-points. The standard approach is to build strings of $\mathbf{k}$-points parallel to a vector of the reciprocal space $\mathbf{G}_i$.

The projection of the polarization along that direction can then be computed as the sum of the string averaged electronic Berry phase, $\varphi_e l$, and the ionic phase, φ_{ion},

$$\boldsymbol{\mathcal{P}}(\lambda)\cdot\mathbf{G}_i = \frac{e}{\Omega_0}\left(\varphi_{el}^{(i)} + \varphi_{ion}^{(i)}\right) \tag{2.25}$$

with

$$\varphi_{el}^{(i)} = \frac{2}{M_\perp^{(i)}} \sum_{l=1}^{M_\perp^{(i)}} \Im ln \prod_{j=0}^{M_1-1} det\left[S(\mathbf{k}_j^{(i)}, \mathbf{k}_{j+1}^{(i)})\right] \tag{2.26}$$

and

$$\varphi_{ion}^{(i)} = 2\pi \sum_{\kappa}^{cell} Z_\kappa R_{\kappa i}, \tag{2.27}$$

where $M_\perp^{(1)} = M_2 \times M_3$ is the number of strings along $\mathbf{G}_1$, each containing M_1 points $\mathbf{k}_j^1 = \mathbf{k}_\perp^{(l)} + j\mathbf{G}_1/M_1$, S is the overlap matrix between Bloch functions:

$$S_{n,m}(\mathbf{k},\mathbf{k}') = \langle u_{n\mathbf{k}} \mid u_{m\mathbf{k}'}\rangle \tag{2.28}$$

and $R_{\kappa i}$ the reduced coordinates of atom κ in the unit cell[14].

A more detailed explanation of the Berry phase approach can be found in [21] and [20].

The changes in polarization can be due to the presence of an electric field, such as for ferroelectric materials, which sustain a spontaneous polarization even when the electric field is removed. Changes may also be induced by the application of a strain, as for piezoelectric materials, and by changes in temperature, as for pyroelectric materials.

Spontaneous polarization, $\boldsymbol{\mathcal{P}}_s$, occurs in any crystal that lacks a center of inversion. In such case, the two states taken into account for the calculation of the $\boldsymbol{\mathcal{P}}_s$ with zero electric field are the actual crystal and a crystal in which $\boldsymbol{\mathcal{P}} = 0$ by symmetry. This can be calculated by constructing a path between the two crystals by "theoretical alchemy", in which the charge of the nuclei is varied, or by large displacements of atoms to change the crystal structure[18].

2.3.1 Use and accuracy

Some examples of changes in polarization computed within the Berry phase approach and DFT are mentioned next.

The spontaneous polarization of $KNbO_3$ calculated as a Berry phase is 35 $\mu C/cm^2$, to be compared with the experimental value of 37, which represents a difference of 5.4%[20]. For $BaTiO_3$ the calculated $\boldsymbol{\mathcal{P}}_s = 37$ $\mu C/cm^2$ for the orthorombic phase, very similar to the experimental value of 36, denoting a small difference of 2.8%[14].

The differences seem to be larger for organic molecular solids. In a recent study where the Berry phase approach was used to compute the $\mathcal{P}_s$ of organic molecular crystals, the error was larger, though the spontaneous polarization is in the same order of magnitude than the experimental value. The calculated $\mathcal{P}_s$ for the optimized structure of a crystal of phenazyne-chloranil acid ($Phz - H_2ca$) was 0.55 $\mu C/cm^2$, compared with an experimental value of 0.76, which corresponds to a 27.6% error. For a crystal of thiourea the theoretical result was 4.9 versus 3.6 $\mu C/cm^2$, that is a 36.1% error[22].

In the same study[22], the importance in computing the polarization as a Berry phase in hydrogen-bonded organic molecular systems is highlighted. The spontaneous electric polarization of ($Phz - H_2ca$) was also computed cutting the intermolecular bonds by supercell calculations, computing the $\mathcal{P}_s$ of the Phz and H_2ca parts of the system separately, and then obtaining a net $\mathcal{P}_s$. The result was of 0.10 $\mu C/cm^2$, very far from the experimental value of 0.76.

2.4 The Abinit code

ABINIT is a free software distributed under the GPU General Public License. Its main program allows to find the total energy, charge density and electronic structure of systems made of electrons and nuclei (molecules and periodic solids) within DFT, using pseudopotentials and a planewave basis. ABINIT also includes options to optimize the geometry according to the DFT forces and stresses, or to perform molecular dynamics simulations using these forces, or to generate dynamical matrices, Born effective charges, and dielectric tensors[4]. A very complete description of its capabilities can be found in reference [23].

Even though some more codes can be used to perform such calculations, Abinit has been chosen for being a free software, having many properties calculations already implemented and its reliability.

2.4.1 Geometry optimization in Abinit

Abinit is able to compute analytically the forces on atoms and stresses on the cell. Such information allows one to start the optimization of atomic positions and unit cell parameters: new trial geometries are generated, for which the corresponding forces and stresses are evaluated. This step is repeated until the requirements on the residual forces and stresses, as defined by the users, are met, and the geometry is considered converged. As mentioned previously, the typical accuracy on such geometry parameters is on the order of a few percent[3], $\sim 2\%$ in distances, 1 degree in angles, and a few tens of cm^{-1} for phonons.

The optimization of a cell size and shape will target the stress tensor defined by the user, which corresponds to a *pressure*[4].

2.5 High Pressures in molecules

Molecules submitted to high pressures undergo very important changes in their physical and chemical properties, giving place to even new materials. Some of the changes that have already been observed are the modification of bonding and structure with compression, pressure-induced phase transitions, new states of electronic and magnetic order, besides the adjustment of electronic, magnetic, structural and vibrational properties[24]. These changes have already been studied in molecules such as water, ammonia, and nitrogen, among others.

Water is one of the most studied molecular solids, it has a complex phase diagram. The most common form of ice is hexagonal ice, ice Ih. Its structure has both covalent and hydrogen bonds between hydrogen and oxygen atoms. The former has a length of 1.00 Å, and the latter, of 1.75 Å[25]. Another ice phase is ice VIII. Theoretical calculations of ice VIII have predicted that the proton moves in two potential wells, but the probability of finding it has a maximum between them. Then, when the distance between the oxygen atoms is reduced due to compression, ice VII is formed, and the potential barrier decreases so the proton can tunnel from one position to another, i.e. transfer from one molecule to another, which is called *proton disorder*. This form of bond is known as low-energy barrier hydrogen bond. This transformation from ice VIII to *proton-disordered* ice VII appears at ~50 GPa. Moreover, when submitted to higher pressures, around 100 GPa, it forms Ice X in which protons are located in the middle of the distance between two oxygen atoms, which is known as *centering* or *symmetrization* of the hydrogen bond. In such structure it becomes an atomic solid[26]. Methane hydrate, another molecular solid, also presents proton disorder and symmetrization of hydrogen at around 40 GPa and 70 GPa, respectively[11].

Another example of high pressure studies on molecules is that of nitrogen. Its molecules present an intersting behavior when submitted to increasing pressures. It goes from a free rotating molecule to a more ordered structure to a polymeric phase. An explanation for the nitrogen phase diagram under high pressures as well as new structures, properties and Raman spectra were found using first principles calculations[27, 28].

High pressure studies are not interesting only because of the structural changes, they can also give answers to the formation and composition of planets, satellites or stars, where extreme conditions are found. Molecular compounds, either as gases, liquids or solids, such as water, ammonia and methane are commonly found in the core or atmosphere of other planets or moons. For example, studies of methane hydrate phase transformations at high pressures by Loveday et al. gave an explanation of the significant amount of methane in the current atmosphere of Saturn's satellite, Titan[29].

Much of the understanding of the mentioned changes is possible due to the study of the modifications of vibrational properties with induced pressure. Optical studies can be performed even at very high pressures, and simulations can be used to understand them.

High pressures are, therefore, a handfull tool to study structural transformations and to tune some properties of materials such as electric, magnetic or vibrational ones.

2.5.1 Diamond Anvil Cell

The Diamond Anvil Cell (DAC) is the device experimentally used to perform high pressure studies. It is adaptable to numerous scientific measurement techniques because of its optical accessibility, miniature size and portability.

In a general way, it consists of two diamond anvils that are pressed against each other, having a gasket in the middle containing the sample. It also contains a hydrostatic pressure transmiting medium and ruby. The latter is used as pressure sensor. There are different types of DACs. The most common type allows to insert a pressure of some 15 GPa, but higher pressures can be reached with more sofisticated types. The temperature can also be a variable[30].

2.5.2 Equation of state

An equation of state (EOS) relates thermodynamic variables such as pressure, volume and temperature. Temperature is often held constant in experiment and isothermal EOS are obtained.

Birch-Murnagham (BM) equation of state formalism[31] has been widely used to fit data in geophysics and condensed matter physics[32], including molecular solids, for which the BM third order EOS has worked well[33]. This equation is given by:

$$P(V) = \frac{3B_0}{2}\left[\left(\frac{V_0}{V}\right)^{\frac{7}{3}} - \left(\frac{V_0}{V}\right)^{\frac{5}{3}}\right]\left\{1 + \frac{3}{4}(B_0' - 4)\left[\left(\frac{V_0}{V}\right)^{\frac{2}{3}} - 1\right]\right\}, \quad (2.29)$$

and $E(V)$ is found by substituting 2.29 into $E = E_0 - \int P dV$:

$$E(V) = E_0 + \frac{9V_0B_0}{16}\left\{\left[\left(\frac{V_0}{V}\right)^{\frac{2}{3}} - 1\right]^3 B_0' + \left[\left(\frac{V_0}{V}\right)^{\frac{2}{3}} - 1\right]^2\left[6 - 4\left(\frac{V_0}{V}\right)^{\frac{2}{3}}\right]\right\} \quad (2.30)$$

In which B_0 and V_0 are the bulk modulus and the volume when $P = 0$, respectively, and B_0', the bulk modulus pressure derivative.

2.6 Methanol monohydrate

Methanol is the simplest alcohol, with the molecular formula CH_3OH. It is mainly obtained from fossil-fuel-based syn-gas though other chemical synthesis have been studied[34]. It is used mostly as solvent[35]. At present, its most promising application is in fuel cells[34, 36].

Methanol-water system has been studied widely[37, 38] in order to understand solute-solvent interactions and presence of hydrogen-bonded compounds at low temperatures. Also, both of them *per se* have been studied extensively experimentally and theoretically under a wide range of conditions of temperature and pressure, many techniques and methods. This also applies for their deuterated compounds, especially for vibrational studies.

This system is important for industrial chemistry as an inhibitor of clathrate formation in gas pipelines[39]. It is also of interest for cosmochemistry, since methanol has been found to be the source of hexamethylenetetramine (HMA), which may be a significant source of prebiogenic compounds in comets and interstellar medium, where conditions[40].

The studies of this system have revealed the formation of a solid phase of methanol monohydrate ($CH_3OH \cdot H_2O$). The solid-liquid phase diagram of the system methanol-water at atmospheric pressure shows a line corresponding to this compound at 50 mole percent methanol and -102°C[37]. The evidence of its existence are X-ray diffraction patterns, nuclear magnetic resonance spectra, powder neutron diffraction and differential scanning calorimetry data[37, 38, 41].

With the use of powder neutron diffraction data and *ab initio* methods, the structure of deuterated methanol monohydrate was solved, at 160 K and atmospheric pressure[42]. Although its structure has been elucidated, no information is available about its properties. Its particular structure is due to the formation of hydrogen bonds which are expected to be altered by high pressures, leading to a modification in its structure and properties, as it happens for other molecular compounds like water and nitrogen.

Other studies show that higher alcohols also form similar compounds and even more complex ones at low temperatures, but they have neither been studied under high pressures. At low temperature, ethanol and propanol also form hydrates at specific compositions, but when the content of water in the system is higher, they form clathrates[38].

Therefore the studies of methanol monohydrate under high pressures can be considered as a model for further studies of similar and more complex molecular solids, specially those containing hydrogen bonds. Besides, it is very likely that it can be found in other planets or moons as a planetary ice, since similar compounds have already been encountered. Therefore, its theoretical studies are important for its identification.

2.6.1 Crystal Structure

The crystal structure for deuterated methanol monohydrate ($CD_3OD \cdot D_2O$), has been solved at 160 K and ambient conditions of pressure by powder neutron diffraction data and *ab initio* methods, finding an orthorhombic crystal with unit cell dimensions a = 4.64910(2) Å, b = 14.08464(7) Å, c = 4.69358(1) Å, and volume V = 307.340 Å^3. The crystal is orthorhombic with space group

$Cmc2_1$ (number 36).

The structure is made of water-water chains, linked by ordered hydrogen bonds extending along the c-axis, which cross link methanol-water chains with disordered hydrogen bonds along the a-axis. These perpendicular chains form sheets which are stacked parallel to the b-axis[42]. This can be viewed in figures 2.2 and 2.3, taken from [42].

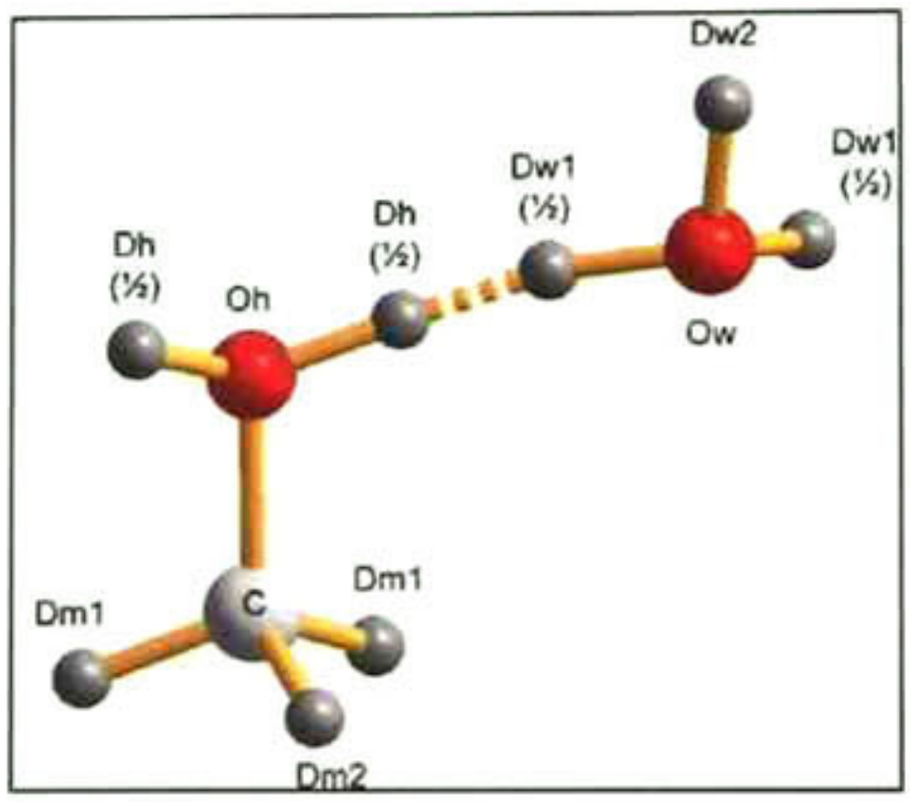

Figure 2.2: Methanol monohydrate molecule with atom labels used by Fortes[42], where the two positions of the disordered proton(in this case, deuterium) are shown by $Dh(^1/_2)$ and $Dw1(^1/_2)$ labels, when it is bonded to the oxygen of the methanol molecule or the water molecule, respectively.

The disordered hydrogen bonds are hydrogen bonds but with a disordered proton between the two oxygen atoms[§], as seen in figure 2.2. A disordered proton, as mentioned in section 2.5, can occupy two possible positions, in one position it forms a bond with one of the oxygens, and in the second position, with the other oxygen; i.e. it is able to move from one molecule to another. In figure 2.2 it is a deuterium atom the one that can either be forming a bond with the methanol-oxygen (position *Dh*) or with the water-oxygen (position *Dw1*).

The proton disordered is possible under certain conditions when the potential barrier decreases so the proton can go from one of the mentioned positions to another by quantum effects of protons (tunneling) or thermal hopping[12].

2.6.2 Interatomic distances

The interatomic distances of methanol monohydrate found in Fortes' study are presented below in section 3.3.1.3, table 3.4, toegether with some common distances for bonds formed between the same kind of atoms present in $CH_3OH \cdot H_2O$.

[§]Or other electronegative atoms such as F, Cl and N, instead of O.

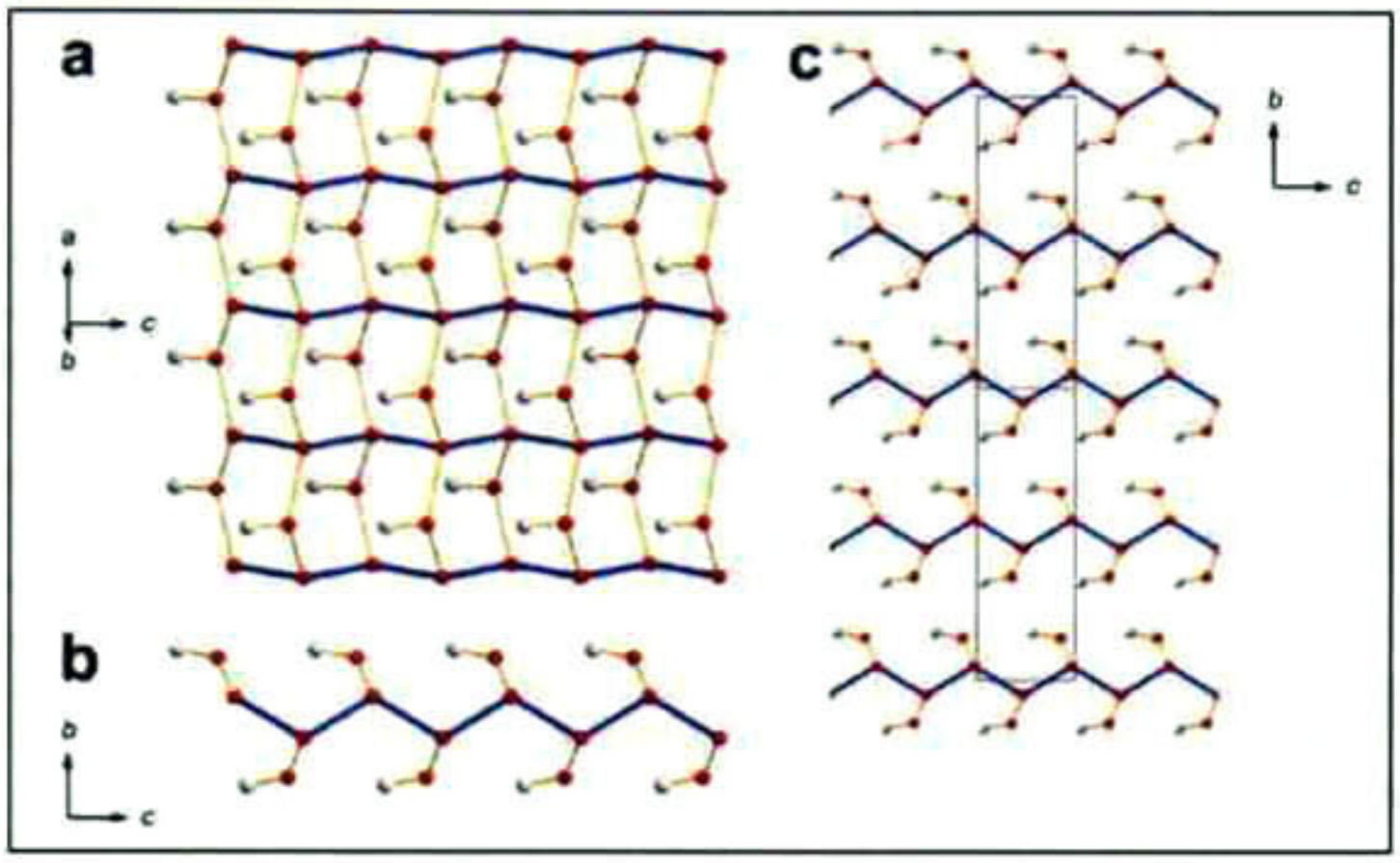

Figure 2.3: Views of experimental methanol monohydrate structure obtained by Fortes[42]. Hydrogen atoms were omitted for clarity. (a) View almost perpendicular to the plane of the H-bonded sheet (the waterwater chains are indicated by the heavy blue bonds). (b) View exactly parallel to the plane of the H-bonded sheet. (c) The packing arrangement of the sheets parallel to the b-axis (two unit cells are marked).

As stated before, hydrogen bonds play a mayor role in the structure of methanol monohydrate. The study of the hydrogen bond is very important especially for chemistry and biochemistry. It is of great importance in the design and construction of molecular *solids*. Its typical distances are 1.60-1.80Å for the O-H···O bond[43].

2.7 X-Ray Diffraction

A diffracted beam may be defined as a beam composed of a large number of scattered rays mutually reinforcing one another. Atoms scatter incident x-rays in all directions, but in some of these directions the scattered beams will be completely in phase and so reinforce each other to form diffracted beams.

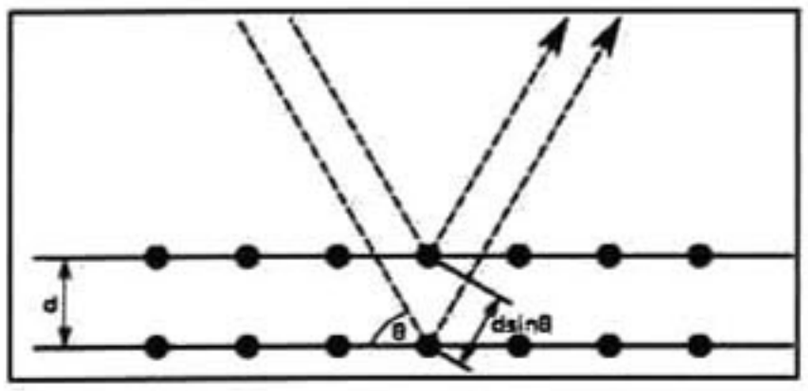

Figure 2.4: X-rays diffraction due to scattering between two planes.

Two scattered rays will be completely in phase if their path difference is

equal to a whole number n of wavelengths, or if

$$n\lambda = 2dsen\theta \tag{2.31}$$

This relation is known as Bragg's law, where d is the interplanar distance and θ is the scattering angle, as seen in figure 2.4. n is called the order of diffraction. The angle usually measured experimentally is 2θ, it is the angle between the diffracted beam and the transmitted beam and is known as the diffraction angle. Diffraction in general occurs only when the wavelength of the wave motion has the same order of magnitude as the repeating distance between scattering centers.

A general relation is obtained by combining Bragg's law and the plane-spacing equation of a particular crystal to predict the diffraction angle of any set of planes. For example, for a tetragonal crystal, with axes a and c, the corresponding general equation is:

$$sin^2\theta = \frac{\lambda^2}{4}\left(\frac{h^2+k^2}{a^2} + \frac{l^2}{c^2}\right) \tag{2.32}$$

Similar equations for other crystal systems can be obtained. Diffraction directions are determined solely by the shape and size of the unit cell. Intensities are determined by the position of the atoms in the unit cell, the density of atoms in the planes, and the number of electrons in the atoms. The intensity of a a diffracted beam is changed or even eliminated by any change in atomic positions[44].

Chapter 3

Crystal Structure

The structure of methanol monohydrate, experimentally found at 160 K and ambient conditions of pressure was described in chapter 2. This structure was taken as starting point to study the crystal structure of methanol monohydrate under pressure by DFT. The results of such subject are presented in this chapter.

3.1 Studied Structures

As an aid for the understanding of the present section and following ones, atoms will be represented according to the scheme shown in figure 3.1, unless otherwise mentioned: carbon atoms in dark gray, oxygen atoms in red, hydrogen atoms in blue and purple. The difference between the two types of hydrogens is described in the next section.

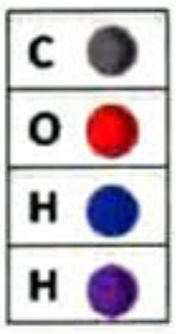

Figure 3.1: Color key convention for atoms used in the present work.

3.1.1 Initial structures

The methanol monohydrate structure experimentally found at 160 K has ordered and disordered hydrogen bonds[42]. In the present work, with the purpose of performing the ab-initio calculations for its structural optimization, initial configurations were proposed based on the mentioned structure. In the studied configurations, the hydrogen atoms from the originally disordered bonds, are located at fixed positions. The positioning of the hydrogens leads to seven different configurations which were named Structure 1 to 7, and are shown in figure 3.2. Each unit cell contains two molecules, and each molecule has 9 atoms.

The hydrogen atoms represented in purple are the ones that were originally (in the experimental structure) in disordered positions and were fixed for this study.

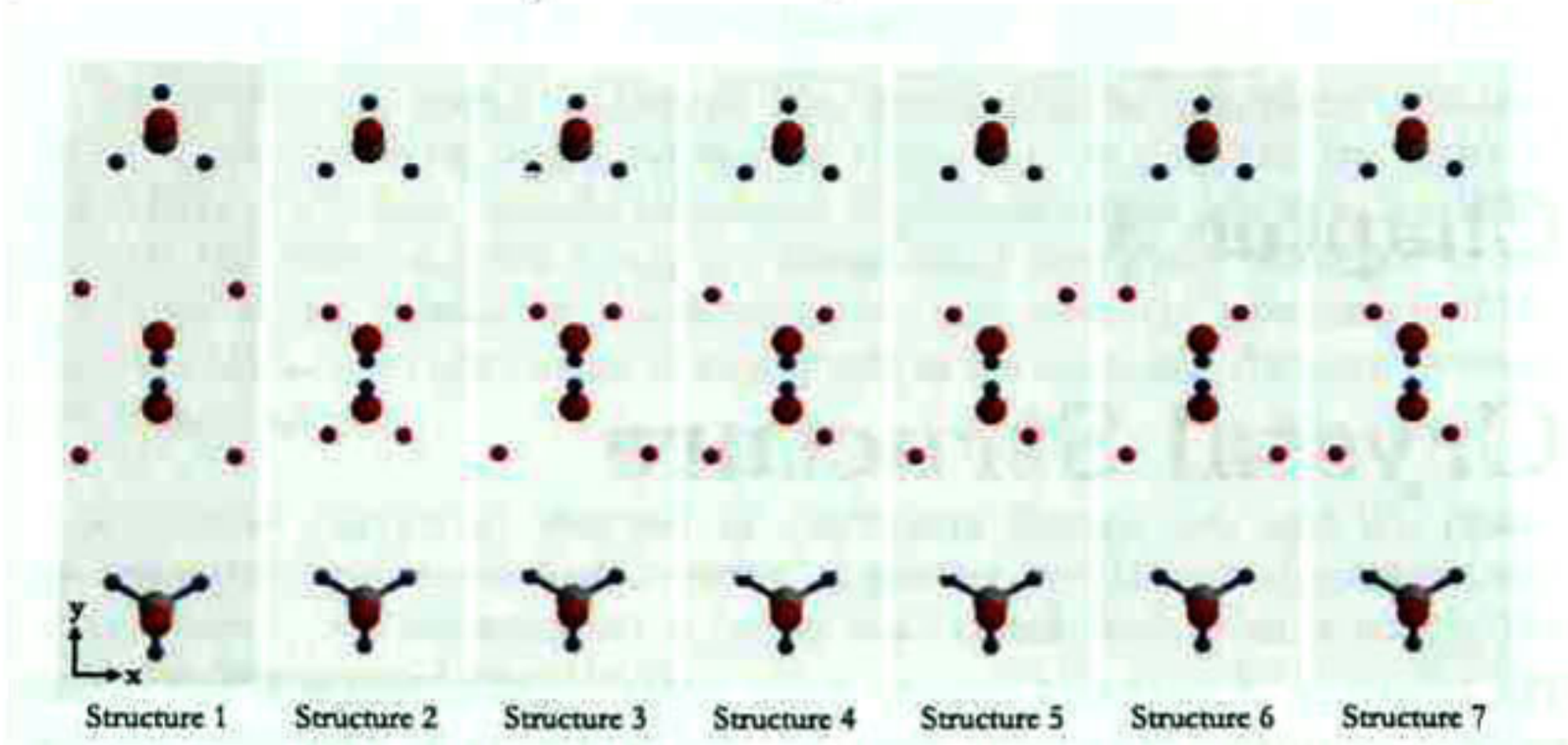

Figure 3.2: Initial configurations for the structural optimization of methanol monohydrate, showing the 18 atoms of the unit cell. The bonds between oxygen atoms and disordered protons (purple) are not shown.

These 18 atoms form the unit cell for the present calculations; and, the primitive vectors used, in cartesian coordinates and bohrs, were:

$$\begin{array}{rrr} 4.3927628639E+00 & 1.3308056085E+01 & 0.0000000000E+00 \\ -4.3927628639E+00 & 1.3308056085E+01 & 0.0000000000E+00 \\ 0.0000000000E+00 & 0.0000000000E+00 & 8.8695807457E+00 \end{array}$$

3.2 Computational details

All total energy calculations were performed with firs principles calculations, within the Abinit code[4], under the Generalized Gradient Approximation. Norm-conserving pseudopotentials GGA(PBE) (Perdew-Burke-Ernzerhof) generated with the package fhi98PP were used[45].

Convergence studies were done to select an appropriate cutoff energy and number of k points in the Brillouin zone. The former was chosen to be 40 Ha* and, the latter, a grid of $6 \times 6 \times 6$ points. A total energy difference of $8.9 \times 10^{-}4$ Ha was found when using this cutoff energy, with respect to using a 45 Ha cutoff energy.

The structural optimization was performed for each structure using as input the configurations mentioned in last section. Their cell geometries were fully optimized, allowing the modification of each cell's shape and volume, at 0 GPa, until the minimum total energy structure was found. The resulting structures were used as input to do the structural optimizations at 1 GPa. All structures†

*Such high cutoffs are needed for convergence of similar systems containing hydrogen atoms.

†Except structure 6, which could not be optimized at 0 GPa, its lowest pressure total energy calculation was the one done at fixed volume.

were optimized under 0, 1, 2, 4, 10, 15, 20, 30 and 40 GPa, using as starting unit cell the result from the previous pressure calculation.

The cells were also optimized taking the same initial structures as input but fixing the unit cell volume and allowing the optimization of the cell geometry. The fixed volumes were V_{exp} = 153.6699 Å^3 and $0.9V_{exp}$, the former corresponds to half the experimental volume of a conventional cell used by Fortes (307.340 Å^3)[42].

Convergence criteria for the structural optimization were set such that one Self-Consistent-Field cycle stopped when forces reached twice a difference less than 1.0×10^{-6} Ha/Bohr, and the structural relaxation stopped when a force below 5.0×10^{-5} Ha/Bohr was reached.

Calculated Volume-Energy pairs of data were fitted to the Birch-Murnagham third order EOS, equation 2.30. This was done using the code *Equation of State*[‡].

Maps of the electronic density have been computed with the abinit utility *Cut3D*.

The cell parameters and position of atoms in the structures were obtained from the optimized structures. By using these data and the software Diamond[§], X-ray diffraction patterns were obtained from the results at experimental volume optimization in order to compare them with experimental patterns.

3.3 Results

The calculated energies in this and next chapters are presented in Hartrees(Ha) per unit cell. Such unit cell is the one used for the calculations and described in section 3.1.1. It consists of two units of methanol monohydrate, ($CH_3OH{\cdot}H_2O$).

The cell parameters are given according to the conventional unit cell used by Fortes in reference [42]. It is drawn in figure 2.3c in section 2.6, and in figure 3.4. It is different from the unit cell used for the calculations, but it can be readily obtained when repeating the latter in space. Such conventional unit cell is delimited by the eight oxygen atoms located at the vertices of the prism in figure 3.4. Its volumen is twice the one of the unit cell used in the calculations.

3.3.1 Optimization at experimental volume

The structural optimization at experimental volume lead to the configurations shown in figure 3.3, that when repeated along the optimized primitive vectors, reproduce the conventional cell, like the one seen in figure 3.4. Along with the

[‡]Equation of State (EOS): Program for fitting total energy data to a model equation of state and extracting various parameters. Written by J. K. Dewhurst, Uppsala, Sweden (2002), Version 1.0.

[§]DIAMOND - Crystal and Molecular Structure Visualization. Demonstration Version 3.0. (C) Copyright 2004 Crystal Impact, K.Brandenburg and H.Putz GbR, Bonn, Germany. Author: Dr. Klaus Brandenburg.

Table 3.1: Cell parameters of structures optimized at experimental volume

Cell Parameters	Structure 1	2	3	4	5	6	7
a (Å)	4.064	4.063	4.060	4.440	4.438	4.453	4.439
b (Å)	15.943	15.939	16.071	14.737	14.723	14.676	14.735
c (Å)	4.744	4.746	4.711	4.697	4.704	4.704	4.699
α (°)	90.000	90.000	89.905	90.000	90.000	90.035	89.988
β (°)	90.000	90.000	90.000	89.279	90.000	89.300	89.295
γ (°)	90.000	90.000	90.000	90.000	90.468	90.003	90.010

differences in the position of their atoms, the structures presented variations in their cell parameters and angles, which are presented in table 3.1. Their space groups are shown in table 3.2. These space groups prevailed at the pressures studied, moving along the Born-Oppenheimer surfaces. Non of the space groups encountered are centrosymmetric, i.e. non of them has a center of inversion as symmetry element.

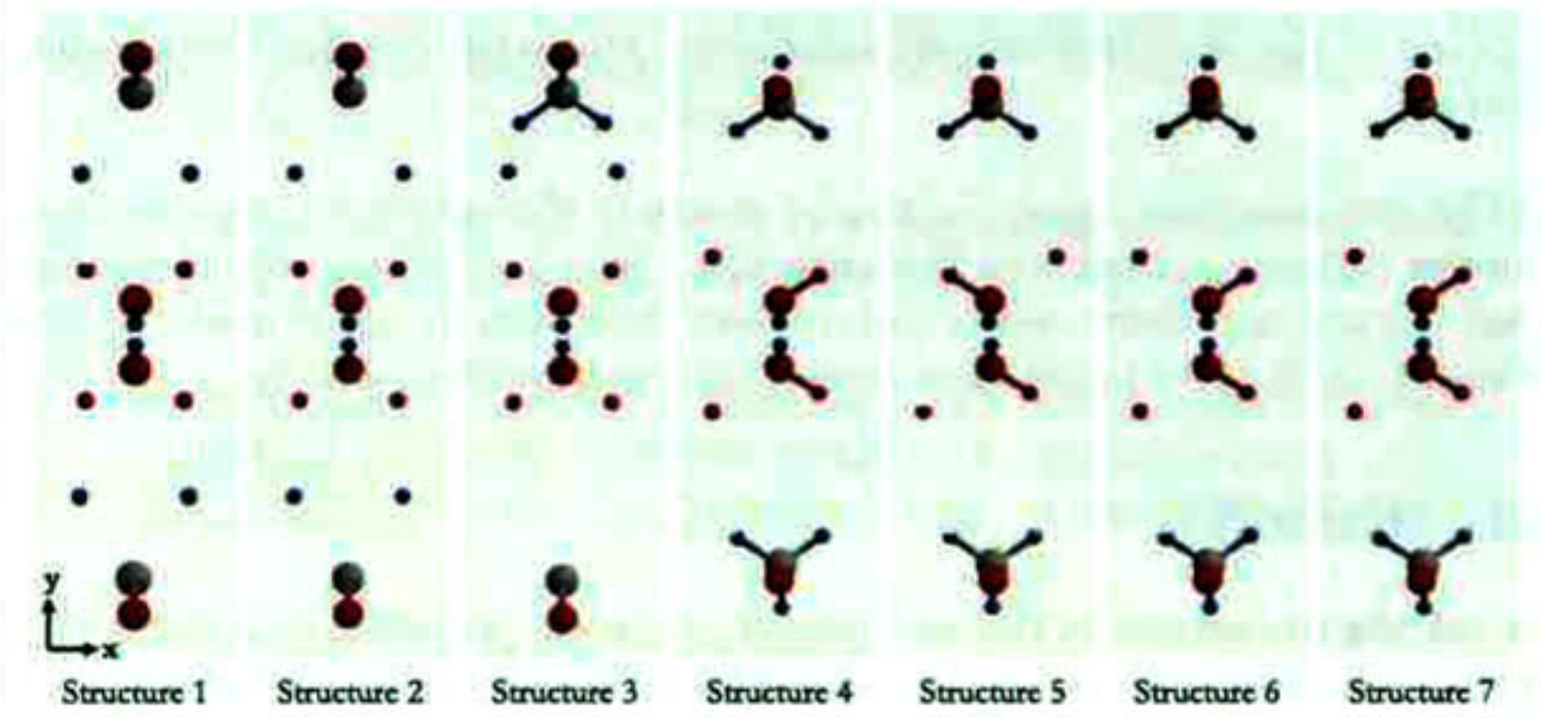

Figure 3.3: Atoms configuration of structures after optimization at experimental volume, showing the xy plane. Configuration of the originally disordered protons (purple) resulted very similar for structures 1 to 3, and for structures 4, 6 and 7.

Some similarities between the configurations can be observed in figure 3.3, by observing the originally disordered hydrogen atoms (purple). The position of these purple protons in structures 1, 2 and 3 resulted in very similar configurations. The four protons are almost equidistant from the central oxygen atoms. In contrast, for the rest of the structures, two hydrogen atoms(purple) are closer to the oxygen atoms of the middle of the picture, than the other two hydrogens. In these sense, structures 4, 6 and 7 also resamble, and structure 5 is different.

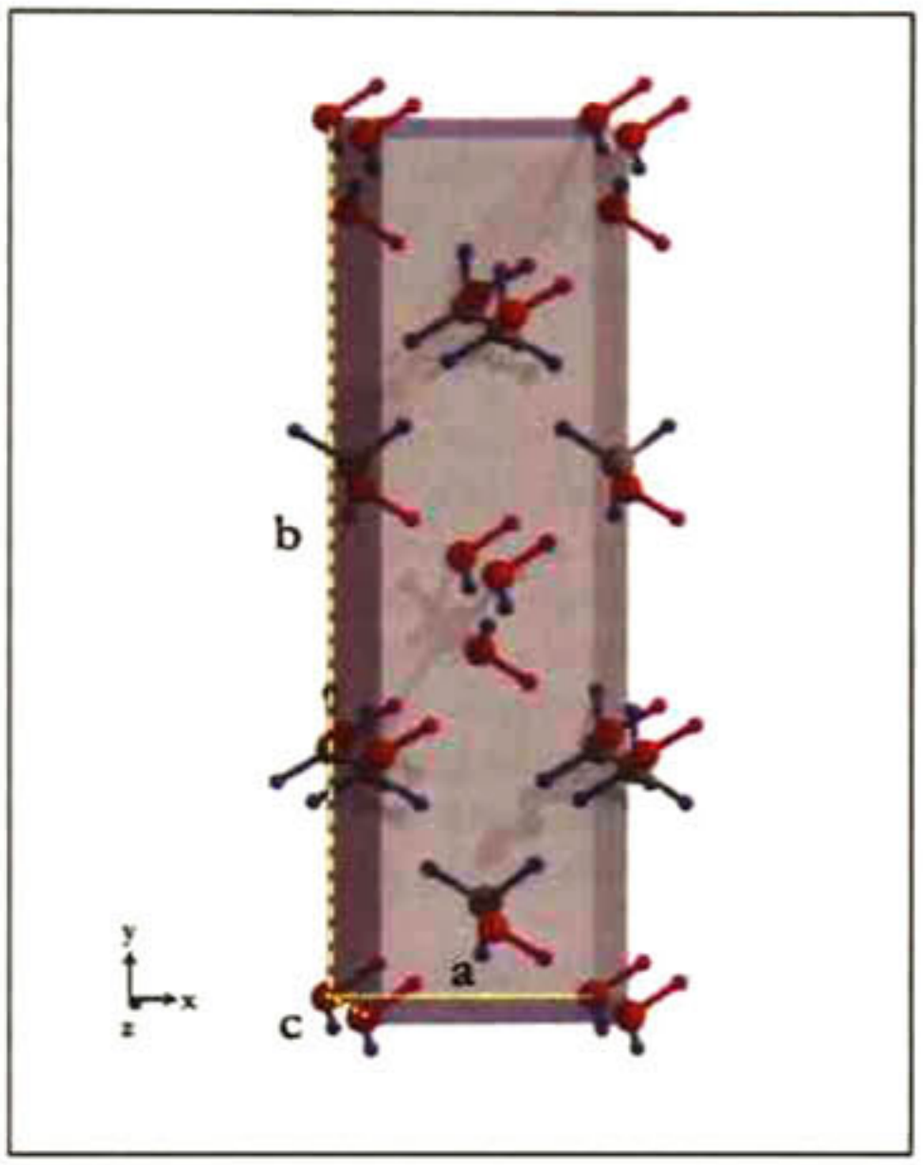

Figure 3.4: Conventional unit cell of structure 4 at experimental volume, delimited by oxygen atoms in the vertices. The cell parameters are indicated by dashed lines.

Table 3.2: Space groups and crystalline systems of structures

Structure	Space Group	Space Group No.	Crystalline System
1	$Cmc2_1$	36	orthorombic
2	$Cmc2_1$	36	orthorombic
3	Cm	8	monoclinic
4	Cc	9	monoclinic
5	$P2_1$	4	monoclinic
6	$P1$	1	triclinic
7	$P1$	1	triclinic

Protons in purple (originally disordered) are bonded to different oxygen atoms depending on the structure seen (1 to 7). Moreover, their configuration changed after optimization, with respect to the initial structures. On the contrary, hydrogen atoms in blue (ordered) remain bonded to the same carbon or oxygen atoms for all structures, and, in the same way that they were in the initial structures. This is not very clear when observing the unit cells of figure 3.3, but it is clear when they are repeated in space. One example is figure 3.4, where the conventional cell of structure 4 is shown. The same kind of bonds are observed for the ordered protons of all structures when the unit cells are repeated.

A more quantitative difference among structures can be obtained by comparing their symmetry groups and cell parameters after geometrical optimization (tables 3.2 and 3.1). Structures 1 and 2 are the most symmetric, i.e. they have more symmetry operations than the rest. They have a mirror plane in the xy plane, an axial glade plane, which is a reflection in the xz plane and a translation in direction z, and one C_2 rotational axis on x. Structure 3 has a mirror plane in the yz plane. Structure 4 has an axial glade plane, like the one of structures 1 and 2. Structure 5 has a C_2. Structures 6 and 7 possess no symmetry operations but the identity, and have all their angles different than 90°

Considering that structures 1 and 2 have the same symmetry, and very similar cell parameters and ground state energies, it can be said that the optimization led in both cases to the same structure. This could also be true for structures 4, 6 and 7 since the disagreement in space groups among them are due to very small differences in their cell parameters. But this is only valid for the structures found at the experimental volume optimization (the pressure corresponding to such volume is presented in table 3.3), since their behavior is different at higher pressures.

Because of the approximations used, total energies obtained by DFT do not have a physical meaning, instead what is really important is the difference in energies. The energies of the seven structures, when optimized at experimental volume, are not directly comparable one to another since they correspond to different pressures (table 3.3). In any case, by performing the energy differences between the different structures with respect to the one with the lowest energy (structure 7), an idea about their relative stability can be obtained. These differences are presented in table 3.3. The structural similarity of the first three structures is confirmed with their very close energies. The energies of structures 4, 5, 6 and 7 are also similar among them. Then, it can be said that in terms of energy, two groups of structures are formed. These groups are seen again when their relative enthalpies are compared, as seen below in figure 3.14, in section 3.3.2.1, where it can be observed that structures 1, 2 and 3 are less stable than structures 4 to 7, at all the studied pressures. Then, the group of structures 1, 2 and 3, less stable, will be referred to as group A henceforth; and the other group, with the remaining structures, group B.

Despite the increase of pressure for structures of group B with respect to group's A for the experimental volume optimization, it is seen below in figure 3.13 (section 3.3.2) that energy increases as pressure increases (volume decrease).

Table 3.3: Energy differences of structures optimized at experimental volume (with corresponding pressures)

Structure i	Pressure GPa	Energy Difference (Ha) ΔE_{i-7}
1	0.3260	1.056E-02
2	0.3284	1.056E-02
3	0.3857	1.054E-02
4	0.6555	4.324E-07
5	0.6607	7.004E-05
6	0.6573	2.452E-06
7	0.6603	0

So, the lower energy of group B is not due to the pressure increase, but to the structures' greater stabilities.

3.3.1.1 Description of structures

The structures obtained form layers or sheets in the xz plane, stacked in the y direction, as shown in figures 3.5, 3.6 and 3.7.

There are zig-zag water-water chains along the z direction, bonded by hydrogen bonds, shown with dashed yellow lines. Methanol-water chains, also in zig-zag, exist along the x direction, also bonded by hydrogen bonds, shown with a dashed violet line. Hydrogen bonds in the z direction are ordered, since the hydrogen atoms that form them, always occupy the same relative position. In contrast, the hydrogen atoms that form the hydrogen bonds along the x direction can occupy one of two possible positions, they are disordered. These two possibilities are shown in figure 3.8. The disordered hydrogens of structure 4, and its likes 6 and 7, occupy one of the two possible positions, while those of structure 5, the other position, as seen in figure 3.6 and 3.7, respectively.

Observing the methanol in the left superior corner of pictures 3.6 and 3.7, the disordered proton is bonded to the oxygen of methanol in structure 4 (fig. 3.6), while the same proton is bonded to the oxygen of water in structure 5 (fig. 3.7).

It should be noticed that the mentioned layers are formed by two constituent layers, one above and one below the blue sheet shown in figure 3.5. For the optimized structure 5, the disordered proton occupies the position shown in figure 3.7 only in the upper part of the layer (or front part in these figures), and the positions in the lower part have the same arrangement than that of the rest of the structures of group B (positions of figure 3.6), as seen behind the gray plane in figures 3.6 and 3.7.

The disorder cannot be seen in structures from group A, where the originally disordered atoms occupy the same relative position for the three final structures.

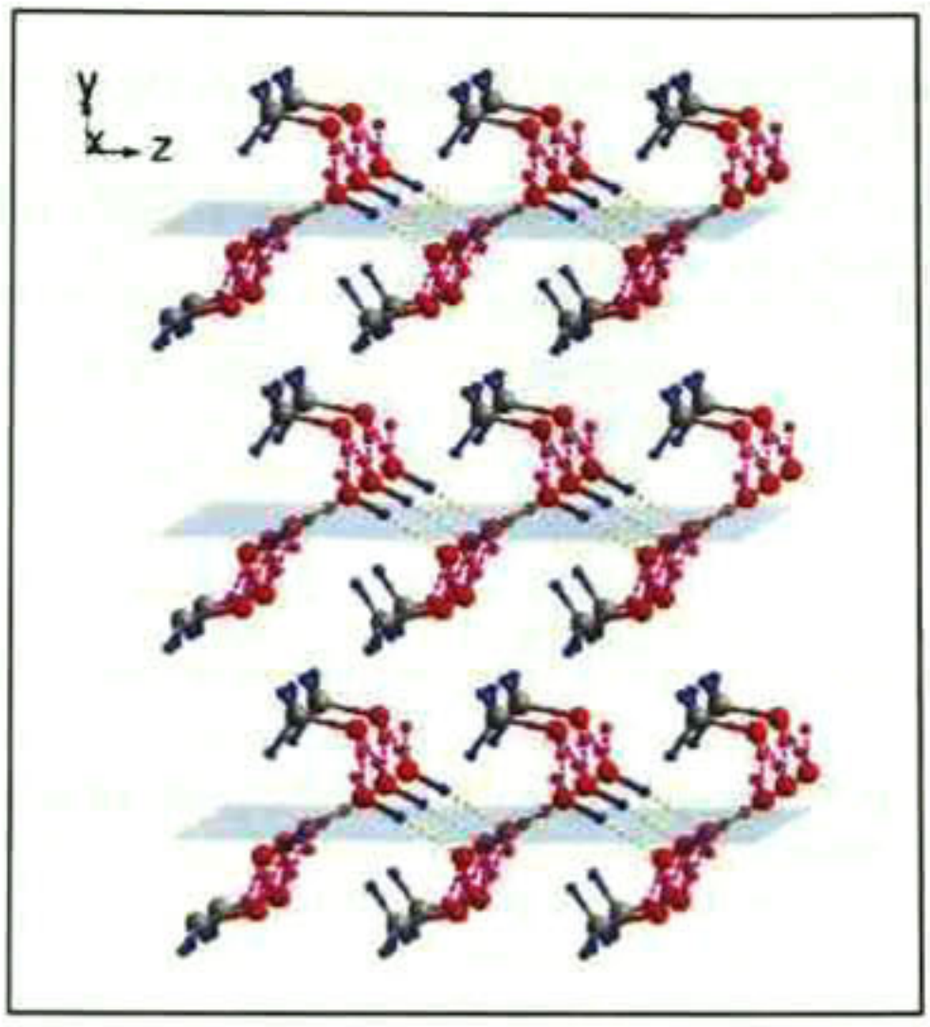

Figure 3.5: Stacking in the y direction of hydrogen bonded layers (of structure 5), showing the ordered hydrogen bonds along the z direction in yellow. The molecules that form the layer are bonded by disordered hydrogen bonds, seen in purple, along the x direction.

Lengths of the ordered hydrogen bonds vary from 1.75 (that correspond to structures of group B) to 1.79 Å (structures 1 and 2), which fall in the common range of a hydrogen bond length, 1.60-1.80 Å[43] (section 2.6.2). For a given structure, all ordered hydrogen bonds have the same length.

The disordered hydrogen bonds of group B have two different lengths, although very close to each other. One of them is ~1.67 Å, for the $\mathbf{HOH}\cdots\mathbf{O}(\mathrm{H})CH_3$ bond, and the other is ~1.71 Å for the $H_2\mathbf{O}\cdots\mathbf{H}OCH_3$ bond. In group A, the distances between the disordered hydrogen atoms and the oxygens are ~1.2 Å, smaller than that of a hydrogen bond, larger than reported covalent O-H bonds (some of them indicated in table 3.5), nevertheless in the van der Waals radio of both atoms (1.52 Å for O and 1.20 Å for H), which means that there is a weak interaction.

The existence of layers with ordered and disordered hydrogen bonds coincides with the description given for the experimental structure.

3.3.1.2 Electronic Density

Figure 3.9 shows one plane of the electronic density of structures 2 and 7, selected because the former belongs to group A and the latter to group B. Figure 3.10 presents different views of the density of structure 7. Both figures correspond to structures optimized at experimental volume, and the density is given

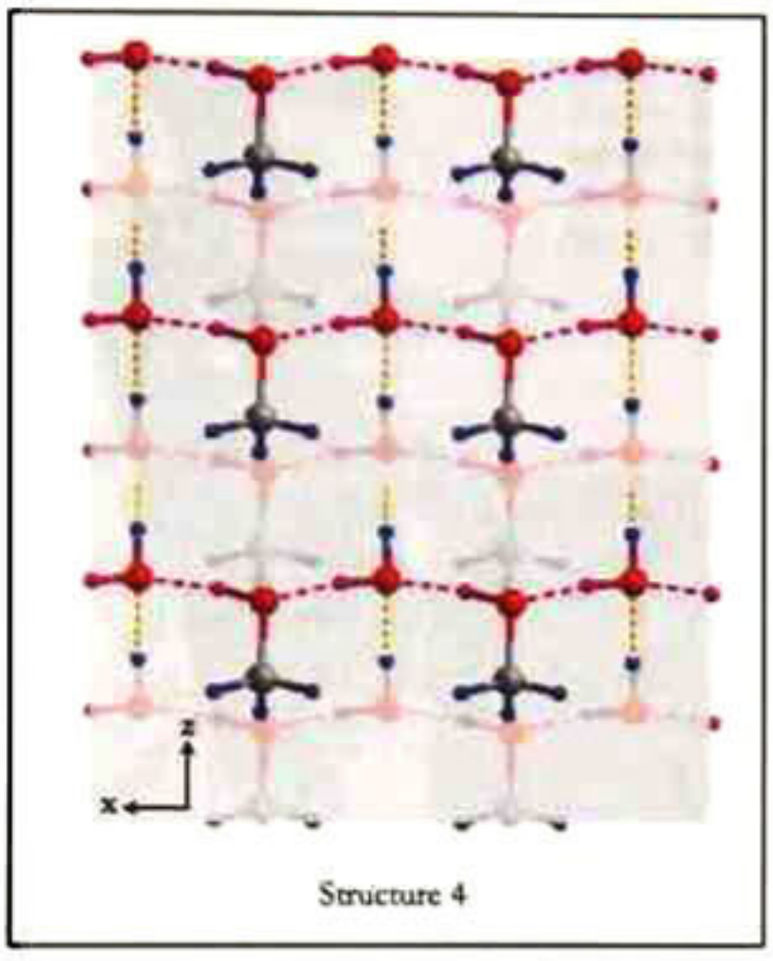

Figure 3.6: View of the xz plane of H bonded sheet of structure 4. The sheets are formed by two layers, which are divided by a gray plane in this picture. The bond between the water-oxygen and the purple proton is always directed to the $+x$ direction, along the water-water chains, in both layers.

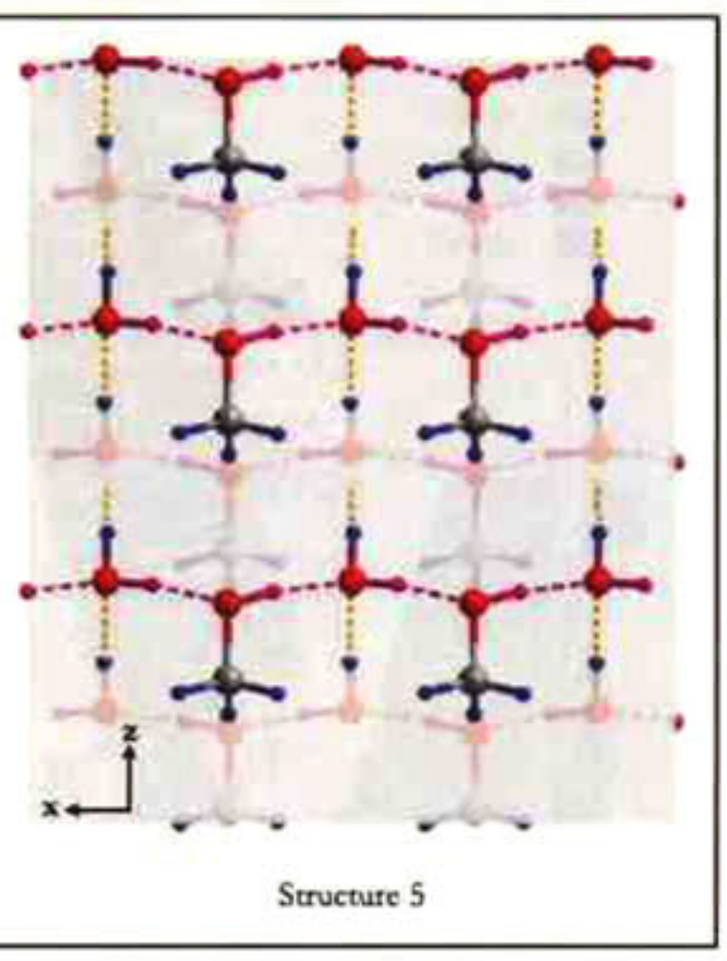

Figure 3.7: View of the xz plane of H bonded sheet of structure 5. The bond between the water-oxygen and the purple proton alternates in the $+x$ and $-x$ directions from one layer to another, along the water-water chains.

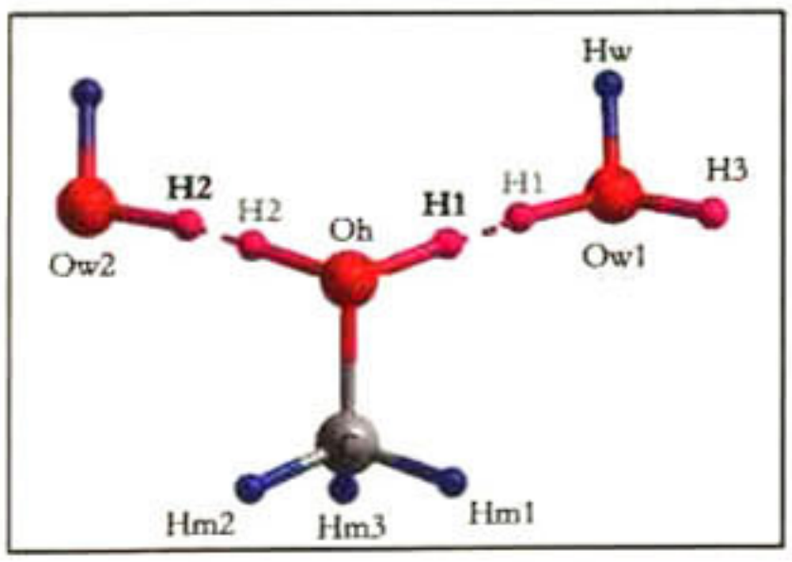

Figure 3.8: Ordered and disordered hydrogen bonds of methanol monohydrate. The disordered protons, H1 and H2, in purple, can occupy any of the two positions shown. One would correspond to the configuration of structure 5, and the other to that of structures 4, 6 and 7. The protons in blue are ordered.

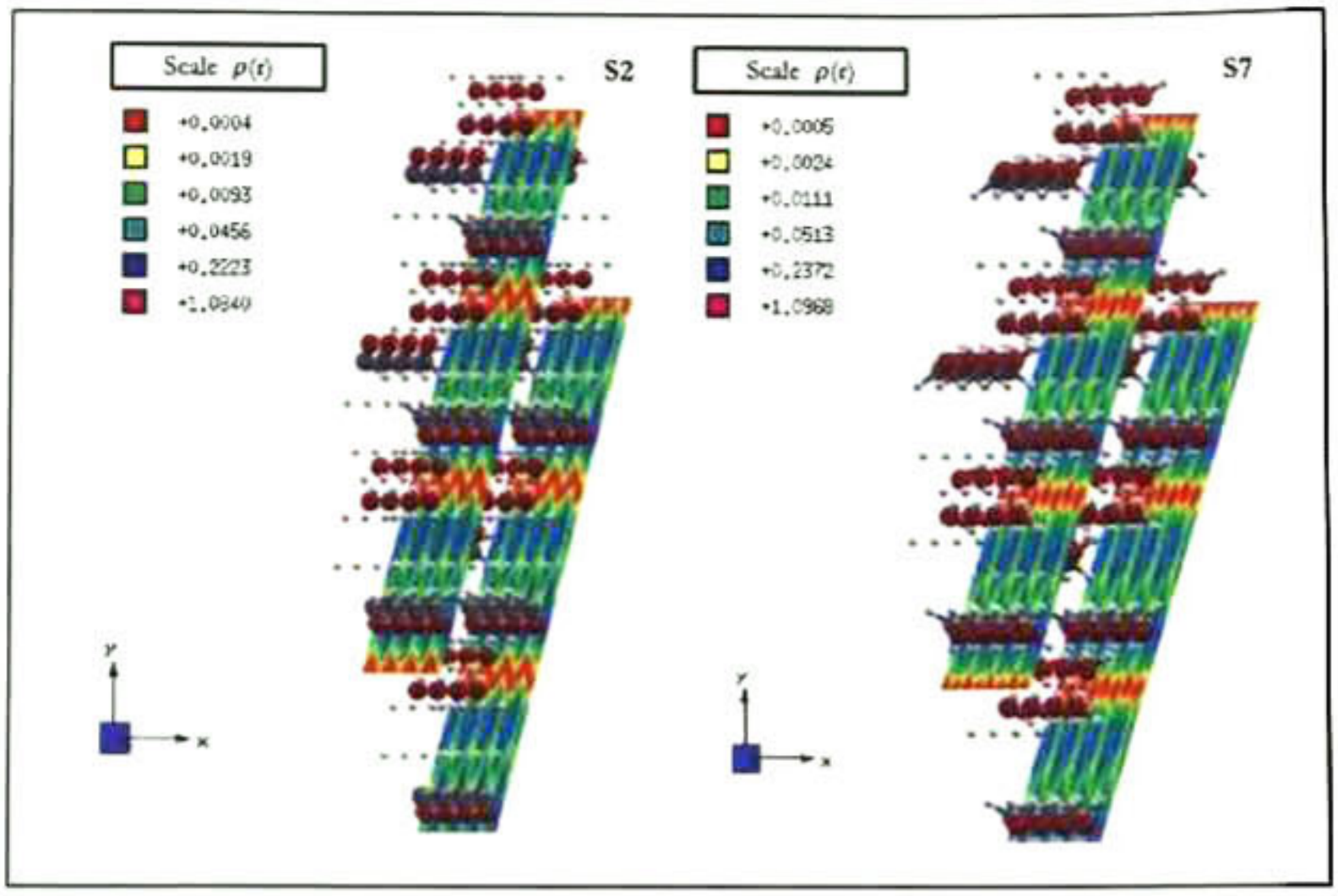

Figure 3.9: Electronic density maps of structures 2 and 7.

in *electrons/Bohr*^{3}[¶]. There are not large differences between the electronic density of structures 2 and 7, only in the water-water interphase, where the spots with lower density (shown in red) are a continuous for structure 2, but delimited by a higher density (yellow) for structure 7.

Analyzing both figures, it can be noticed that the maximum density (violet), 1.0968 electrons/Bohr^3, is located around water oxygen atoms, which is expected because oxygen has the higher atomic number and is the most electronegative atom of all the present atoms (see figure 3.10, picture *d*). In this figure, in pictures *b* and *d*, the electronic density of the methanol-water chains in the x direction can be appreciated (in this direction is where the disorder positions are). In contrast, the density in the water-water chains in the z direction is low, as seen in picture *a* and *c*.

3.3.1.3 Comparison with experimental data

The structures optimized at experimental volume are the ones that can be compared with the experimental structure elucidated in Fortes' study[42]. The percentage differences in cell parameters between the optimized and experimental structures are presented in Table 3.4. It is clear that the parameters of structures of group B are much closer to experimental ones than those of group A. But even the lattice parameter differences for group B, when compared with experiments, are larger than the common error range for DFT mentioned in section 2.1.9. Nevertheless, it is appropriate to notice that experimental data corresponds to a temperature of 160K, ambient conditions of pressure (1 atm

[¶] 1 $electrons/Bohr^3 = 6.7483 electrons/\AA^3$

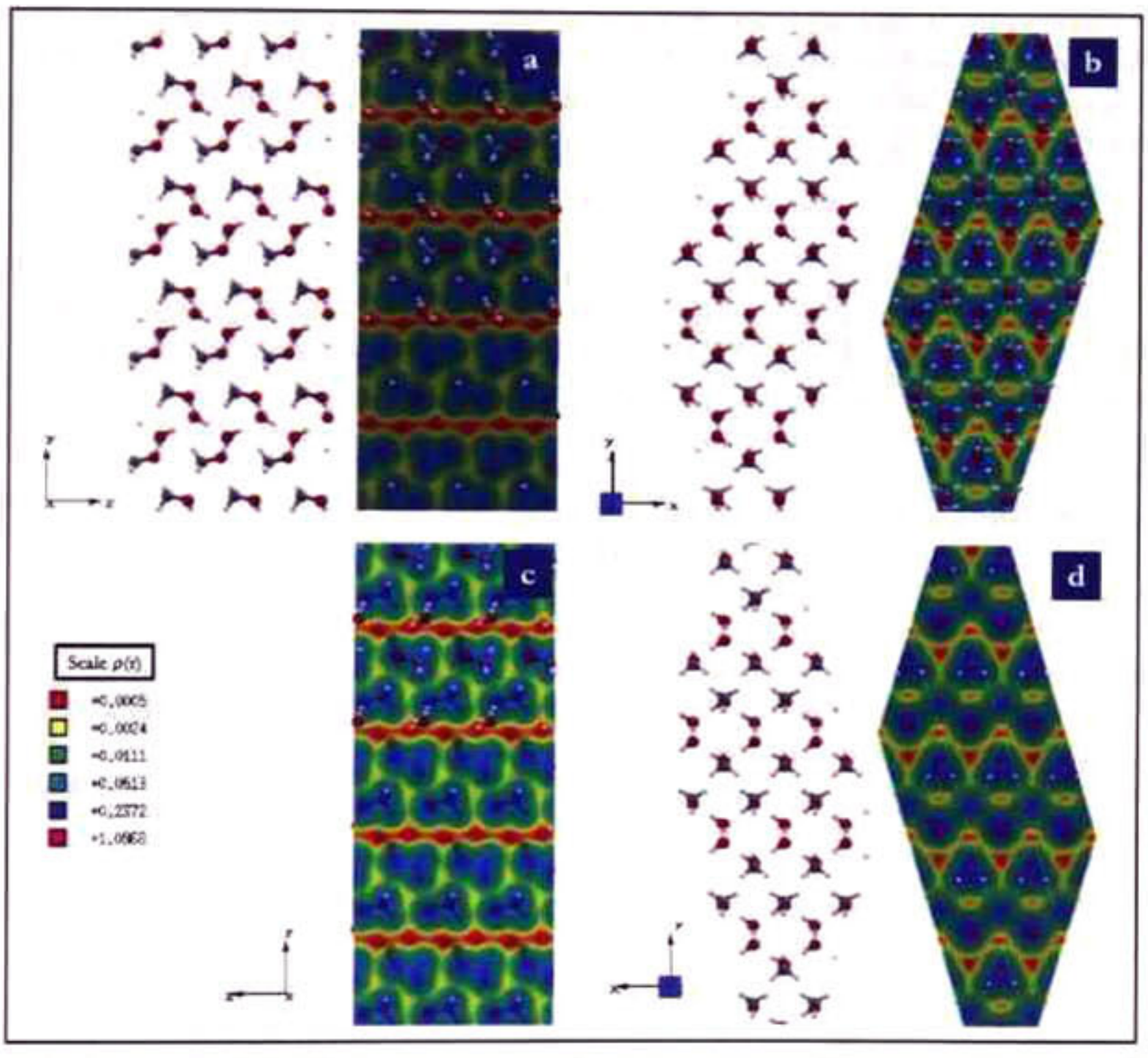

Figure 3.10: Electronic density map of structure 7 along different planes, defined by rotations on y axis, of 0°for a), 90°for b), 180°for c), and 270°for d).

Table 3.4: Percentage differences between calculated and experimental cell parameters

Cell Paramcters	Structure 1	2	3	4	5	6	7
a	-12.6	-12.6	-12.7	-4.5	-4.5	-4.2	-4.5
b	13.2	13.2	14.1	4.6	4.5	4.2	4.6
c	1.1	1.1	0.4	0.1	0.2	0.2	0.1

$\approx 1.013 \times 10^{-4}$GPa) and the deuterated compound; besides, when Van der Waals interactions are present, as for this compound, the error becomes larger. In spite of the facts mentioned, the obtained errors are not far from 3% (for group B).

As seen above in table 3.3, the optimization performed by fixing the volume to the experimental value, did not lead to a pressure of $\sim 1atm$. This situation as well as the differences in cell paramcters, in addition to the reasons presented previously, can be due to the proton disorder. Sugimura et al. discussed that when the proton can occupy two positions it has a larger volume to move in, and therefore the pressure exerted by it in the crystal is reduced[12]. The proton disorder is not implicit in each studied structure, but in the combination of them; then, this reduction in pressure cannot be observed and a higher pressure is obtained for the given volume. With the slight decompression due to proton disorder the atoms can be more separated. Since the disorder is present in the x direction, the calculated a can be smaller than the actual a, which is seen in the negative differences of table 3.4. The shrinkage of the layers augments the electronic density of them, conducting to a larger electronic repulsion between the layers, and therefore, to larger b parameters.

Some specific distances and angles found in theory and experiment for methanol monohydrate, methanol(molecule), α-methanol (solid), ice Ih, water dimers and water-methanol complex are presented in table 3.5 using the nomenclature given in figures 2.2 (label notation used by Fortes in reference [42]), 3.11 and 3.12. These last two figures show the atom labels used in this work. Some of the reported compounds possess deuterium instead of hydrogen atoms, as specified in the table. The last two columns are the results obtained for structures 1 and 7. Their distances and angles are in general very similar to the ones of the other structures of their groups, A and B, respectively.

The covalent C-H bond is the least affected by the chemical environment of each compound, since the C-H distances do not vary much even for the different considered compounds, it is ~ 1.09 for all of them, except the one for methanol monohydrate, which is clearly smaller than the rest. The calculated distances agree well with the most common values.

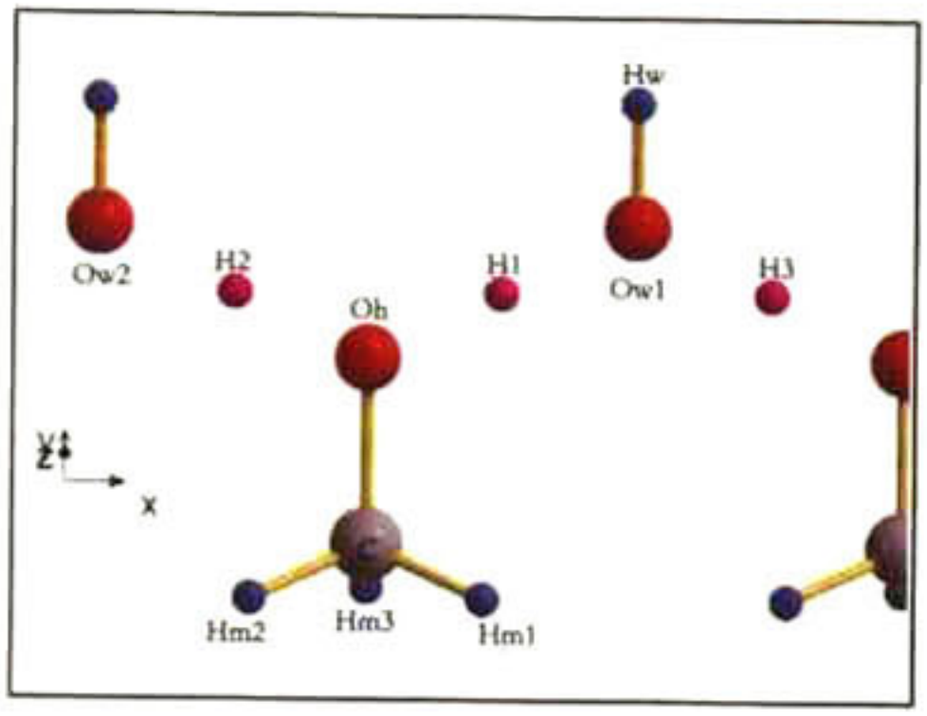

Figure 3.11: Atom labels convention used in the present work. Here H1 and H2 are equidistantly located from Oh, but this changes for the different structures.

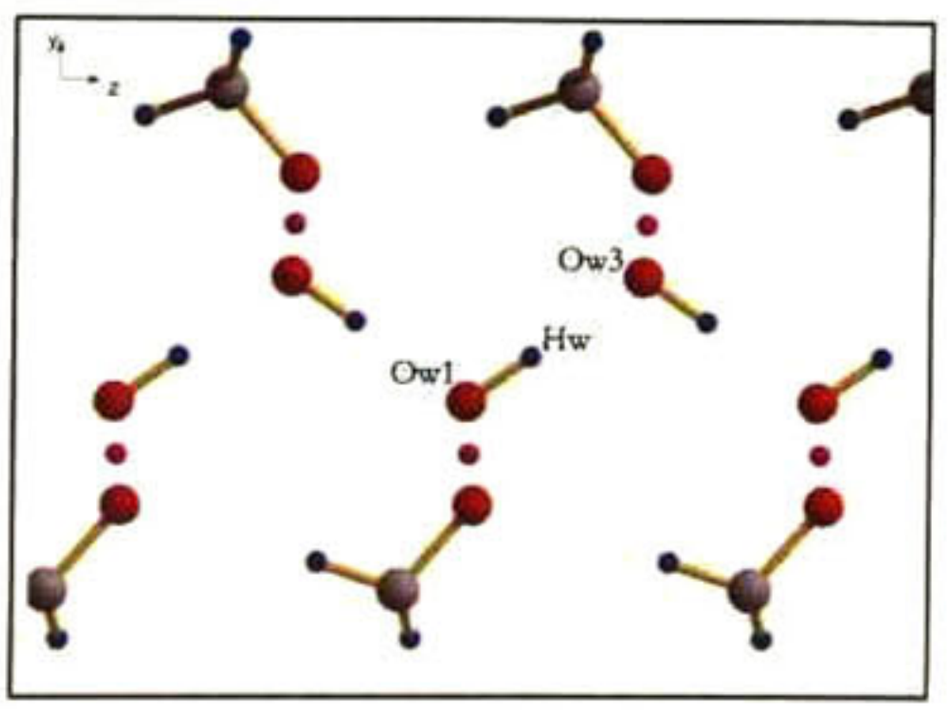

Figure 3.12: Atom labels convention used in the present work, where *Ow1* and *Ow3* belong to two different water molecules that form a hydrogen bond with *Hw*.

Table 3.5: Interatomic distances and angles for related compounds

	Interatomic distances d(Å) and angles $\angle$(deg)							
	$CD_3OD \cdot D_2O$ exp.[b]	CH_3OH exp.[o]	CD_3OD exp.[p]	Ice Ih	H_2O dimers exp.[t]	H_2O - CH_3OH complex, theor.[u]	Structure 1 at exp. vol.	Structure 7 at exp vol.
d_{C-H}	1.059(4)[c]	1.0936(32)	1.091(7)	-	-	1.090	1.0953[c]	1.0951[c]
	1.059(3)[d]	-	1.084(5)	-	-	1.085	1.0932[x]	1.0944[x]
	-	-	1.068(7)	-	-	-	1.0932[y]	1.0911[y]
d_{O-H}	0.906(5)[e]	0.9451(34)	0.959(6)	0.983-1.002[q]	0.9573	0.962[e]	1.1933[z]	0.9917[z]
	-	-	-	-	-	-	1.1933[aa]	1.6661[aa]
	0.955(5)[f]	-	-	-	-	0.971[f]	1.2342[ab]	1.7098[ab]
	-	-	-	-	-	-	1.2342[ac]	0.9998 [ac]
	0.966(4)[g]	-	-	-	-	0.960[g]	0.9889[g]	0.9900[g]
d_{C-O}	1.405(4)	1.4246(24)	1.410(4)	-	-	1.431	1.4275	1.4318
d_{O-O} [a]	2.743(5)[h]	-	-	2.745(6)[r,s]	2.976(-30)	2.840	2.7805[h]	2.7383[h]
	2.733(3)[i]	-	-	2.767(2)[r,s]	-	2.997[v]	2.4273[i]	2.6983[i]
$\angle_{H-C-H}$	111.35(15)[j]	108.63(70)	108.7(7)	-	-	-	107.72[j]	108.35[j]
	104.68(14)[k]	-	108.3(4)	-	-	-	108.77[k]	109.21[k]
$\angle_{C-O-H}$	-	108.53(48)	106.5(5)	-	-	108.3	110.18[ad]	107.42[ad]
	-	-	-	-	-	-	110.18[ae]	109.51[ae]
$\angle_{H-O-H}$	121.5(4)[l]	-	-	107.0(7)[r]	104.56	104.6[n]	113.25[l]	111.64[l]
	107.8(4)[m]	-	-	-	-	-	114.04[m]	112.32[m]
	109.1(2)[n]	-	-	-	-	-	107.78[af]	112.43[af]
	-	-	-	-	-	-	107.78[ag]	106.91[ag]
$\angle_{O-H-O}$	-	-	-	-	-	166.1[w]	178.40[w]	174.21[w]
	-	-	-	-	-	179(1)[w,v]		

[a] Oxygen atoms that form a hydrogen bond. [b] From ref. [42] at atmospheric pressure and 163 K

See fig. 2.2/3.11 or 3.12 [c] C-Dm2/C-Hm3. [d] C-Dm1/C-Hm1 or H2, [e] Oh-Dh/Oh-H1 or H2, [f] Ow-Dw1/Ow1-H1 or H3, [g] Ow-Dw2/Ow1-Hw, [h] Ow-Ow/Ow1-Ow3, [i] Oh-Ow/Oh-Ow1, [j] Dm1-C-Dm1/Hm1-C-Hm2, [k] Dm1-C-Dm2/Hm1-C-Hm3, [l] Dh-Oh-Dh/H1-Oh-H2, [m] Dw1-Ow-Dw1/H1-Ow1-H3, [n] Dw1-Ow-Dw2/Hw-Ow1-H1 or H3.

[o] From ref. [46] at atmospheric pressure and room temperature. [p] α-phase of solid deuterated methanol, from ref [47] experimental data at 160 K.

[q] Normal form of ice, from ref [48], from several spectroscopic studies. [r] D_2O ice Ih, from ref. [49], at atmospheric pressure an 20 K, average value of Monte Carlo modelling.

[s] Bonds in different directions in the same system. [t] From ref. [50], partially deuterated water dimers studied by molecular beam electric resonance spectroscopy

[u] From ref. [51], by quantum mechanical studies. [v] From reference [52], experimental data.

See fig. 3.11: [w] Oh-H1-Ow1, [x] C-Hm1, [y] C-Hm2, [z] Oh-H1, [aa] Oh-H2, [ab] Ow1-H1, [ac] Ow2-H2, [ad] C-Oh-H1, [ae] C-Oh-H2, [af] Hw-Ow1-H1, [ag] Hw-Ow1-H13

For the O-H bonds, the distances obtained for structure 7 are closer to the reported data than those of structure 1. It can be seen that structure 7 has one covalent O-H bond with one of the hydrogen atoms and, one hydrogen bond with the other, H1 or H2. That does not happen for structure 1, where both distances are the same. These bonds are formed by the originally disordered hydrogen atoms, and the calculated distances are larger than the reported ones (except for ice Ih). The difference is smaller for the ordered O-H bonds of the water molecules (g). For such bonds and the C-H ones, the distances obtained for the two groups of structures resemble. They are both covalent and not much affected by the disordered proton position.

The reported distances for the C-O bond are diverse, so it can be said that they are more affected, than other bonds, by the chemical environment of the molecules in which they are. The calculated distances are closer to the ones of liquid methanol (o) and the H_2O - CH_3OH complex (u), and, again, larger than methanol monohydrate.

The distance between two oxygen atoms, in which one of them is a proton donor and the other an acceptor, to form a hydrogen bond, is commonly reported in studies of such bonds and the *symmetrization* of the bond. The one in the yz plane (h) is larger than that of the xy plane (i), which coincides with the methanol monohydrate distances, but the differences between the two calculated ones is larger, especially for structure 1.

The calculated C-H-C angles are similar to those of liquid and solid methanol, but conspicuously different from the ones of Forte's study. The C-O-H angles are also similar to the reported ones.

For the H-O-H angle involving the oxygen of the methanol part and two originally disordered hydrogen atoms(l) (see figure 3.11), the differences between the calculated ones and the methanol monohydrate's are large. The optimized structures angles are smaller. As the differences in interatomic distances are not so large, it can be said that the optimized structures are more compact and that the mentioned layers shrinkage is carried out by the reduction of this angle, leading to a smaller a cell parameter and to a mayor space between layers. For the same angle, but with the oxygen of the water in the middle (m), the calculated angles are now more open, but the difference is not as large as in the previously mentioned bond. The other H-O-H bond (n, af, ag) is formed by an ordered hydrogen atom of the water molecule, and a disorder one. The calculations are close to the angle of ice Ih and a bit smaller than Forte's, except for one of the bonds in structure 7, which shows that it only forms one O-H covalent water like bond with one of the hydrogen atoms, in this case H3.

For the O-H-O bond there is a big difference in the reported angles in the water-methanol complex, the theoretical (166°) being much smaller than the experimental (179°). The calculations of this work resemble more to the experimental value.

In general, the differences are within or not considerably larger than the DFT common errors.

3.3.2 Behavior under pressure

3.3.2.1 Energy and Enthalpy

The total energy per unit cell versus volume of unit cell plot is presented in figure 3.13. Again, in terms of energy, structures are separated into two groups, as seen in the optimization at experimental volume. The difference is more noticeable at larger volumes that correspond to lower pressures. In this and next graphs, lines are not a fitting, they are only drawn to guide the eye.

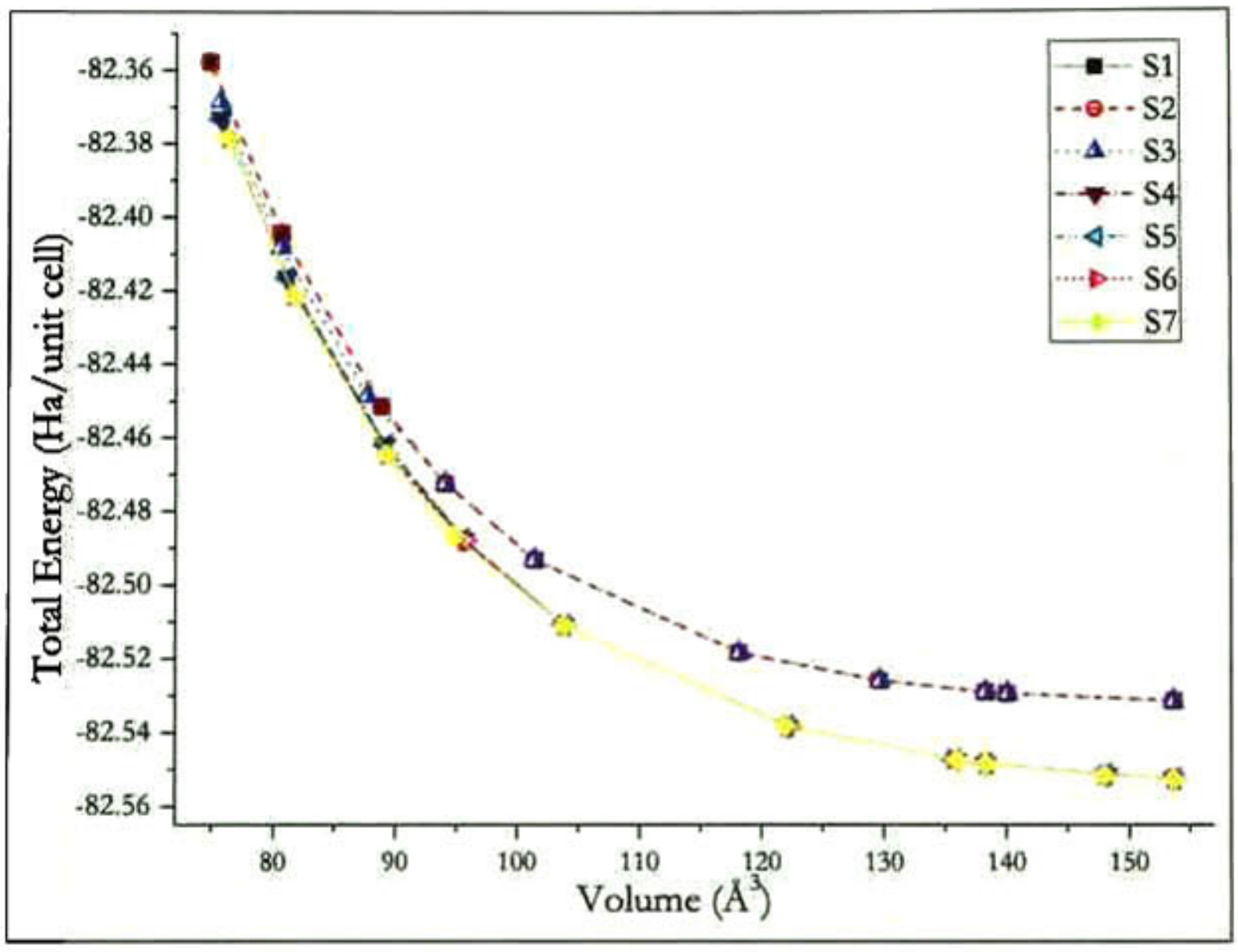

Figure 3.13: Total Energy vs. Volume, where two groups of structures are observed, which have very small energy differences among them. S stands for structure. The group with higher energy, A, is formed by structures 1, 2 and 3, and the one with lower energy, B, is formed by structures 4 to 7.

The structure with the lowest energy is not the same for all pressures. It varies among structures 4, 6 and 7, though structure 5 is very close up to 15 GPa. For low pressures, up to 10 GPa, the four of them have energy differences so small that are within the error of the calculations. At 15 GPa, structure 7 is less energetically stable than the other three, with an energy difference of $\sim$ 0.001 Ha/unit cell (0.34 kcal/mol). From 20 to 40 GPa, structures 6 and 7 have the lowest energies, with a difference of 0.005 GPa at 40 GPa with respect to structures 4 and 5, and of $\sim$ 0.01 Ha/unit cell with respect to structure 3. At low pressures, up to 4 GPa, the energy difference between group A and B is of $\sim$ 0.02 Ha/unit cell (6.3 kcal/mol).

For comparison, the energy barrier between eclipsed and staggered confor-

mations of ethanol is of 3 kcal/mol, and is reached at ambient conditions, so the carbon-carbon bond can freely rotate. Then, it is likely that structures from group B can go from one to another at ambient conditions[53].

The enthalpy of each structure was calculated according to equation 2.13. Structure 7 was taken as a reference, so the difference between the enthalpy of each structure and structure 7 is shown in figure 3.14. Again, the two groups of structures are distinguished and the difference in their enthalpies becomes smaller as pressure increases, indicating the possibility of the inversion in stabilities at higher pressures. Such inversion is expected, that is, the symmetrization of the hydrogen bond, as it happens at high pressures for water or methane hydrate (section 2.5). But to prove it, more calculations are necessary, including different crystalline systems to find the more stable structure at such pressures. This is because the structures considered in this work derivate from a geometry found at low pressures and might not prevail at very high pressures. In spite of this, an approximation of the symmetrization pressure is done in section 3.3.2.3. The smallest enthalpy difference between groups A and B is at 40 GPa between structures 3 and 7, where it is of 0.00357 Ha/unit cell (that is 0.0971 eV/unit cell = 4.6867 kJ/mol = 1.1201 kcal/mol).

The structures' enthalpies are very close. At low pressure, up to 10 GPa, all structures of group B could exist. Because of their similar enthalpies, they might go easily from one configuration to another. Although the difference in energy with group A could be considered an energy barrier(symmetrization of proton), proton tunneling could exist. This energy barrier diminishes when increasing the pressure, as seen in the shortening of the enthalpy differences between group A and B, which favors the disorder of protons.

In terms of enthalpy, when the pressure increases, going from 15 to 20 GPa, structure 3 separates from the rest of structures of group A, and structure 6 from group B. Structure 7 separates before, between 10 and 15 GPa, all of them becoming more energetically stable with such separation. As seen below, this occurs with a marked distortion of the systems.

3.3.2.2 Compression

The variation of cell parameters with pressure is presented in figure 3.15, where it can be observed that the changes in a and c were small, and the one of b is much larger.

The compressibility of structures 1 to 7 is shown in figure 3.16, i.e. d/d_0 vs. P, where the data considered as initial, for example V_o, is the one used for or obtained from the optimization at experimental volume. For the volume, the slope is larger at the beginning of the compression, i.e. at low pressures. The solid reduces its volume up to 50% at 40 GPa, and such change is mainly due to the reduction of cell parameter b. For the first group of structures, a remains almost constant, while for the second group it reduces a little. c reduces in a similar amount for all structures. Such compressibility data can be compared with experimental one, when available.

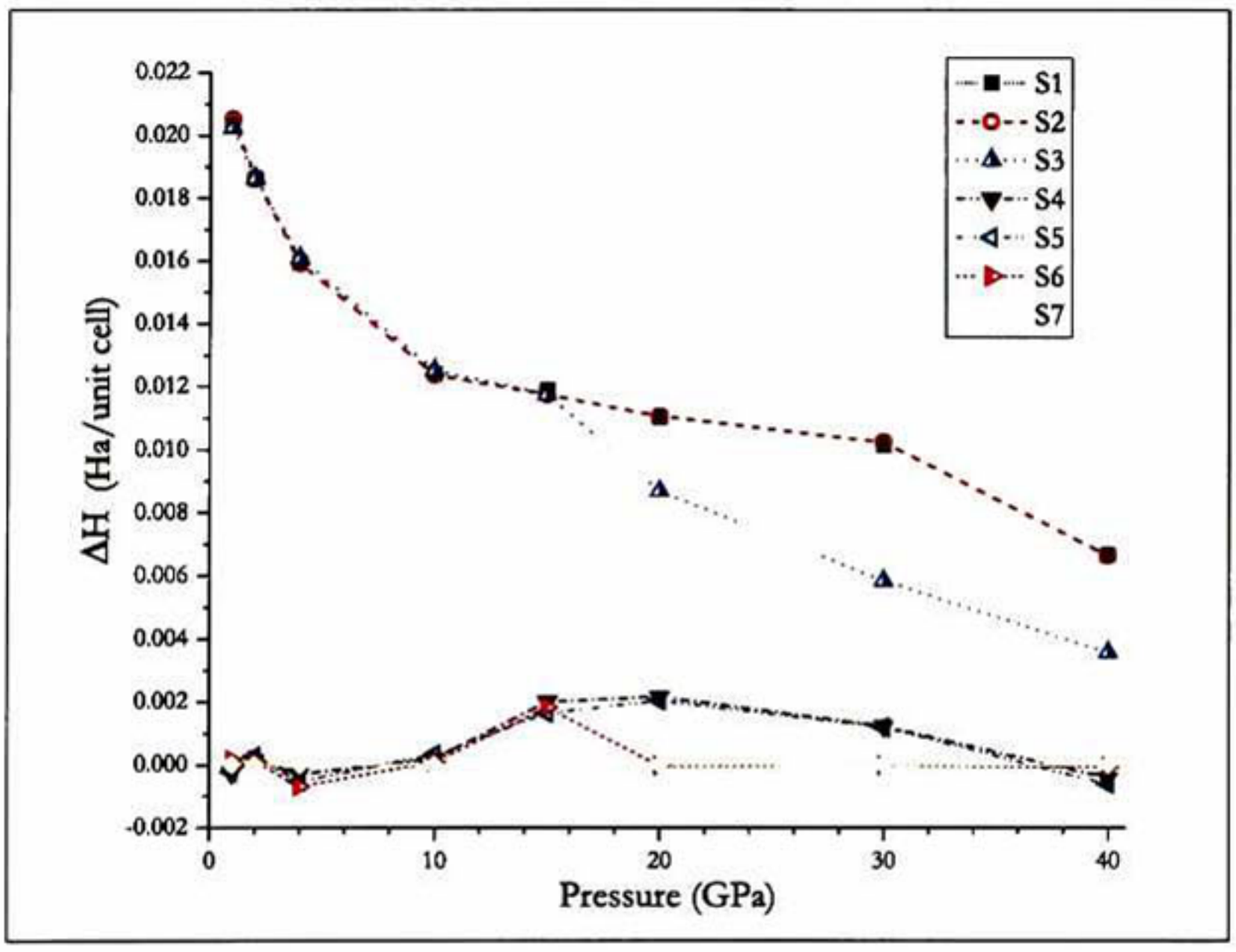

Figure 3.14: Enthalpy vs. Pressure. Structure 7 was taken as a reference, so ΔH is H of each structure minus H of structure 7. The enthalpy difference between structures of group A and B shortens with pressure, so an inversion of stabilities is expected at higher pressures. This means that the structures tend towards the symmetrization of the H bond.

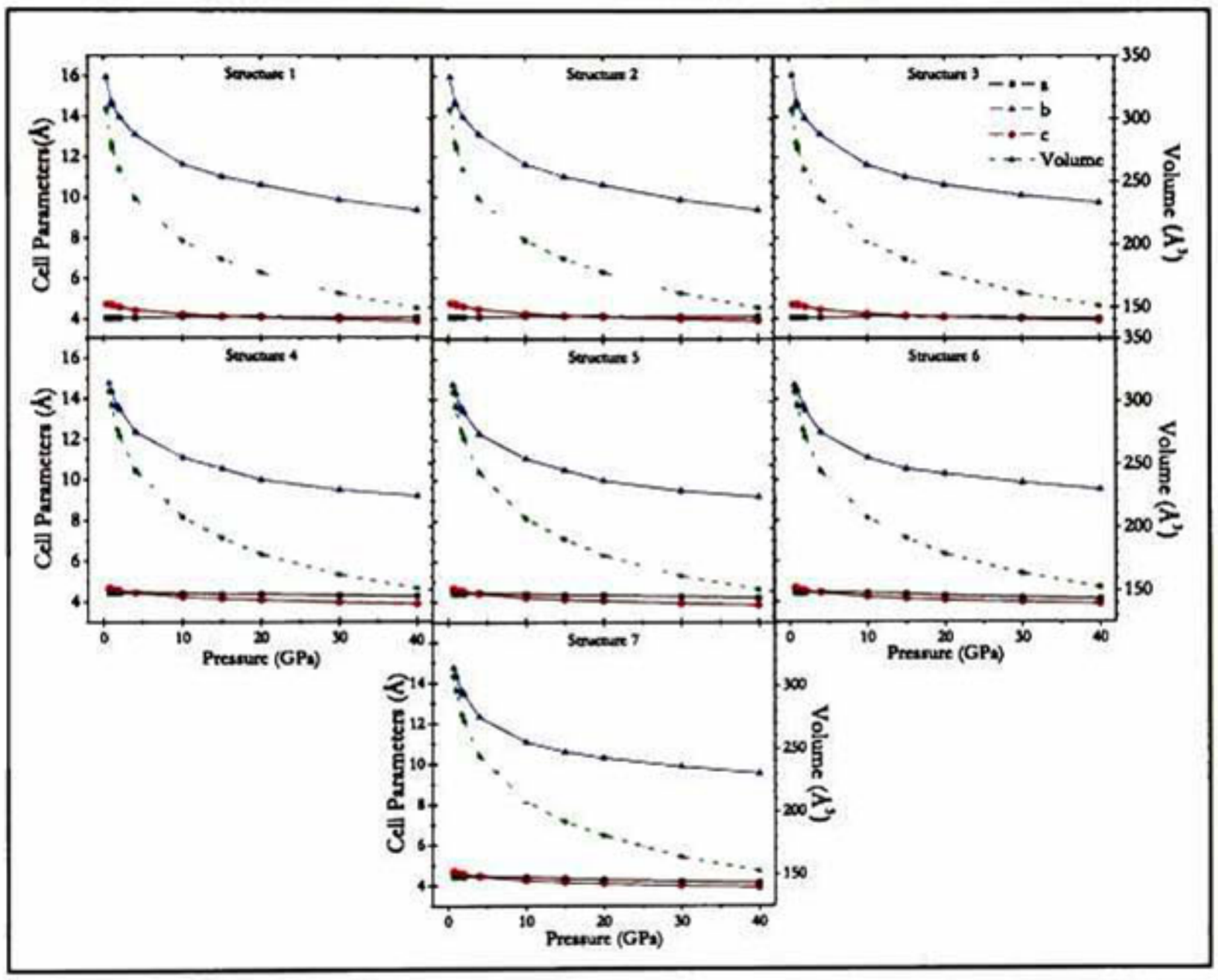

Figure 3.15: Cell parameters variation with pressure of each structure. The variations were very similar for all structures, being b the parameter that compressed the most.

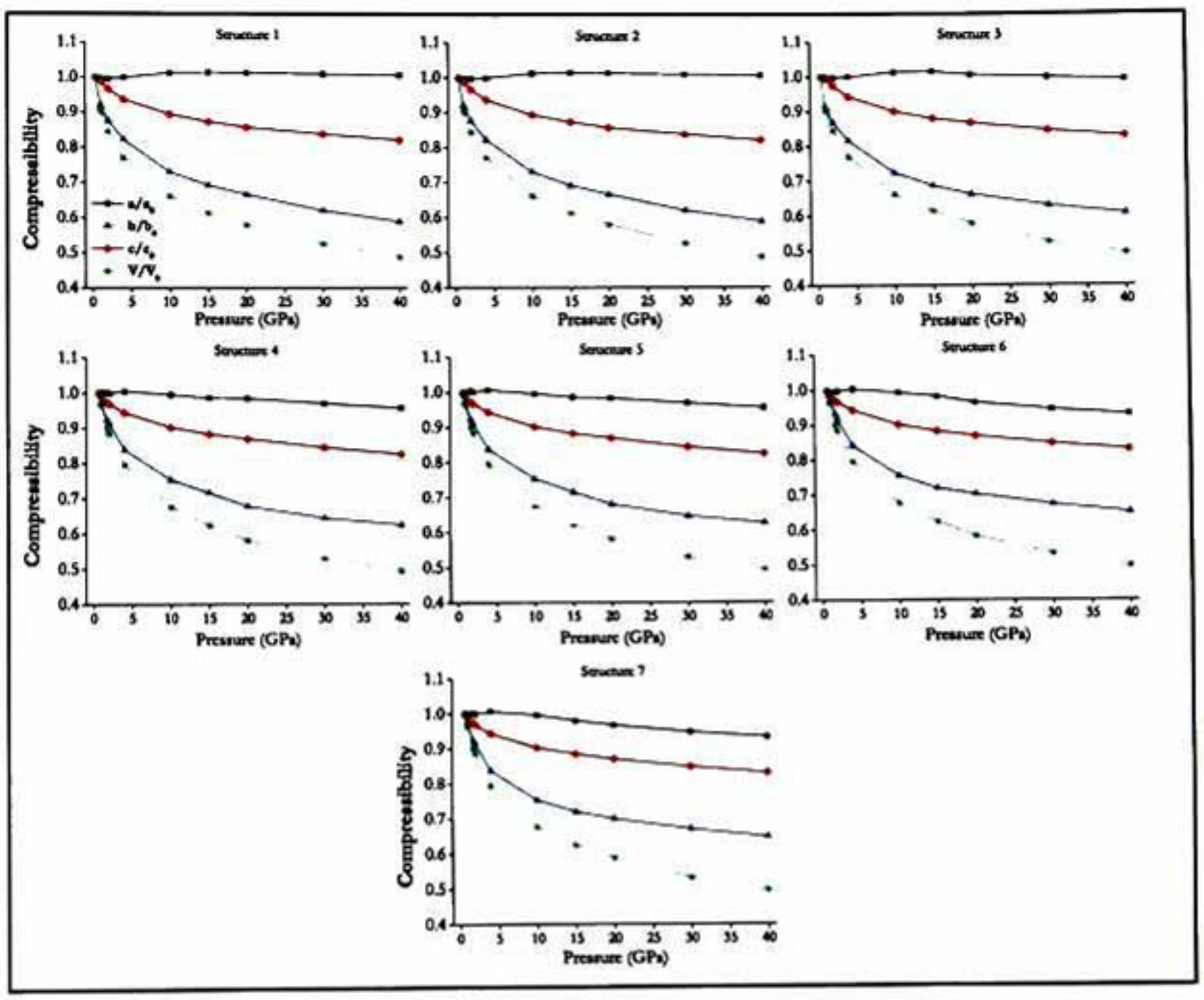

Figure 3.16: Compressibility of each structure, where the reference values d_0 correspond to those of the optimization at experimental volume. The variation was very similar for all structures.

Figure 3.17 is a view of the evolution of the conventional cell of structure 7 under pressure. The more noticeable change is the distortion it undergoes when going from 10 to 15 GPa. This can also be seen in figure 3.18, which shows the distortion of α, β and γ with respect to a right angle. Structures 1 and 2 have all their angles equal to 90°so they are not plotted. The distortion of the cell is given by a large change of α at the mentioned pressures. This also happens for structures 3 and 6, but when going from 15 to 20 GPa. As observed above, this distortion energetically stabilizes the structure (fig. 3.14. The β angles of structures 4, 6 and 7 also suffer changes, but not so marked. γ remains nearly constant, except for structure 5, for which it varies slightly.

If experimental studies were done, monitoring the changes of angles of the cell with pressure, could give a clear idea of the existence or not of a predominant structure, noting if a marked distortion of the network does or does not occur, and at what pressure is given.

The mechanism of compression of the structures can be analyzed from figure 3.17. The layers of molecules get closer in the y direction and also the atoms that form the layers approach. The O-H part of the water molecule with the ordered

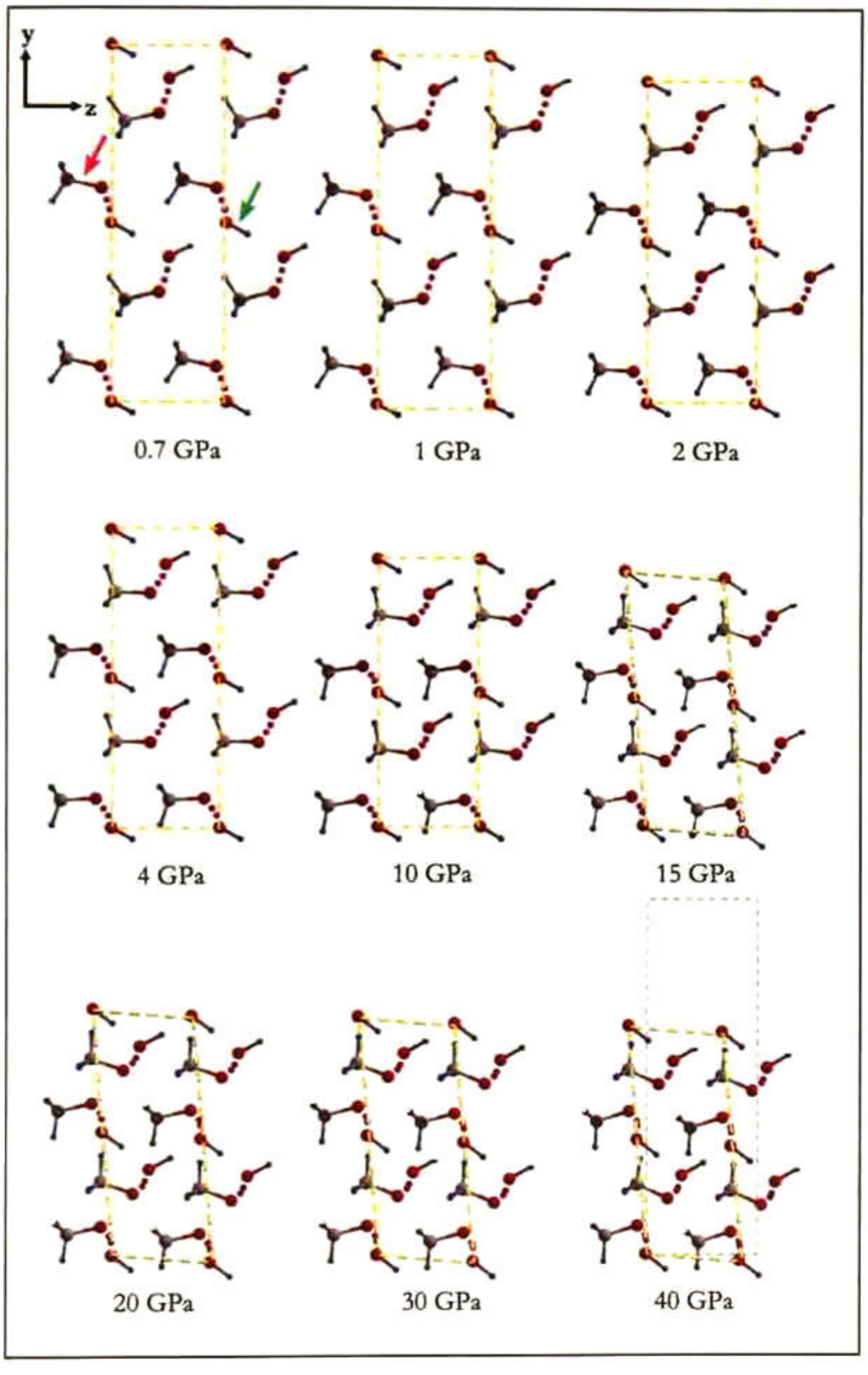

Figure 3.17: Evolution of structure 7 with pressure. The dashed gray rectangle at 40 GPa indicates the size at 0.7 GPa, pressure corresponding to the experimental volume.

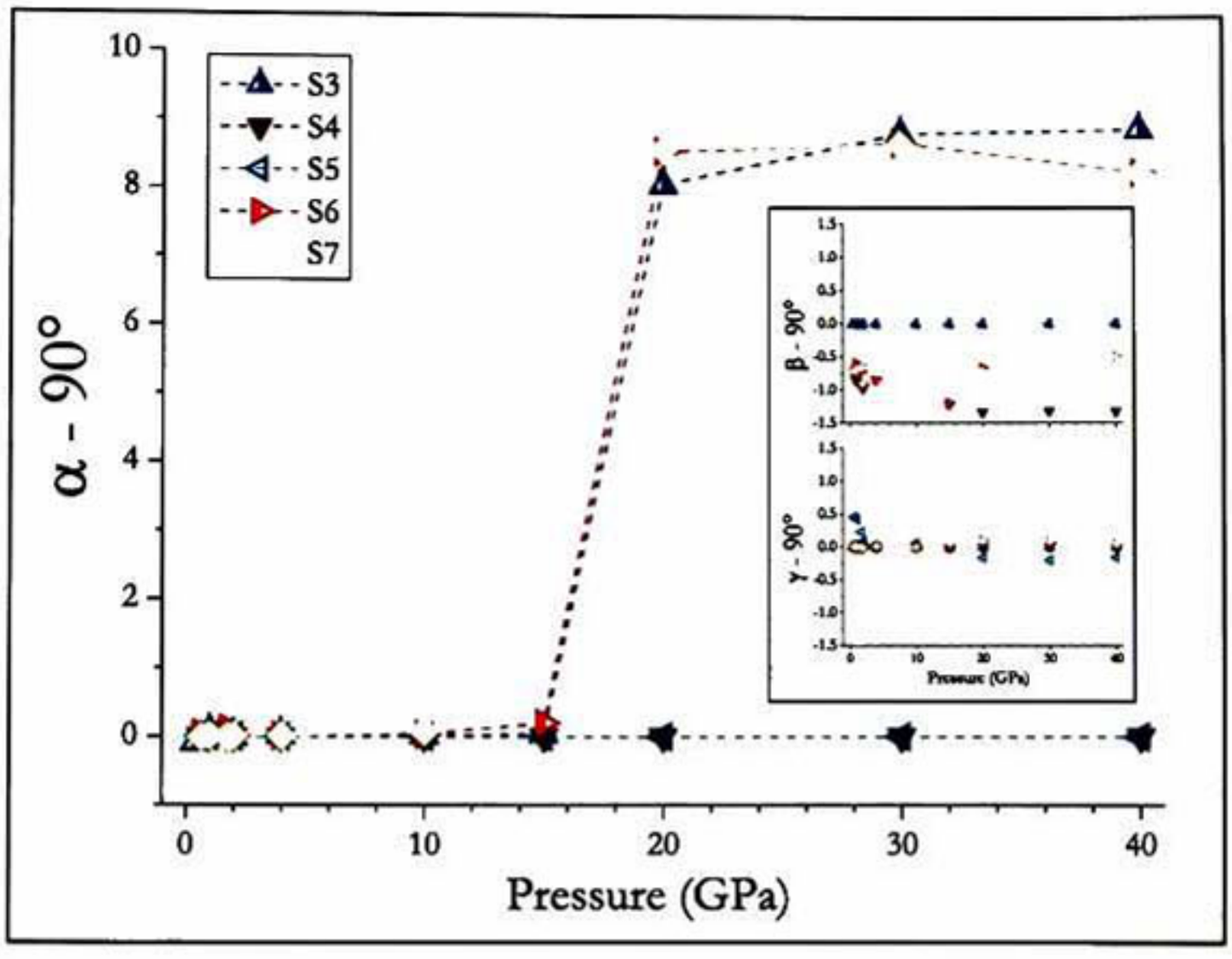

Figure 3.18: Distortion of α, β and γ with pressure of structures 3 to 7.

proton remains practically unchanged (pointed with a green arrow), except for the approach in the y direction. In contrast with the water part, the methanol molecules change their orientation constantly as pressure increases. This can be observed by following the orientation of the C-O bond (pointed with a pink arrow) with respect to the z axis. In the superior part of the layer(see the pink arrow), the carbon with its hydrogen atoms goes down with respect to the oxygen, it is almost parallel to the axis at 4 GPa, and keeps going downward. The carbon of the inferior layer does the opposite, the C atom goes upward. They are aligned at 4 GPa. The disordered protons seem to approach one to the other with pressure augmentation, but they are not in the same plane. This only shows they become more symmetric, like the protons in structure 1 which appear to be only one because there is one just behind the other, as viewed in figure 3.19. The mechanism of compression seems to be the same for structure 1.

The change of some specific interatomic distances with pressure is presented in the following figures. Figure 3.20 presents the relative change of some distances of structures 3 and 7. For structure 3, all the plotted distances become a little smaller with P increase, except for Ow1-Hw which becomes larger. A change in slope is observed between 15 and 20 GPa for some O-H distances, which will be analyzed below.

Interatomic distances of structure 7 have a very similar variation to that of structure 3, except for the Oh-H2 and Ow1-H1, which noticeably become smaller. These are the hydrogen bonds of structure 7, they can be easily reduced in comparison with the covalent ones, and therefore the mechanism of compression depends on their distance reduction.

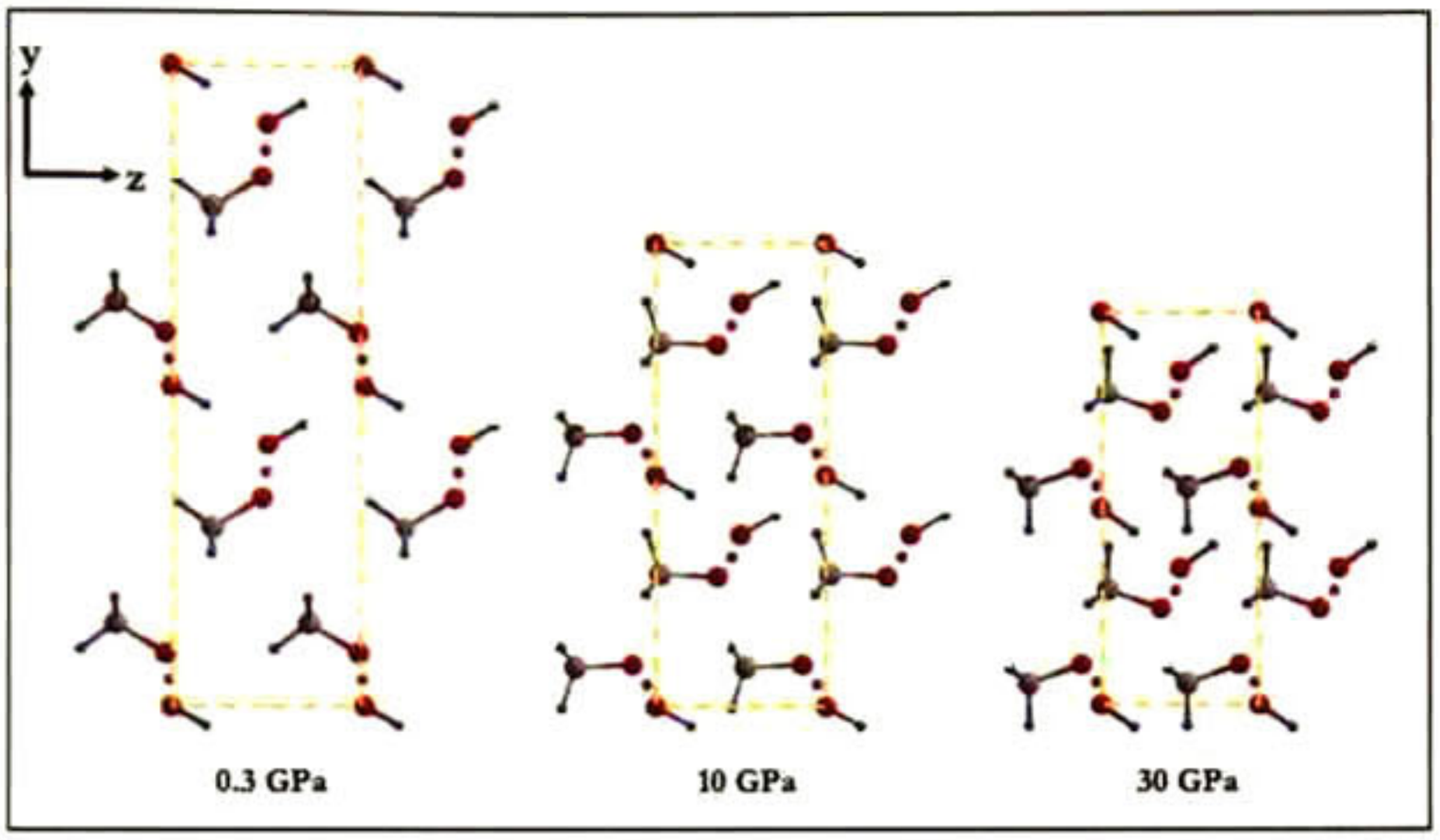

Figure 3.19: Evolution of structure 1 with pressure.

The compression of covalent C-H and C-O bonds is small, regular and similar for both structures, so only the other distances are analyzed more carefully and for all structures in figure 3.21.

The Oh-H1 and Oh-H2 are clearly different for group A and group B of structures. In group A, they have very similar values, $\sim 1.20\mathring{A}$ and do not vary much with P increase; though those of structure 3 separate slightly after 15 GPa. The behavior is comparable with Oh-H1 for group B, here the distance of structures 4 and 5 separates from 6 and 7, also at 15 GPa. For the Oh-H2 of group B the situation is different, the bond is very compressible and the group is divided in two after 15 GPa. This hydrogen bond of structures 6 and 7 -the more distorted structures- is capable of continuing reducing greatly, and not so much for structures 4 and 5. Ow1-H1, being the other hydrogen bond of structures of group B, has a very akin behavior. And the Ow2-H2, being the covalent O-H bond of water for group B, has an alike behavior to the Oh-H1, covalent methanol bond in group B. Ow1-Hw is the only bond that enlarges, and this happens for all structures.

The distances and angles of structure 5, in figure 3.21, correspond to the inferior part of the layers, in which the relative position of the proton was the same that for the rest of group B at experimental volume. Having this in mind and that the enthalpies of the structures of group B are close to each other, and according to the discussion of the previous paragraph, the originally disordered proton has more possible positions after 15 GPa, leading to a more disordered crystal.

The modification of some internal angles for structures 3 and 7 is presented in figure 3.22. It can be seen that the Oh-H1-Ow1 angle closes at the beginning

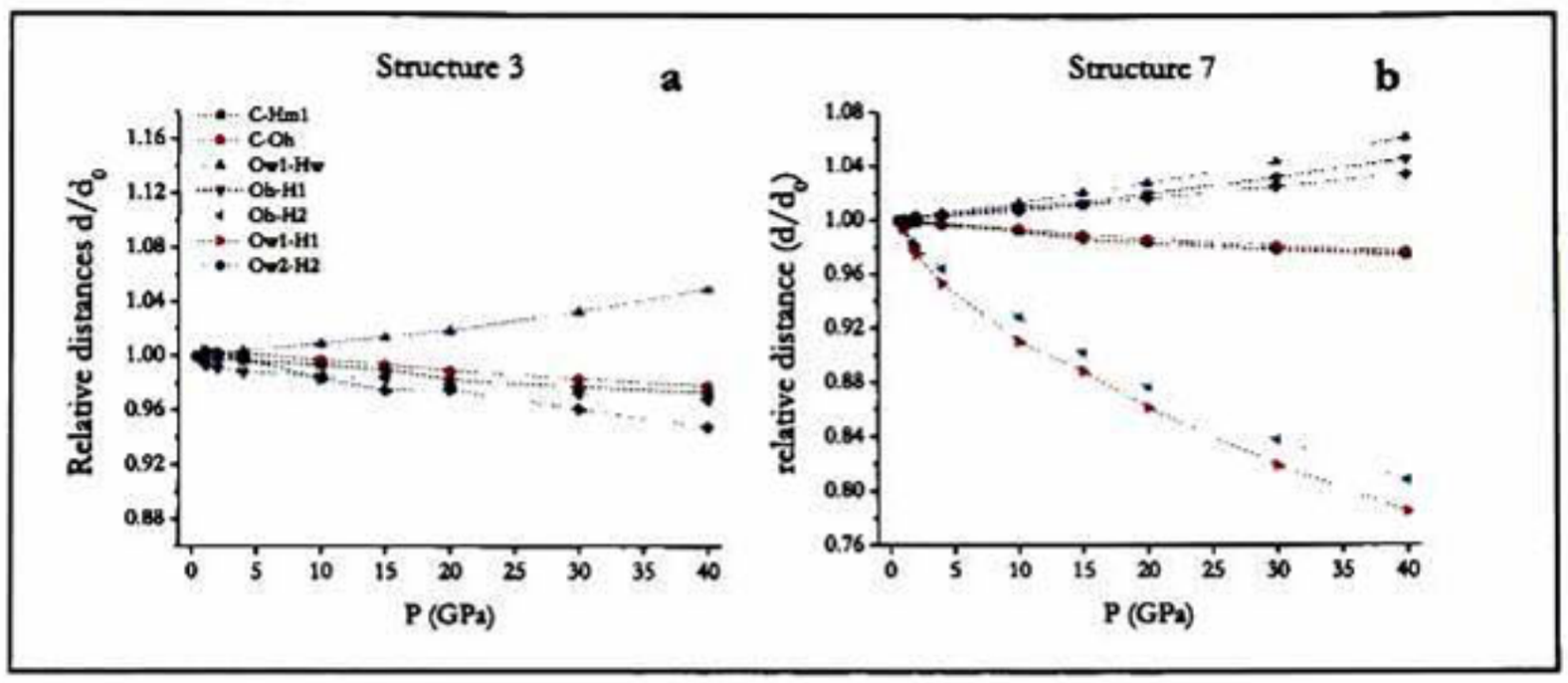

Figure 3.20: Some relative interatomic distances change as a function of pressure for a) structure 3 and b) structure 7.

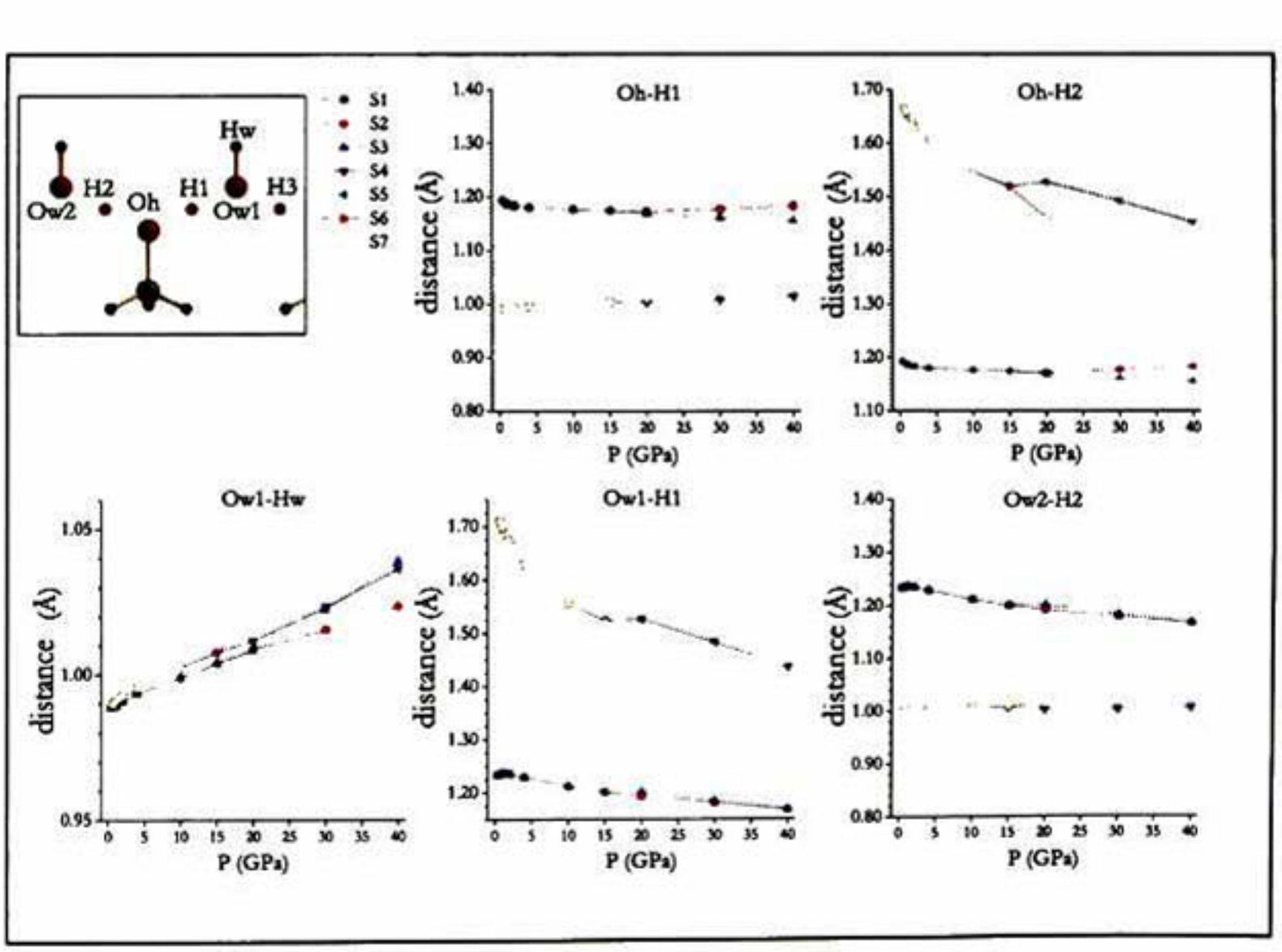

Figure 3.21: Some interatomic distances change as a function of pressure for all structures.

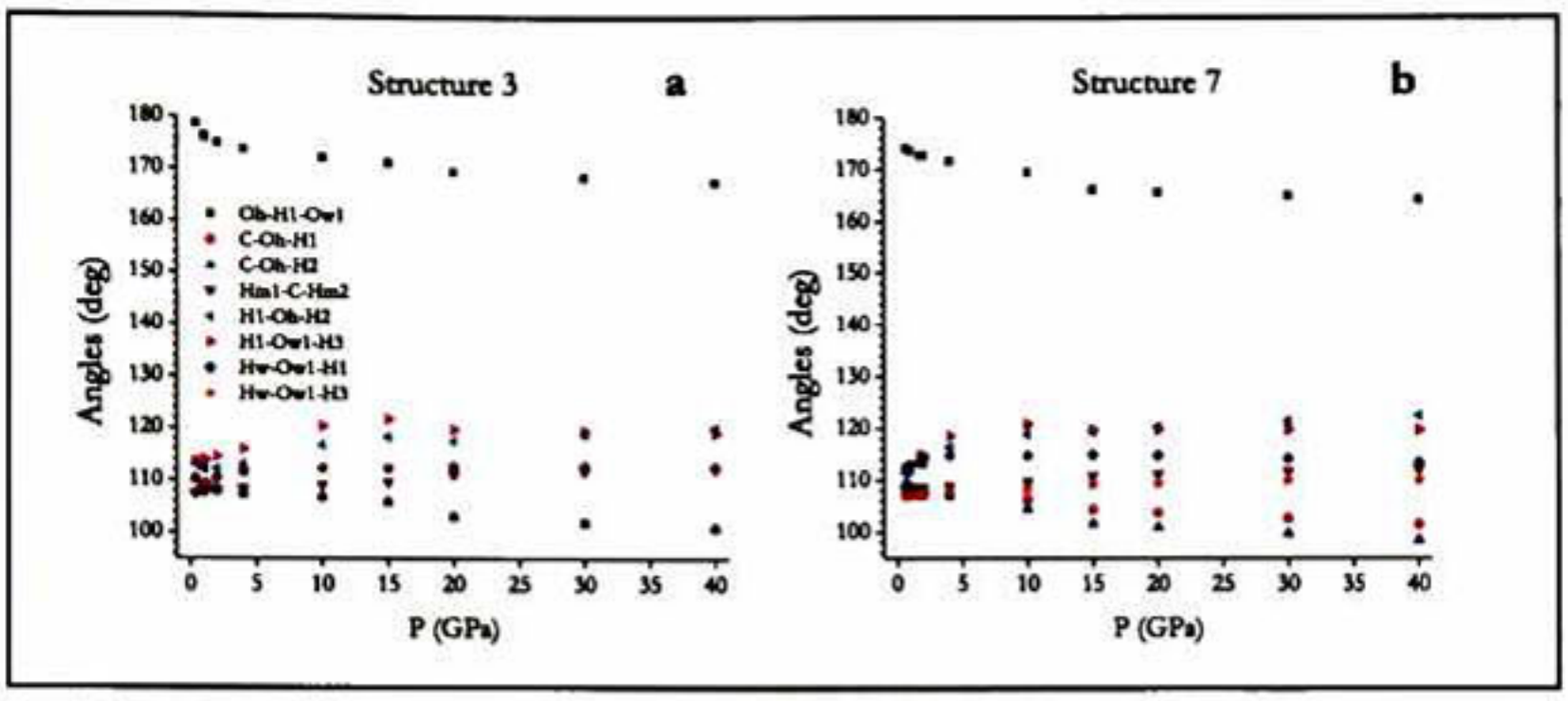

Figure 3.22: Some interatomic angles change with pressure for structures a) 3 and b) 7.

Table 3.6: Parameters of Birch-Murnagham third order equations of state

EOS parameters	Structure 1	2	3	4	5	6	7
V_0, Å^3	154.473	154.474	161.021	165.066	165.020	177.875	184.619
E_0, eV	-2245.785	-2245.785	-2245.802	-2246.383	-2246.379	-2246.419	-2246.430
B_0, Ha/ua^3 $\times 10^{-3}$	0.237	0.237	0.160	0.202	0.201	0.101	0.066
B_0', Ha/ua^4	5.979	5.979	6.878	5.551	5.576	7.262	8.869
B_0, GPa	6.987	6.987	4.705	5.950	5.918	2.979	1.947

of the compression and then it remains almost constant. This closure is compensated by the opening of H1-Oh-H2 and H1-Ow1-H3, the three along the x direction, resulting on the very small change of the a parameter observed in figure 3.16. The water part remains pretty much constant, its angles Hw-Ow1-H1 and Hw-Ow1-H3 barely change.

No experimental measurements of methanol monohydrate under pressure exist to directly compare the results obtained, but the observed changes are expected to occur, although the corresponding pressures may vary a little. This could happen because of the mentioned factors of approximations, van der Waals forces and proton disorder, besides of the temperature at which the measurements be done. However, these factors should not affect the results at high pressures as much as they did for low pressures.

3.3.2.3 Equation of State

The resulting parameters for the EOS (equation 2.30) are shown in table 3.6.

This results are important since they can be compared with experimentally obtained EOSs. Also, the inverse of the bulk modulus is a measure of the compressibility: the smaller B_0, the more compressible the structure is. Then from table 3.6 it can be seen that the most compressible is structure 7, and structures 1 and 2 the least. In general, the computed bulk moduli are similar to those

of ice VII and water, which are $\sim$ 5.02 and $\sim$ 2.2 GPa, respectively; and are far from the less compressible ice X and steel, with $B_0 \sim 145$ and ~ 160 GPa, respectively. They are much further from the highly incompressible diamond, with B_0 of 442 GPa. Therefore it can be stated that the studied structures present a high compressibility for a solid[12].

An estimation of the pressure at which the enthalpies of group A and B are the same can be done using the EOSs found. This was done for structures 3 and 7, and their enthalpies are the same at 54 GPa. So the symmetrization of the proton could occur at this pressure. This result is important for the study of such effect, since the observed pressures at which symmetrization occur for other compounds, such as ice and methane hydrate, are higher, of 100 and 70 GPa, respectively. Then, this smaller pressure makes it easier to experimentally study the effect. Nevertheless, more calculations, considering different structures and configurations, are needed to assure this.

3.3.3 X-Ray Diffraction Patterns

X-ray diffraction (XRD) patterns, obtained from the structures calculated at experimental volume, are shown in figure 3.23. They are compared with an experimental result from reference [41]. Both were performed with $\lambda = 0.179021$ nm from Co $K\alpha$ radiation. In the experimental pattern the starred peaks correspond to hexagonal ice, and the unassigned ones, presumably to methanol monohydrate, in a mixture of methanol and water annealed at 160 K.

X-ray patterns of structures 1 and 2, and 6 and 7 are very similar, so only one of each pair is presented. In the rest, the intensities and number of peaks varied, mainly because of the differences in the structure's symmetries.

The most characteristic peak in the experimental XRD pattern is that around 30° This diffraction angle is present in all the structures but with small differences due to the differences in lattice parameters, and corresponds to the (130) plane. Structure 4's pattern is the one that matches best the experimental one. The peak around 44°also matches very well. But other peaks fit better for other structures, e.g. the one at 34°, seen in structure 3. A perfect fitting cannot be expected because the possibility of the existence of all the structures, at least of group B; also because of the factors already mentioned in section 3.3.1.3. Then, peaks' displacement or elimination are feasible.

Computed patterns are in general similar to experimental, but more calculations are needed that include temperature and be able to find the existence of each structure at a given temperature.

Even though only some patterns are shown, the computed results permit to obtain patterns at the different pressures for which structures have been optimized. They could then be compared with experimental difractograms when available.

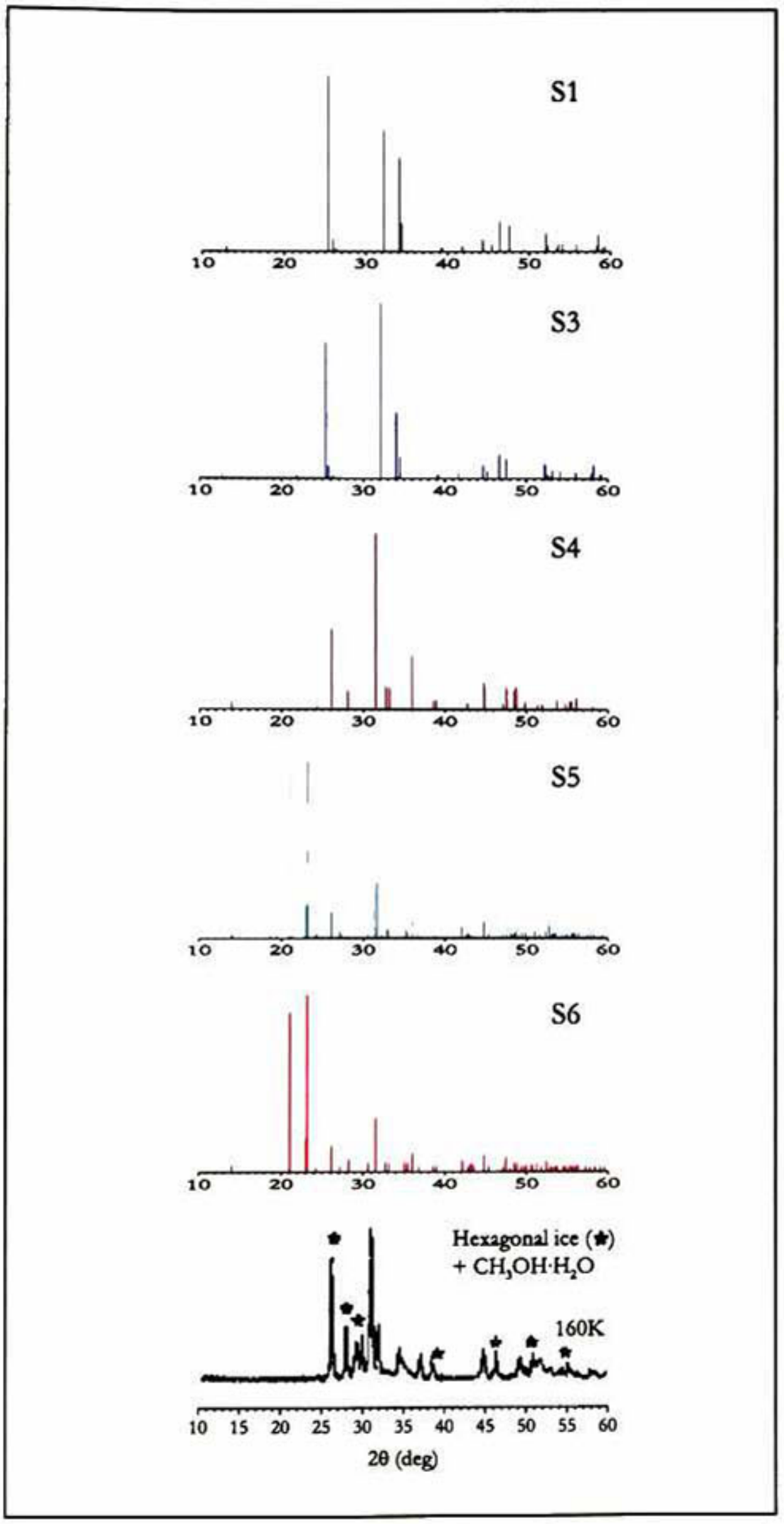

Figure 3.23: X-Ray diffraction patterns of structures 1, 3, 4, 5 and 6 with experimental volume, and experimental difractogram of a mixture of hexagonal ice (starred peaks) and methanol monohydrate from [41].

Chapter 4

Polarization

Structural changes lead to changes of properties, one of them is the electric spontaneous polarization. The structure of methanol monohydrate crystal as well as its change with pressure were studied in last chapter. In the present one, the optimized structures were used to compute the spontaneous polarization of the solid, and its evolution with pressure, within the Berry phase approach described in section 2.3.

4.1 Studied Structures

Polarization was computed from the resulting optimized structures 1 to 7 under 1, 2, 4 and 10 GPa, and the one optimized at the experimental volume.

4.2 Computational Details

These calculations were done using the Berry phase formulation implemented in abinit and based on the theory mentioned in section 2.3. They were done under a zero electric field. The cutoff energy was set to 40 Ha for all cases and the k-point grid was varied according to the structures' symmetry.

Structures 1 and 2, with space group no. 36, have a mirror plane in the yz plane, therefore, polarization in the x direction should be canceled. They also possess an axial glide plane, which is a reflection in the xz plane and a translation in direction z, thus polarization in y direction also cancels. Therefore, its polarization was only computed in the z direction using a k-point grid of $6 \times 6 \times 24$.

The polarization of the remaining structures was computed in all directions and with a k-point grid of $20 \times 20 \times 20$.

4.3 Results

The calculated spontaneous electric polarization, $\boldsymbol{\mathcal{P}}_s$, of the bulk crystal for structures 1 to 7 under pressure is presented in figures 4.1 a) and b), in x and z direction, respectively. The polarization in y was zero or very close to zero for

all structures, then it is not presented in the graphs. The structures with the highest values of spontaneous polarization were 4, 6 and 7 and this occurred in the x axis direction, and it can be seen it is tunable with pressure. Structures of group A presented spontaneous polarization only in the z direction.

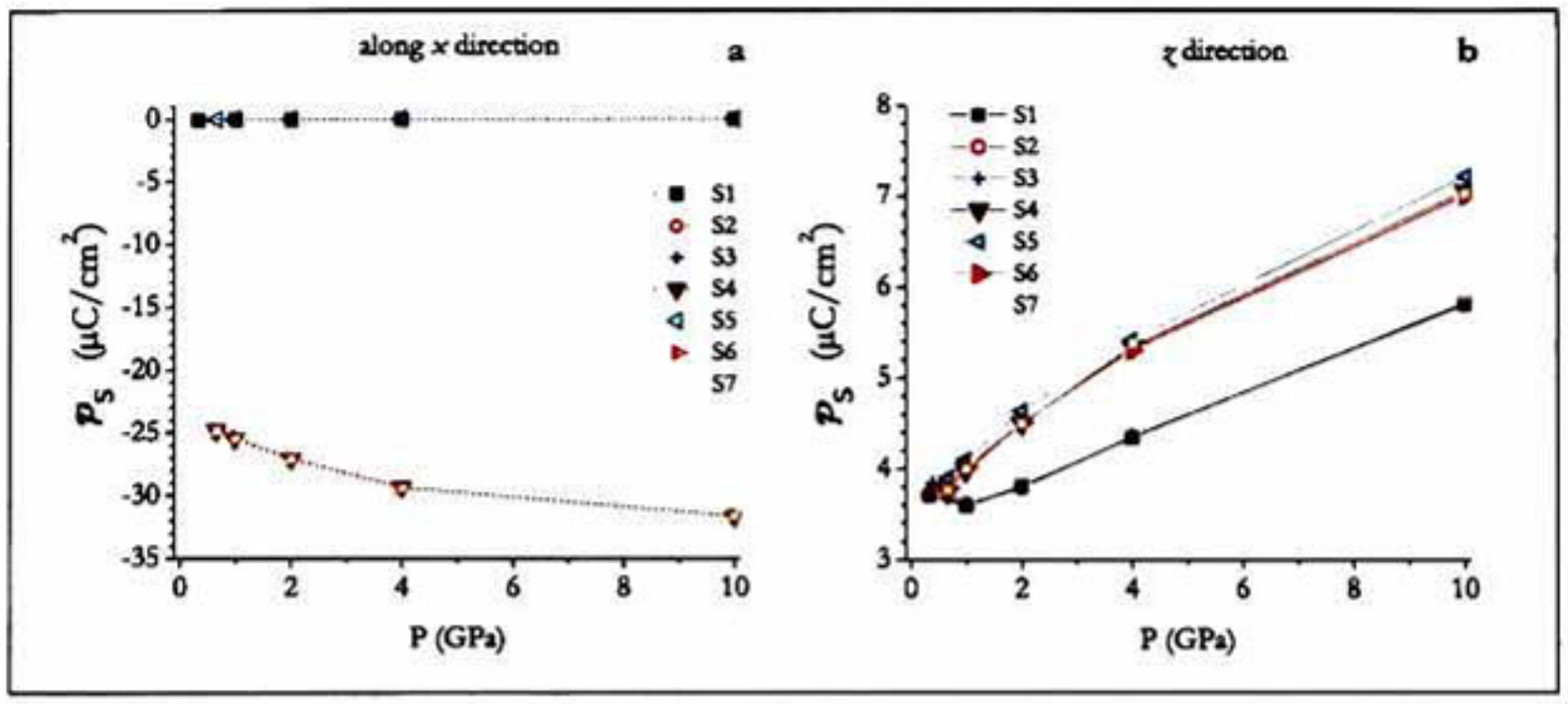

Figure 4.1: Spontaneous polarization of structures under pressure along a) x direction and b) z direction. Structures 4, 6 and 7 show a high polarization along the x direction.

The polarization in the y direction resulted in zero for structures 1, 2, 4 and 5; and near zero for the rest of the structures, but the values obtained for them are within the error of the calculation. Like structure 1 and 2, structure 4 also has the axial glide plane explained in the prior section (4.2), which leads to the cancellation of the $\mathcal{P}_s$ in the y direction.

Structure 5 has the operation symmetry of a C_2, which none of the other structures of group B has. This causes structure 5 to have null polarization in direction y and x.

As seen in figure 4.1, polarization along x is high for the structures of group B, except 5. This shows how a simple change in the structure can modify so much a property of the system. Such structural change can be seen in figures 3.3, in chapter 3, where the difference in the configuration of atoms in structure 5 with respect to 4, 6 and 7 (group B), can be seen in the middle of the pictures, and is only that the disordered protons (purple) bonded to the superior water-oxygen are interchanged.

A view of the xy plane of the conventional unit cell of structures 4 and 5 is also presented in figure 4.2. The orientations of the O-H bonds of water and methanol originate the polarization in direction x in structure 4. The symmetry of each configuration causes that the polarization vanishes in the y direction in both structures, and also in the x direction for structure 5.

Structure 5 represents one of the two positions that the disordered proton can take, as explained in section 3.3.1.1. Consequently, the methanol mono-

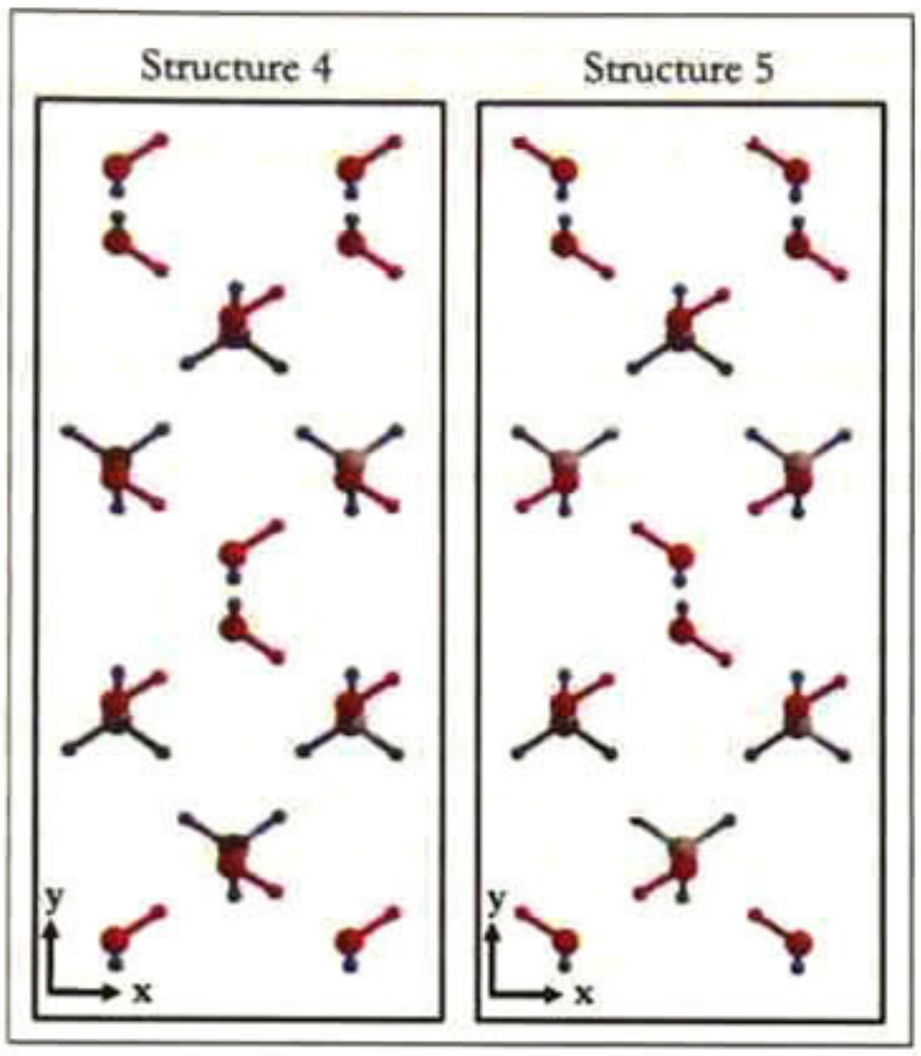

Figure 4.2: Configurations of structures 4 and 5, in which it can be seen that the orientation of the O-H bonds originate the polarization in the x direction in structure 4, and that the symmetry causes the polarization to vanish in the y direction in structures 4 and 5, and also in the x direction for structure 5.

hydrate can present this two values of spontaneous polarization of 0 and ~25 $\mu C/cm^2$, or a combination of them, when the proton is disordered. If the stable structure happens to be only one of the configurations, then it would present only one of the encountered values.

Yet, the distribution of the relative existence of each configuration cannot be determined by the calculations done in this thesis, but with calculations that would require much computational time. Nor is clear which the minimum energy configuration is below 10 GPa (section3.3.2.1).

4.3.1 Comparison with other materials

The resulting values of the spontaneous polarization in x are high when compared to the values of other organic solids. For example, the calculated $\boldsymbol{\mathcal{P}}_s$ for crystals of thiourea ($SC(NH_2)_2$) and squaric acid ($C_4H_2O_4$) are 4.9 and 17.1, respectively (the later is only in the x direction)[22].

Ferroelectric materials present spontaneous polarization and experimental information of them is extensive. Therefore, they are used here to compare them with the calculated values of $\boldsymbol{\mathcal{P}}_s$ of the methanol monohydrate, in spite of the fact that methanol monohydrate has not been proved to be a ferroelectric, since polarization was not calculated under different electric fields.

It should be mentioned that crystals presenting a permanent dipole may not show their polarization value until a change had been applied to them, and order the molecules in the crystal. Such change can be an electric field, a mechanical stress or temperature.

In the field of ferroelectrics, there is a relatively new branch, which is organic ferroelectrics. Examples of them have not been abundant. Organic ferroelectrics have become important for materials science since their invention may find many new applications of their lightness, flexibility and non-toxicity in the emerging field of organic electronics[54].

In a recent review of organic ferroelectrics some experimental spontaneous polarization values are reported. For single-component organic molecules, the vinylidene fluoride oligomer is the one with the largest reported value, which is $\boldsymbol{\mathcal{P}}_s = 13\ \mu C/cm^2$ at room temperature[54]. This value is similar to the $\boldsymbol{\mathcal{P}}_s$ of its polymers polyvinylidene fluoride and copolymers of vinylidene fluoride with trifluoroethylene, $\sim 10\ \mu C/cm^2$ These polymers have been extensively studied in order to use them in electronics[55]. A value slightly larger was found for an organic-inorganic compound, a salt of diazabicyclo[2,2,2]octane (dabco) with inorganic tetrahedral anions. Its spontaneous polarization can be as high as 16 $\mu C/cm^2$ at room temperature.

But yet, the most used ferroelectrics are inorganic compounds, which have much larger spontaneous polarization and higher dielectric constants. To have an idea of their characteristic $\boldsymbol{\mathcal{P}}_s$, $BaTiO_3$ presents a $\boldsymbol{\mathcal{P}}_s$ of 26 $\mu C/cm^2$, and $PbTiO_3$, of 75, both at room temperature[54]. A very large spontaneous polarization is that of $BiFeO_3$ single crystals, of 100 $\mu C/cm^2$[56].

Hence, the spontaneous polarization found for methanol monohydrate configurations 4, 6 and 7, are large when compared with other organic materials; but still far from the largest values found for inorganic materials.

Chapter 5

Vibrational Characterization and Dielectric Constant

Thc phonon frequencies and dielectric constant of the structures of methanol monohydratc under pressure were computed using DFPT, and are presented in this chapter.

5.1 Studied Structures

The DFPT calculations were performed in the structures 1 to 7, previously optimized under 1, 2, 4 and 10 GPa, and the one optimized at the experimental volume.

5.2 Computational Details

Response function calculations at Gamma, based on the DFPT described in section 2.2, were done in order to obtain the phonon frequencies and dielectric constants of the structures.

The cutoff energy was again set to 40 Ha and the k-point grid to $6 \times 6 \times 6$. The resulting output was analyzed by the abinit utility Anaddb (Analysis of Derivative Data Base).

5.3 Results

5.3.1 Vibrational modes and frequencies

The 54 vibrational modes of methanol monohydrate were obtained for each structure, corresponding to the $3N$ modes of the 18 atoms-unit cell. Structures 1, 2 and 3 have some imaginary phonon frequencies, which means these structures are metastable under the studied conditions. This means that they migth

exist, but they represent an ustable structure configuration, so when the structure of methanol monohydrate has this configuration, it would go to a more stable one, such as structures 4 to 7. The latter ones do not present negative frequencies for their vibrational modes, therefore they show dynamical stability. The structures have the expected three acoustic modes with low frequencies, close to zero cm^{-1}

By performing group theory analysis in the zone center, the next decomposition of the modes is obtained: $15A_1 + 12A_2 + 12B_1 + 15B_2$ for structures 1 and 2, $32A' + 22A''$ for structure 3, $27A' + 27A''$ for structure 4, $27A + 27B$ for structure 5, and 54 A modes for structures 6 and 7. All of them are active in both Raman and IR spectroscopies, except A_2, which is not active in IR.

The vibrational modes are characterized by their symmetry. This symmetry is given by the code for each obtained mode, so in this way modes can be identified and analyzed under pressure. It is assumed that the modes preserve their symmetry under compression.

The vibrational modes frequencies of structures 1, 3, 4, 5 and 6 are presented in figures 5.1, 5.2, 5.3, 5.4 and 5.5, respectively. The negative frequencies of structures 1 and 3 can be seen, which belong to the unstable modes.

For most of the modes, their frequencies increase with the increase in pressure, they harden; but, for some of them, their frequencies decrease.

The frequencies and change in frequencies with pressure for structure 1 and 2 are very similar in the studied interval of pressures. This also happens for structure 6 with respect to 7. As mentioned in chapter 3 structures 1 and 2 have the same space group, so they can be considered as the same structures, as well as structures 6 and 7.

The results obtained are very important for vibrational spectroscopies, such as Raman and Infrared ones. At the frequencies obtained, peaks are expected to be observed in a Raman or IR spectrum, depending on the selection rules of each. Nevertheless, more calculations are needed to predict the relative intensities of the peaks.

With the information obtained, each mode can be directly observed, to see what kind of atoms and movements give place to each mode and frequency.

For example, the modes that cause the instability of structures of group A involve stretching between the symmetric protons and oxygen atoms.

It is well known that modes with high vibrational frequencies correspond to the stretching of strong bonds, such as stretching of C-H or O-H bonds. The C-H stretching is usually found at a frequency of $3000 - 2850$ cm^{-1}[57]. Hence, observing the mode of structure 6 or 7, with a frequency of 3022 cm^{-1} at 0.7 GPa, it can be seen that it corresponds to a streching mode of the C-H bond. This is presented in figure 5.6, the arrows represent the relative displacements of the atoms when they are vibrating in the particular mode of vibration. It is

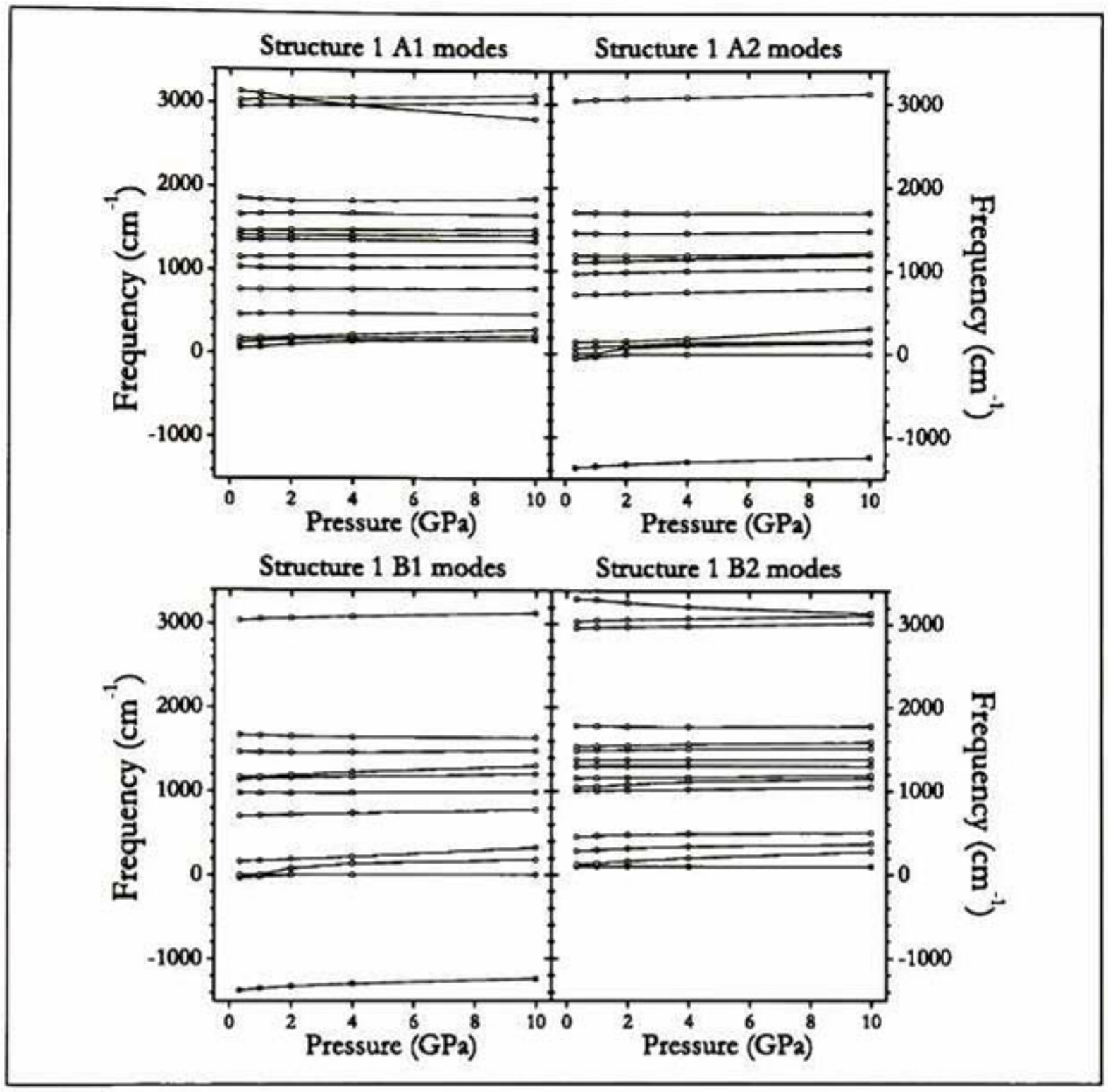

Figure 5.1: Pressure variation of the vibrational modes of structure 1.

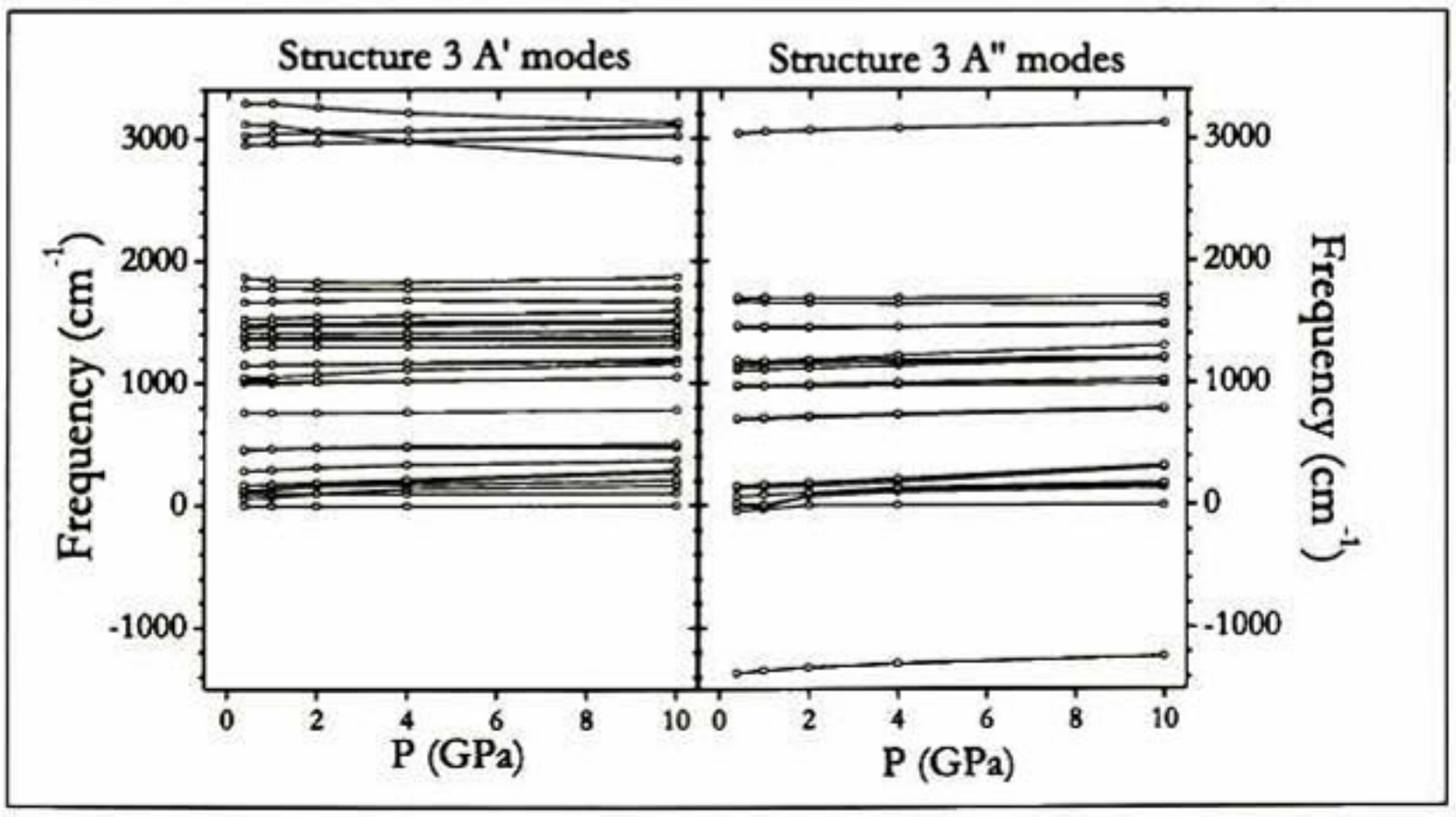

Figure 5.2: Pressure variation of the vibrational modes of structure 3.

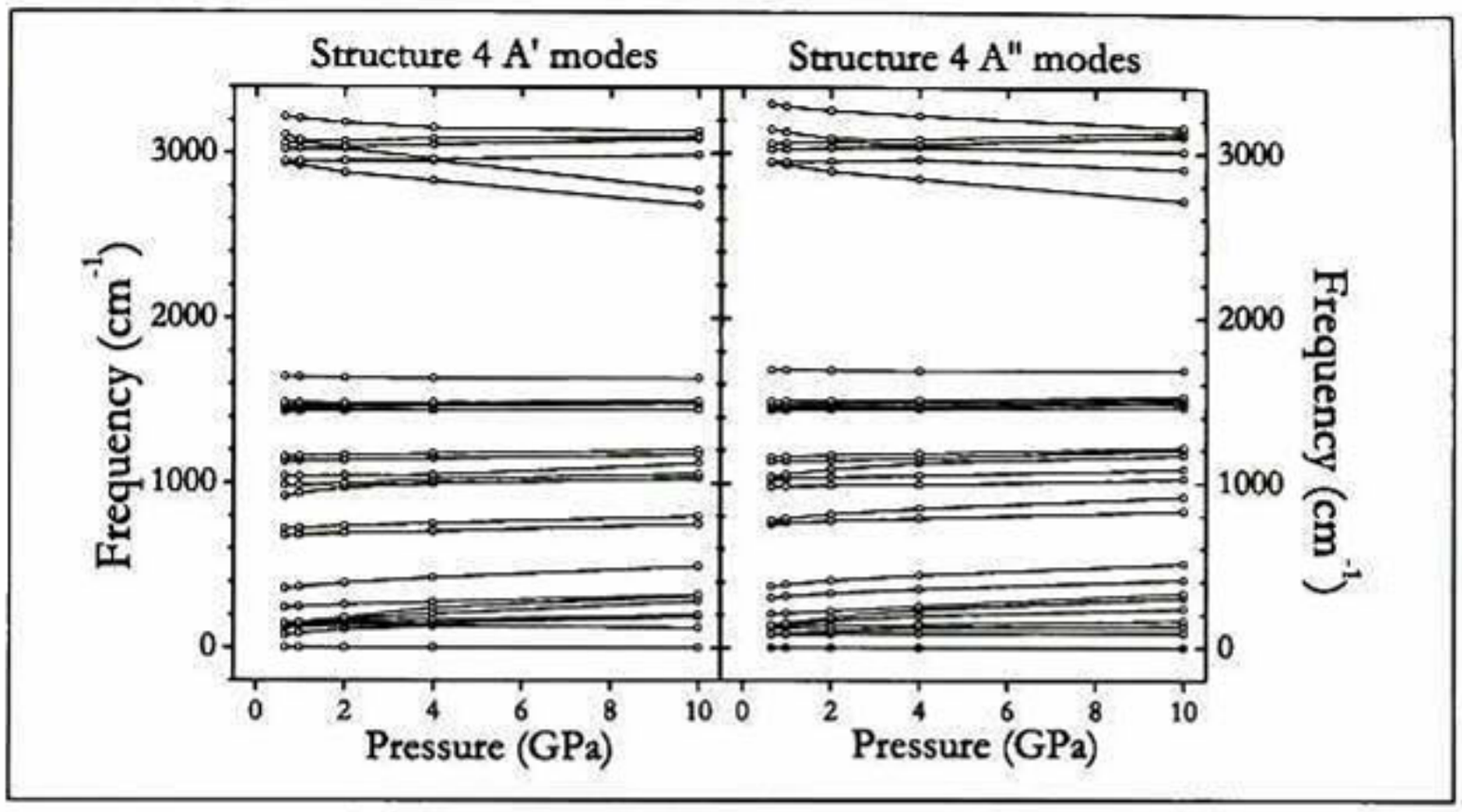

Figure 5.3: Pressure variation of the vibrational modes of structure 4.

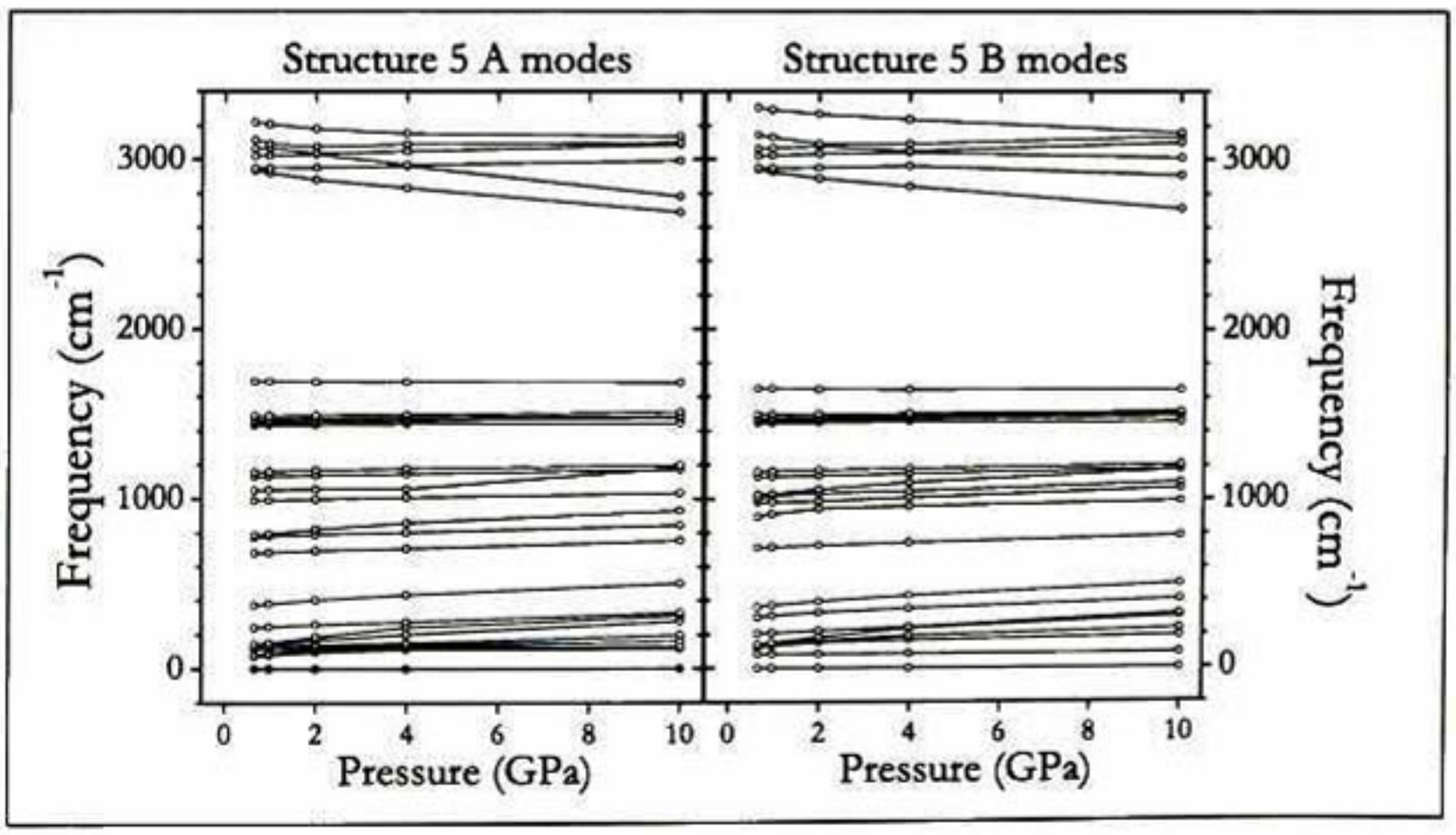

Figure 5.4: Pressure variation of the vibrational modes of structure 5.

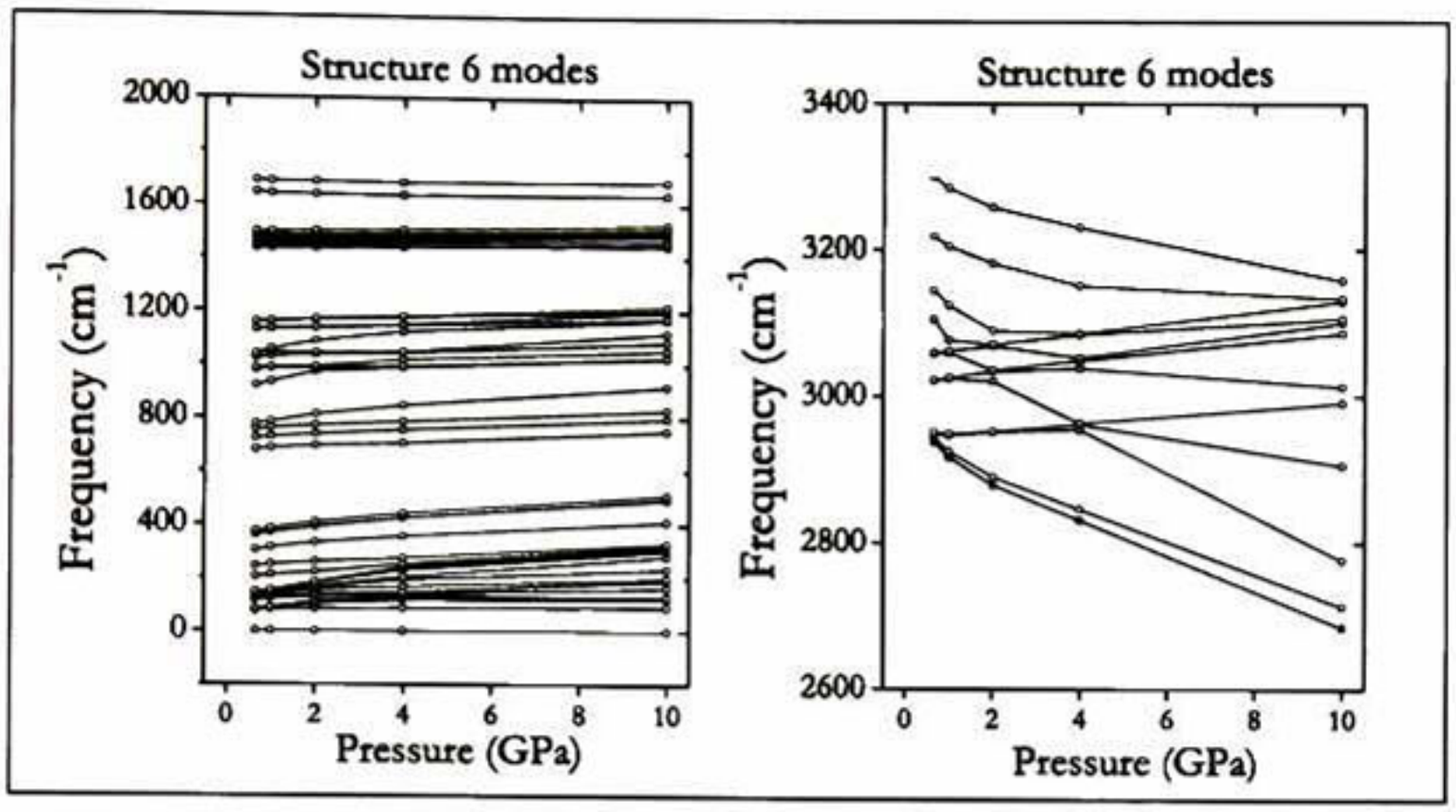

Figure 5.5: Pressure variation of the vibrational modes of structure 6.

also the data point marked with light pink triangles in figure 5.5.

The mode with the higher vibrational frequency of structure 6 (orange squares in figure 5.5), corresponds to an O-H streching in water molecules, mainly, and it is combined with the O-H stretching in methanol, not as intense as the first stretching. Its frequency is 3299 cm^{-1} at 0.7 GPa and is shown in figure 5.7. The usual range for the O-H stretching modes is 3700 - 3600 cm^{-1}, but it decreases when hydrogen bonds are present. For example, it is observed in the 3500 - 2500 cm^{-1} range for hydrogen-bonded alcohol dimer[57]. This agrees perfectly with the obtained results.

In the acoustic modes all atoms move together. The rest of the modes include wagging, rocking, sissoring, as well as some other stretching modes of different parts of the methanol monohydrate.

5.3.2 Dielectric constant

The dielectric constant results complements the dielectric characterzation of methanol monohydrate, along with the spontaneous polarization calculated in chapter 4.

The dielectric constants found were small when compared with some other organic materials. The results obtained are shown in table 5.1. Due to the negative frequencies obtained for the structures of group A, their dielectric constant could not be computed.

The dielectric constant of all of them are equal at a given pressure, except for the one of structure 5 at 2 GPa. Then it can be said that this property is not noticeable affected by the structural differences in the studied configurations.

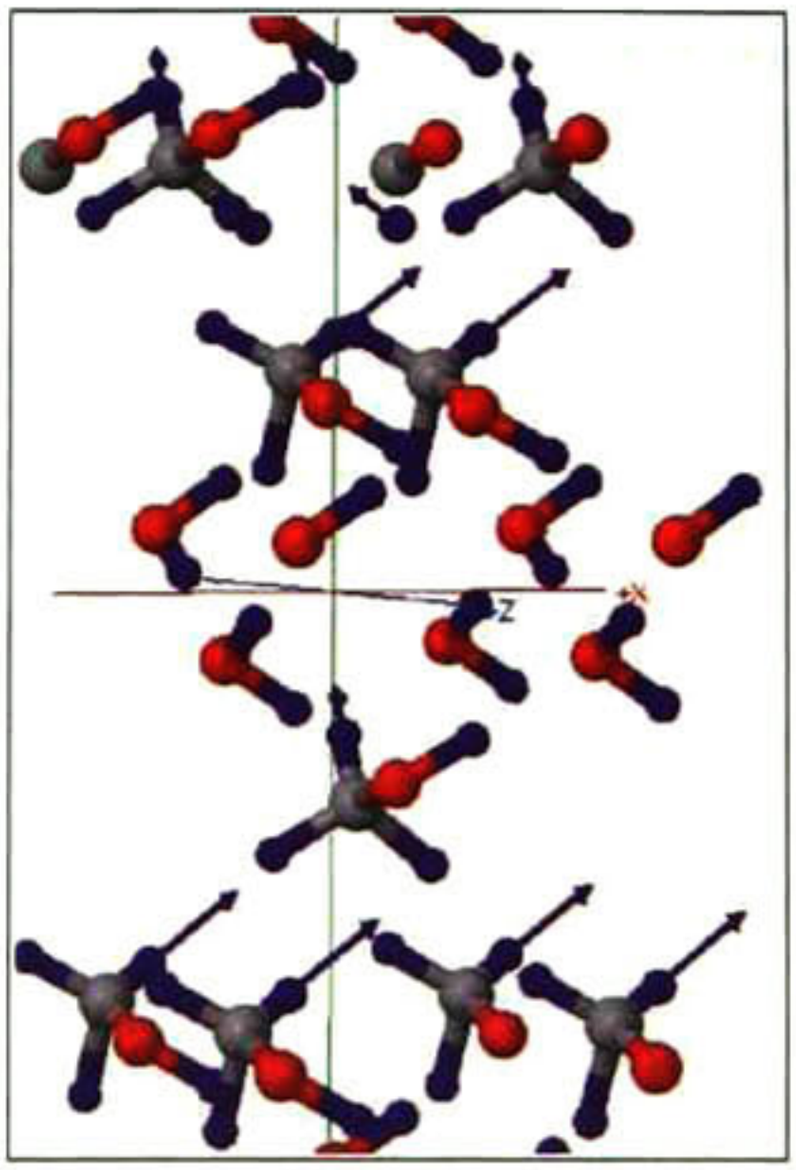

Figure 5.6: High frequency vibrational mode of structure 7 at 0.7 GPa (experimental volume), where the arrows indicate the direction and intensities of the movement of the atoms. This mode is a C-H streching at 3022 cm^{-1}

Table 5.1: Calculated dielectric constants of structures 4 to 7.

	Structure			
P(GPa)	4	5	6	7
0.7	5.3	5.3	5.3	5.3
1.0	5.4	5.4	5.4	5.4
2.0	5.6	5.7	5.6	5.6
4.0	6.0	6.0	6.0	6.0
10.0	6.8	6.8	6.8	6.8

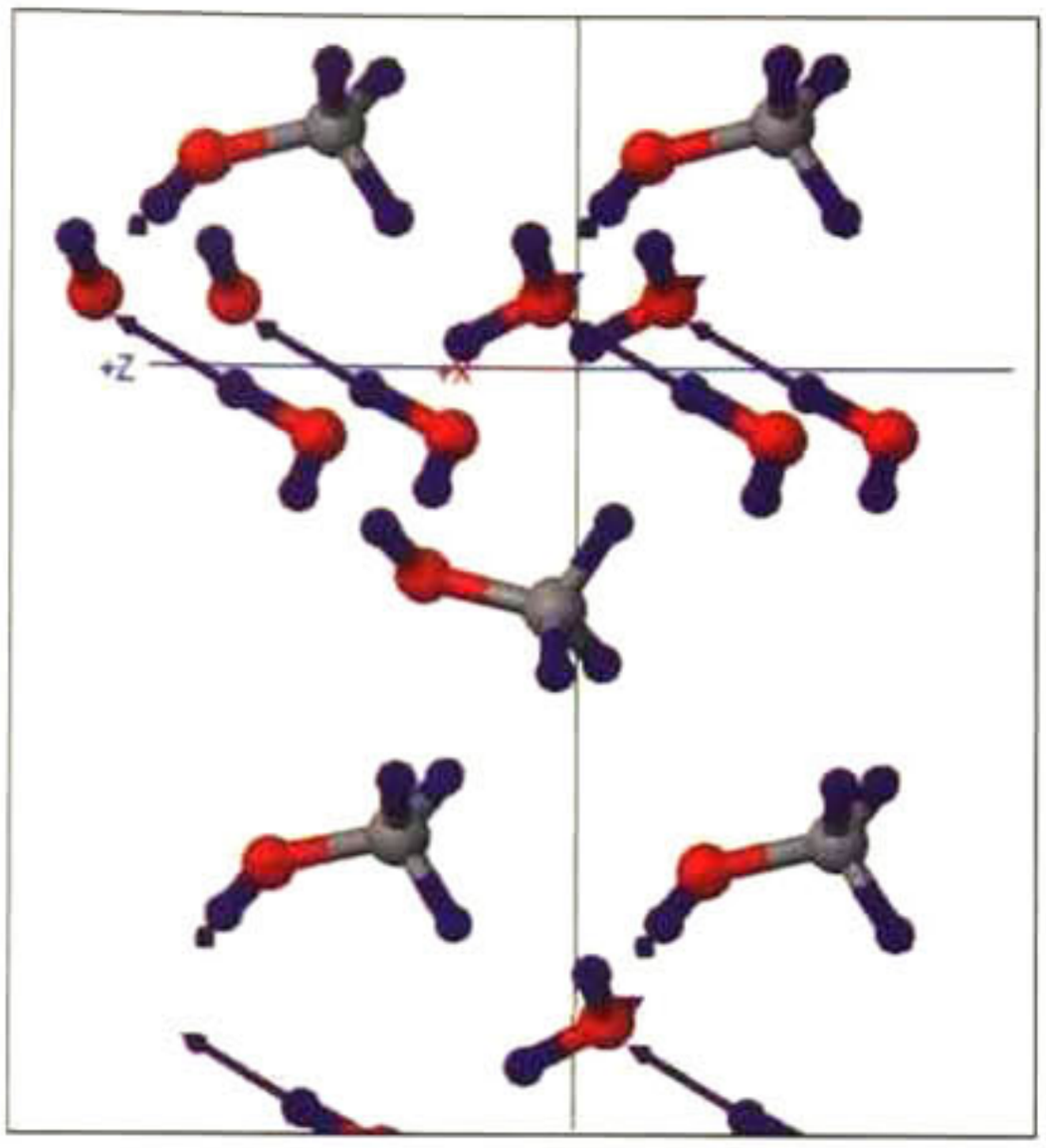

Figure 5.7: High frequency vibrational mode of structure 6 at 0.7 GPa (experimental volume), where the arrows indicate the direction and intensity of the movement of the atoms. This mode is a O-H streching at 3299 cm^{-1}

Anyway, it has been observed in this work that structures 6 and 7 might be the same structure up to 10 GPa, and therefore, have the same properties. Also, structure 4 is very similar to them.

These computed dielectric constants values are comparable with those of the vinylidene fluoride oligomer and the salt of diazabicyclo[2,2,2]octane (mentioned in chapter 4), both of 6 at room temperature[54]. The dielectric constant of thiourea is 30 at room temperature, and it can be as high as 10^4 at its Curie temperature, of 169 K. $BaTiO_3$ dielectric constant also presents this value at its T_C of 381 K. These are some of the largest reported values.

At least, for ferroelectric materials, the dielectric constant increases with temperature increase, up to the Curie temperature, then it decreases. This has been observed also for hydrogen-bonded organic ferroelectrics, so the dielectric constant of methanol monohydrate may also increase with temperature.

Chapter 6

Conclusions

In this work, methanol monohydrate has been theoretically studied. We have performed a complete structural, electronic and vibrational characterization of such system as a function of pressure.

Seven different structural configurations were considered in our calculations. They were proposed based on powder neutron diffraction experimental measurements.

Two groups of structures were found in terms of energy. The one of higher energy was named group A and was formed by structures 1 to 3. The one of lower energy was named group B and was formed by structures 4 to 7.

Methanol monohydrate configurations of group B are more energetically stable than those of group A at the studied conditions, i.e. from 0.3 to 40 GPa, and 0 K.

The small energy differences among the structures of group B may result in an easy transformation of the configurations from one to another, by the movement of the protons from one disorder position to another, either by proton tunneling or proton hopping.

Methanol monohydrate is dynamically stable under the studied range of pressures (0.3-10 GPa) and 0 K, in the configurations of group B.

The dynamical stability of methanol monohydrate in the configurations of group B, and the dynamical instability of group A was confirmed by the vibrational characterization, in which negative vibrational frequencies were found.

The stable configurations correspond to those where the protons are not localized symmetrically between two oxygen atoms, but bonded to only one of them.

The compression mechanism of the structures involves a reorientation of the methanol molecules and a reduction in the hydrogen bonds lengths.

The structures present a high compressibility along the b axis (y direction).

According to the calculated EOS, the symmetrization of the protons for methanol monohydrate is expected to occur when the system be submitted to 54 GPa.

Methanol monohydrate also presents a high spontaneous polarization when compared with other organic solids, of 25 $\mu C/cm^2$ along the x direction at experimental volume. The spontaneous polarization can be adjusted with pressure and it can go up to 31 $\mu C/cm^2$ at 10 GPa.

Such results are relevant to planetary science since the large polarization of the methanol monohydrate can induce some orientation of other molecules for them to arrange in larger molecules, which could be prebiogenic factors; and to the study of organic electronics and technology.

54 vibrational modes and its frequencies for each structure were identified. The high frequency modes correspond to the stretching of C-H and O-H bonds. In the lower frequency modes, some other types of vibrations were observed.

The dielectric constant of methanol monohydrate was computed, obtaining a value of 5.3 at experimental volume.

Cell parameters, compressibility curves, X-ray diffraction patterns and vibrational mode frequencies were calculated, which can be compared with experimental data when available, in order to identify and understand the methanol monohydrate.

Perspectives

To study the same structures but with different approximations for the exchange correlation energy and in particular with functionals that include corrections for the intermolecular interactions. Based on that, we can see the effects of such corrections on the optimized structures and properties calculated. It is not expected to have a large influence on the structure but it could change some of the electronical properties.

To perform calculations for these structures that permit to investigate the effects of temperature. In particular, ab initio molecular dynamics, where temperature is a variable or Rahman-Parrinello molecular dynamics, where temperature and pressure are considered basic variables.

To study the properties of structures at higher pressures (> 10 GPa), along with more possible configurations. Since structural changes were observed at 15 - 20 GPa, it could lead to important changes in properties and structures. As in other hydrogen bonded materiales, it is expected that pressure is able to increase the number of phases, when the hydrogen network is varied as the unit cell changes.

To compare the results with experimental data of methanol monohydrate, when available, or to start collaboration with experimental groups which are able to perform such experiments.

To write 2 scientific papers: one about the structural evolution of methanol mnonohydrate under pressure, along with the vibrational characterization, and one with the dielectric properties of methanol monohydrate at different pressures.

Bibliography

[1] P. Hohenberg and W. Kohn, "Inhomogeneous electron gas," *Phys. Rev.*, vol. 136, pp. B864–B871, 1964.

[2] W. Kohn and L. J. Sham, "Self-consistent equations including exchange and correlation effects," *Phys. Rev.*, vol. 140, no. 4A, pp. A1133–A1138, 1965.

[3] X. Gonze, G.-M. Rignanese, M. Verstraete, J.-M. Beuken, Y. Pouillon, R. Caracas, F. Jollet, M. Torrent, G. Zerah, M. Mikami, P. Ghosez, M. Veithen, J.-Y. Raty, V. Olevano, F. Bruneval, L. Reining, R. Godby, G. Onida, D. Hamann, and D. Allan, "A brief introduction to the abinit software package," *Zeit. Kristallogr.*, vol. 220, pp. 558–562, 2005.

[4] `http://www.abinit.org/`.

[5] K. Burke, "The ABC of DFT," 2003. http://dft.rutgers.edu/kieron/beta.

[6] M. Payne, D. Allan, M. Teter, T. Arias, and J. Joannopoulos, "Iterative minimization techniques for *ab initio* total-energy calculations: molecular dynamics and conjugate gradients," *Reviews of Modern Physics*, vol. 64, no. 4, pp. 1045–1097, 1992.

[7] K. Capelle, "A bird's-eye view of density-functional theory," *Brazilian Journal of Physics*, vol. 36, pp. 1318–1343, 2006.

[8] N. Argaman and G. Makov, "Density functional theory: An introduction," *Am. J. Phys.*, vol. 68, no. 1, pp. 69–79, 2000.

[9] L. E. Díaz Sánchez, *Anisotropías magnéticas de primeros principios.* PhD thesis, Cinvestav, Unidad Querétaro, 2009.

[10] H. J. Monkhorst and J. D. Pack, "Special points for brillouin-zone integrations," *Phys. Rev. B*, vol. 13, no. 12, pp. 5188–5192, 1976.

[11] T. Iitaka and T. Ebisuzaki, "Methane hydrate under high pressure," *Phys. Rev. B*, vol. 68, no. 17, p. 172105, 2003.

[12] E. Sugimura, T. Iitaka, K. Hirose, K. Kawamura, N. Sata, and Y. Ohishi, "Compression of H_2O ice to 126 GPa and implications for hydrogen-bond symmetrization: Synchrotron x-ray diffraction measurements and density-functional calculations," *Phys. Rev. B*, vol. 77, no. 21, 2008.

[13] M. Walker, C. A. Morrison, D. R. Allan, C. R. Pulham, and W. G. Marshall, "A new high pressure phase of sodium formate dihydrate; an experimental and computational study," *Dalton Trans.*, pp. 2014–2019, 2007.

[14] V. Marek, *First principles study of the nonlinear responses of insulators to electric fields: applications to ferroelectric oxides.* PhD thesis, Universite de Liege, 2005.

[15] X. Gonze, "First-principles responses to atomic displacements and homogeneous electric fields: implementation of a cojugate-gradient algorithm," *Phys. Rev. B*, vol. 55, no. 16, pp. 10337–10354, 1997.

[16] X. Gonze, "Perturbation expansion of variational principles at arbitrary order," *Phys. Rev. A*, vol. 52, no. 2, pp. 1086–1095, 1995.

[17] X. Gonze and C. Lee, "Dynamical matrices, born effective charges, dielectric permittivity tensors, and interatomic force constants from density-functional perturbation theory," *Phys. Rev. B*, vol. 55, no. 16, pp. 10355–10368, 1997.

[18] R. M. Martin, *Electronic structure: basic theory and practical methods.* Cambridge University Press, 2005.

[19] G. G. Raju, *Dielectrics in electric fields.* Marcel Dekker, 2003.

[20] R. Resta, "Macroscopic polarization in crystalline dielectrics: the geometric phase approach," *Rev. Mod. Phys.*, vol. 66, no. 3, pp. 899–915, 1994.

[21] R. D. King-Smith and D. Vanderbilt, "Theory of polarization of crystalline solids," *Phys. Rev. B*, vol. 47, no. 3, pp. 1651–1654, 1993.

[22] F. Ishii, N. Nagaosa, Y. Tokura, and K. Terakura, "Covalent ferroelectricity in hydrogen-bonded organic molecular systems," *Phys. Rev. B)*, vol. 73, no. 21, p. 212105, 2006.

[23] X. Gonze, J.-M. Beuken, R. Caracas, F. Detraux, M. Fuchs, G.-M. Rignanese, L. Sindic, M. Verstraete, G. Zerah, F. Jollet, M. Torrent, A. Roy, M. Mikami, P. Ghòsez, J.-Y. Raty, and D. Allan, "First-principles computation of material properties: the abinit software project," *Comput. Materials Science*, vol. 25, no. 3, pp. 478–492, 2002.

[24] R. Hemley, "Effects of high pressure on molecules," *Annu. Rev. Phys. Chem.*, vol. 51, pp. 763–800, 2000.

[25] E. Isaacs, A. Shukla, P. M. Platzman, D. R. Hamann, B. Barbiellini, and C. A. Tulk, "Covalency of the hydrogen bond in ice: A direct x-ray measurement," *Phys. Rev. Lett.*, vol. 82, no. 3, 1999.

[26] A. Goncharov and R. Hemley, "Probing hydrogen-rich molecular systems at high pressures and temperatures," *Chem. Soc. Rev.*, vol. 35, pp. 899 907, 2006.

[27] R. Caracas, "Raman spectra and lattice dynamics of cubic gauche nitrogen," *J. Chem. Phys.*, vol. 127, p. 144510, 2007.

[28] R. Caracas and R. Hemley, "New structures of dense nitrogen: pathways to the polymeric phase," *Chem. Phys. Lett.*, vol. 442, pp. 65–70, 2007.

[29] J. S. Loveday, R. J. Nelmes, M. Guthrie, S. A. Belmonte, D. R. Allan, D. D. Klug, J. S. Tse, and Y. P. Handa, "Stable methane hydrate above 2 GPa and the source of Titan's atmospheric methane," *Nature*, vol. 410, pp. 661 663, 2001.

[30] S. M. Peiris and G. J. Piermarini, *Static Compression of Energetic Materials*, ch. 1, Diamond Anvil Cell Techniques, pp. 1–74. Springer Berlin Heidelberg, 2008.

[31] F. Birch, "Finite elastic strain of cubic crystals," *Phys. Rev.*, vol. 71, no. 11, pp. 809–824, 1947.

[32] D. Anderson, *Theory of the Earth.* Blackwell Scientific Publications, 1989. Oxford.

[33] S. M. Peiris and J. C. Gump, *Static Compression of Energetic Materials*, ch. 3, Equations of State and High-Pressure Phases of Explosives, pp. 99–126. Springer Berlin Heidelberg, 2008.

[34] G. A. Olah, "Beyond oil and gas: The methanol economy," *Angewandte Chemie International Edition*, vol. 44, no. 118, pp. 2636–2639, 2005.

[35] A. Esteban, V. Hernández, and K. Lunsford, "Exploit the benefits of methanol," *Proceedings, Annual Convention-Gas Processors Association*, no. 79, pp. 45–81, 2000.

[36] P. Biedermann, T. Grube, and B. Höohlein, *Methanol as an energy carrier.* Forschungszentrum Jlich, Zentralbibliothek, Verlag, 2006.

[37] G. Miller and D. Carpenter, "Solid-liquid phase diagram of the system methanol-water," *J. Chem. Eng. Data*, vol. 9, no. 3, pp. 371–373, 1964.

[38] K. Takaizumi and T. Wakabayashi, "The freezing process in methanol-, ethanol-, and propanol-water systems as revealed by differential scanning calorimetry," *Journal of Solution Chemistry*, vol. 26, no. 10, pp. 927–939, 1997.

[39] E. Sloan, *Clathrate hydrates of natural gases.* Marcel Dekker, 1990. New York.

[40] M. Bernstein, S. Sandford, L. Allamandola, S. Chang, and M. Scharberg, "Organic compounds produced by photolysis of realistic interstellar and cometary ice analogs containing methanol," *Astrophys. J.*, vol. 454, p. 327, 1995.

[41] H. Nakayama, D. Brouwer, Y. Handa, D. Klung, J. Tse, C. Ratcliffe, X. Zhu, and J. Ripmeester, "Methanol: clathrate hydrate former or inhibitor," *Am. Chem. Soc. Div. Fuel Chem.*, vol. 42, pp. 516–520, 1997.

[42] A. D. Fortes, "The crystal structure of methanol monohydrate ($CD_3OD \cdot D_2O$) at 160 k from powder newtron diffraction," *Chem Phys Let*, vol. 431, no. 4–6, pp. 283–288, 2006.

[43] D. Braga, F. Grepioni, and G. Orpen, *Crystal Engineering: From Molecules and Crystals to Materials*, pp. 89–106. Kluwer Academic Publishers, 1999.

[44] B. D. Cullity and S. R. Stock, *Elements of X-Ray Diffraction.* Prentice Hall, third edition ed., 2001.

[45] M. Fuchs and M. Scheffler, "Ab initio pseudopotentials for electronic structure calculations of poly-atomic systems, using density-functional theory," *Comput. Phys. Commun.*, vol. 119, no. 1, pp. 67–98, 1999.

[46] R. M. Lees and J. G. Baker, "Torsion-vibration-rotation interactions in methanol. i. millimiter wave spectrum," *J. Chem. Phys.*, vol. 48, no. 12, 1968.

[47] B. H. Torrie, O. S. Binbrek, M. Strauss, and I. P. Swainson, "Phase transitions in solid methanol," *Journal of Solid State Chemistry*, vol. 166, no. 2, pp. 415–420, 2002.

[48] W. F. Kuhs and M. Lehmann, *Water science reviews 2*, ch. 1. The structure of ice Ih. Cambridge University Press, 1986.

[49] V. M. Nield, J. C. Li, D. K. Ross, and R. W. Whitworth, "Disorder in ice Ih," *Physica Scripta*, vol. T57, pp. 179 183, 1995.

[50] J. A. Odutola and T. R. Dyke, "Partially deuterated water dimers: Microwave spectra and structure," *J. Chem. Phys.*, vol. 72, no. 9, pp. 5062–5070, 1980.

[51] K. N. Kirschner and R. J. Woods, "Quantum mechanical study of the non-bonded forces in watermethanol complexes," *J. Chem. Phys. A*, vol. 105, no. 16, pp. 4150–4155, 2001.

[52] P. A. Stockman, G. A. Blake, F. J. Lovas, and R. D. Suenram, "Microwave rotation-tunneling spectroscopy of the water–methanol dimer: Direct structural proof for the strongest bound conformation," *J. Chem. Phys.*, vol. 107, no. 10, pp. 3782–3790, 1997.

[53] R. T. Morrison and R. N. Boyd, *Organic Chemistry.* Prentice Hall, 6th ed., 1992.

[54] S. Horiuchi and Y. Tokura, "Organic ferroelectrics," *Nat. Mater.*, vol. 7, pp. 357–366, 2008.

[55] S. Horiuchi, R. Kumai, and Y. Tokura, "Hydrogen-bonded donoracceptor compounds for organic ferroelectric materials," *Chem. Commun.*, pp. 2321–2329.

[56] D. Lebeugle, D. Colson, A. Forget, and M. Viret, "Very large spontaneous electric polarization in bifeo[sub 3] single crystals at room temperature and its evolution under cycling fields," *Appl. Phys. Lett.*, vol. 91, no. 2, p. 022907, 2007.

[57] B. H. Stuart, *Infrared Spectroscopy: Fundamentals and Applications.* Analytical Techniques in the Sciences (AnTS), John Wiley & Sons, 2004.

EL JURADO DESIGNADO POR LA UNIDAD QUERÉTARO DEL CENTRO DE INVESTIGACIÓN Y DE ESTUDIOS AVANZADOS DEL INSTITUTO POLITÉCNICO NACIONAL, APROBÓ LA TESIS DE MAESTRÍA DEL LA C. ROSA ELENA DÁVILA MARTÍNEZ TITULADA: "METHANOL MONOHYDRATE UNDER PRESSURE: A FIRST PRINCIPLES STUDY", FIRMAN AL CALCE DE COMÚN ACUERDO LOS INTEGRANTES DE DICHO JURADO, EN LA CIUDAD DE QUERÉTARO, QRO., A LOS VEINTICINCO DÍAS DEL MES DE MARZO DEL DOS MIL DIEZ.

DR. ALDO HUMBERTO ROMERO CASTRO

DR. SEGIO JOAQUÍN JIMÉNEZ SANDOVAL

DR. GERARDO TORRES DELGADO